Master Thesis

submitted within the UNIGIS MSc. programme
at the Department of Geoinformatics - Z_GIS
University of Salzburg, Austria
under the provisions of UNIGIS India framework

Impervious Surface Probability Distribution Mapping of Kathmandu Valley

By

Deepak Kumar Shah
u105532

A thesis submitted in partial fulfilment of the requirements of
the degree of
Master of Science (Geographical Information Science & Systems) – MSc (GISc)

Advisor (s):

Dr. Him Lal Shrestha

Kathmandu, 20-11-2021

Science Pledge

By my signature below, I certify that my thesis report is entirely the result of my own work. I have cited all sources of information and data I have used in my thesis report and indicated their origin.

20th Nov 2021 PedPatil

Place and Date **Signature**

Acknowledgments:

I would like to gratefully acknowledge my thesis supervisor Dr. Him Lal Shrestha, the Associate professor and Coordinator of UNIGIS Program at Kathmandu Forestry College (KAFCOL) for his helpful comments, communication, and advice on all related parameters and guidance through the thesis.

I am very much thankful to Dr. Ambika Prasad Gautam and Dr. Upama Koju of KAFCOL for their critical comments and helpful suggestions. I am especially indebted to Ms. Tanuja Shrestha an employee of ICIMOD for the fruitful discussion on different aspects of Deep Learning and Dr. Mir Abdul Matin Theme Leader of Geospatial Theme at ICIMOD, who supported me during my thesis period.

I would like to acknowledge International Centre for Integrated Mountain Development (ICIMOD) where I used the workstation. I am also thankful to SERVIR-HKH for providing GEE asset access, Google Cloud Service (GCS) for storing data, and all the spatial knowledge. I would also like to acknowledge the data providers such as OSM, GEE, and Survey Departments of Nepal.

I am gratefully thankful to my wife Aradhana Sah, sister Archana Sah, brother Roshan Sah and my mom and dad who have been a great support during my academic period.

Abstract:

The Impervious Surface is known as hidden urbanization and a key factor for the ecological performance of the environment. Impervious surface is directly proportional to urbanization and the increase in urbanization leads to an increase in impervious surface. Remote Sensing integrates the art and science of earth-released sensing smoothly to the newest computerized image handling interpretive tools and methodologies. The Remote Sensing approach has been effective in identifying impervious surfaces with the help of different Indices which sometimes lacks in generalizing the overall impervious surface. Mapping of impervious surface are useful in the sustainable planning of urban areas and this impervious layer can be fed in water runoff modelling.

In this study, the Deep Learning method which is a subset of the Machine Learning approach is applied to map the probability distribution of the Impervious Surface of Kathmandu Valley. The training dataset in which Open Street Map features such as building and selected road type has been considered as impervious surface and the cloudless Sentinel-2A composite image optical bands of 10-meter spatial resolution and some calculated indices such as NDVI, NDWI, MNDWI, NDBI, SAVI, and IBI is considered as a predictor for the impervious surface. The dataset was extracted programmatically from the different highly urbanized areas of Nepal. The configuration of the Deep Learning Model used here is the UNet model with patch size 64X64 pixels, Adam as an optimizer, MSE as a Loss function, RMSE as a metric, and sigmoid as final activation function to produce probability layer of impervious surface.

Three different combinations of features such as optical bands only, optical bands with indices, and selected optical bands and indices were considered to train the model and find the probability distribution of impervious surfaces. The Test RMSE score of three different is 0.1991, 0.1976, and 0.1985. All three models were successful in separating the impervious surface from the pervious surface.

Table of Contents

List of Tables

List of Figures

List of Maps

Abbreviations

CBS	Central Bureau of Statistics
IS	Impervious Surface
LULC	Land Use/Land Cover
NDVI	Normalized Difference Vegetation Index
NDBI	Normalized Difference Built-up Index
IBI	Index-Based Built-up Index
CBCI	Combinational Biophysical Composition Index
ENDISI	Enhanced Normalized Difference Impervious Surface
MLC	Maximum Likelihood Classifier
AI	Artificial Intelligence
ML	Machine Learning
DL	Deep Learning
CNN	Convolution Neural Network
FCNN	Fully Convolution Neural Network
GPU	Graphical Processing Unit
TPU	Tensor Processing Unit
TF	Tensorflow
OSM	Open Street Map
GEE	Google Earth Engine

API	Application Programming Interface
RMSE	Root Mean Squared Error
MSE	Mean Squared Error
SAVI	Soil Vegetation Index
NDWI	Normalized Difference Water Index
MNDWI	Modified Normalized Difference Index
AF	Activation Function
ReLU	Rectified Linear Unit
HPF	High Pass Filter
PCA	Principal Component Analysi

Chapter-1: Introduction

1.1 Background

Nepal is a country of South Asia, situated in the lap of the Himalayas. The border area is surrounded by China in the North and India in the East, West, and South. The extension of Geographical location is from 26° 22' North to 30° 27' North latitude and 80° 04' East to 88° 12' East longitude. Nepal is divided into three physiographic belts known as Terai, Pahad, and Himal.

The total urban population of Nepal consists of 17% of the population resided in 58 designated urban areas (CBS, 2012). Similarly, with the addition of 159 municipalities in 2014/2015, 40% population resides in 217 designated urban areas. Although the growth rate in the intercensal decade was 3.43%, the normal yearly growth between 1981-2011 has stayed at a high pace of 5.3% and the urban-rural growth differential in 2011 was 2.4% (MoUD, 2017) and more detail growth rate is given in below Table 1.2.

Table 1.1: Urban Growth Pattern in Nepal (Adapted From, CBS, 2012; Choe & Pradhan, 2010; MoUD, 2017)

Parameters	1961	1971	1981	1991	2001	2011	2014/15
Number of urban areas	16	16	23	33	58	58	217
Urban population (%)	3.6	4.0	6.4	9.2	13.9	17	40
Urban growth rate (%)	4.40	3.23	7.55	5.89	6.65	3.43	N/A

Natural population growth, rural-to-urban migration, and reclassification of rural areas into urban areas are the factors in Nepal's urbanization (Devkota, 2012).

Urbanization in Nepal is mostly dominated by some huge and medium-sized urban areas. And Kathmandu Valley is the center of Nepal's Urbanization growth. Kathmandu is the only city with millions of population and the level of urbanization of Kathmandu Valley, including three districts Kathmandu, Lalitpur, and Bhaktapur is around 96.97% (MoUD, 2017). Kathmandu Valley has 40% of the total urban Population (Rana & Marwasta, 2015). In several places of Kathmandu, the average urban population density is 10,000 People per square kilometers as per Census 2011. Seven driving variables have influenced the dynamic pattern of urban growth in the Kathmandu valley: physical circumstances, public service accessibility, economic opportunities, land market, population increase, and political environment (Devkota, 2012).

Urbanization has not just effect on decreasing the deeply rooted agricultural land to non-agricultural land but it has adverse effects and implications on the quality of life, preservation of the environment and other natural amenities, farming income, sustainable agricultural production, as well as public interests of the open space, farming tradition and landscape preservation standards (Rana & Marwasta, 2015).

Because of expansion in urbanization the haphazard development has additionally been expanding. The expansion in urbanization has prompted the expansion in impervious surface and lots of development project includes and deal with the burgeon in impervious surfaces. Impervious Surface is characterized as the cover of soils with impenetrable material like concrete, metal, glass, landing area, and plastic(Scalenghe & Marsan, 2009). Impervious Surfaces are mainly constructed surfaces are rooftops, sidewalks, roads, and parking lots, and surfaces like this can be found in urbanized regions with commercial, industrial, transit, and medium to high-density residential land uses (Barnes et al., 2000).

There has been no study of impervious surface in Kathmandu Valley and how deep it is rooted on the soil of the Valley. Although we have seen some of the adverse events of impervious surface implications such as flash floods, water pollution, increase in temperature, less green area, depletion in ground water, water runoff, and other natural calamities. A proper study is required to analyze the extent of the impervious surface of the Kathmandu valley.

1.2 Literature Review

A literature review is an inquiry and assessment of the existing literature in your given subject or area of topic. It establishes the current state of knowledge in the field of the issue or topic you're writing about. It's a detailed overview of prior research on a subject. The literature review recognizes the efforts of earlier researchers, assuring the reader that your study is well-thought-out. The literature review is an important step for the overall completion of the thesis.

1.2.1 Impervious Surface

According to the oxford dictionary, an impervious surface is something that does not allow liquid or gas to pass through. Duley (1940) refers to the impervious surface as “soil seal” which means a layer that limits the infiltration of water through soil and is defined as the cover of soils with impenetrable materials like concrete, metal, glass, and plastic (Scalenghe & Marsan, 2009). Impervious Surfaces are mostly man-made structures such as roads, sidewalks, driveways, parking-lot, airports, industrial areas, commercial areas. Surfaces that allow little or no rainwater penetration into the earth are termed impervious surfaces. Impervious surfaces, apart from exposed natural rock cropping are entirely human-made and constitute an artificial feature of most ecosystems.

According to Strohbach et al. (2019), the impervious surface is also known as the “hidden urbanization” and is an important factor for the ecological performance of the built environment, in particular for water balance. He also describes that there is an increase in impervious surface particularly in commercial or non-commercial area housing and found out there is a gap between the development plans and actual implementation.

Impervious surfaces are approximately 100 percent hydrologically active and significant percentages of such surfaces may be found in urbanized regions with commercial, industrial, transportation, and medium to high-density residential land uses(Novotny & Chesters, 1981),.

Arnold & Gibbons (1996) states that, the impervious land cover has long been a feature of urban, it has only lately become recognized as an environmental indicator. He also added that the highways and rooftops are the most common and immediately recognized kinds of impermeable surface, sidewalks, patios, bedrock outcrops, and compacted soil are some other examples and the percentage of land covered by impermeable surfaces grows when development changes the natural environment which is extremely varied between communities and a significant component in the built environment's ecological performance.

1.2.2 Cause of Impervious Surface

Impervious Surface is directly proportional to Urbanization. The increase in urbanization leads to an increase in the impervious surface and it is one of the major indicator to measure the urbanization process and ecological environment (Liu et al., 2020).

According to Scalenghe & Marsan (2009), the loss of structure due to the impact of rain or soil laboring, the dispersion of colloids, and compaction are some of the causes that have been discovered that might lead to the impermeabilization of the soil surface. There have been many contributions as to what drives urbanization which ultimately leads to the impervious surface; some of the explanations cited include industrialization, commercialization, and migration, natural growth, socially beneficial services, opportunities for work, and other things(Bodo, 2019).

The major causes to increase in impervious surface area are as follows:

1.2.2.1 Rural to Urban Migration

The voluntary movement of people (as individuals, family units, or large groups) from their native lands (places of birth or residency) to a new spot to settle down partially or completely, due to economic and technological growth or advancement in their desired destination, is defined as migration (Bodo, 2019).

Tacoli (2018) describes that in low and middle-income countries, urbanization is driven by net rural-urban movement in response to greater economic possibilities in cities, or by a lack of opportunities in rural regions. He also states that there is a strong relationship between economic activity and urbanization. There are more educational institutions, health facilities, attractive housing amenities, strong road networks, and larger marketplaces for people to get comfortable life (Bodo, 2019).

Due to these factors as people are migrating to an urban area, there is an increase in development in housing, roads, industry, and other activities which finally leads to an increase in impervious surfaces.

1.2.2.2 Rural to Urban Transformation

According to Bodo (2019), there is an increase in demand of people for different facilities such as employment, schools, the hospital in rural areas due to which it slowly grows to a smaller town, the smaller town grows too large town and large town become cities. He also states that, with the development of commercial and industrial operations, policymakers are likely to channel the building of essential social amenities, health, and housing facilities to sustain the tempo of economic growth or to promote new firms in the region. Political factors and socio-economic factors have a major role in transforming rural to urban. As the urban land have a relatively higher price than rural areas, so after increasing different facility to rural areas the price of land becomes high, which are being sold for housing, industries and other for others development activities (Rana & Marwasta, 2015).

These are the reasons for which many rural areas are transforming to an urban area and as a result development in impervious surfaces to fulfill the growing demand for different facilities.

1.2.2.3 Lack of Policy

Government negative policies and programs available in various nations throughout the world have the greatest effect on urbanization today.

According to Devkota (2012), due to a lack of policy initiatives and institutional coherence, Nepal's metropolitan centers have been plagued by a slew of socioeconomic and infrastructure issues. In the lack of a solid strategy for the regulation and administration of rapidly expanding urban growth, unregulated and unplanned urban expansion has resulted in a slew of issues, including shortages in fundamental urban services, encroachment on public lands, slums, and spreading settlement.

Scott (2008) talks about the lack of policy regarding the intraurban specifically targeted to the management and reordering of existing urban areas and urban space have led to rapid urbanization at the highest degree. The urban sprawl or the construction of rapid-transit systems is immediately and intrinsically an element of the urban question. He also talks about the interaction of practical conditions and political arguments that, for the most part, exist well beyond the domain of the urban and he has defined it (even if they have numerous indirect urban consequences); the latter is inextricably linked to definite articulations of urban space.

This lack of strict policy towards urbanization has caused haphazard and unsustainable development and led to an increase in impervious surfaces.

1.2.3 Impacts of Impervious Surface

Increasing imperviousness has an impact on the esthetic nature of the streams and landscapes dramatically, indicates a move away from forest and rural areas to more suburban and urban settings, and is a way of estimating urban sprawl. These changes have enormous implications for the quality of life of millions of people (Barnes et al., 2000).

Some of the major impacts due to advancement in the impervious surface are as follows:

1.2.3.1 Impacts on water

The flow of water into a porous system like the soil is typically characterized by the law of Darcy, which is a gradient that governs the flow of water as well as resistance or permeability, respectively. Various variables impact hydraulic conduction and can affect the hydrological and mechanical behavior of the soil (Assouline, 2004; Baumhardt et al., 1990; Bonsu, 1992) and one of the major impacts of impervious surface is on water quantity as well as quality.

According to Scalenghe & Marsan (2009), the most evident finding is that artificial sealing of the soil surface (impervious surface) renders it impervious to water movement. This, along with the thermal consequences, suggests that the underlying soil's water regime has been substantially changed. In addition to the overall drop in soil moisture content, there is a fall in water tables in urban areas, which reduces the pace of chemical reactions.

Similarly, Barnes et al. (2000) explain that as watershed zones are developed for residential, commercial, industrial, and transit usage, there will be significant changes in local hydrological cycles, and the paving of previously vegetated regions is followed by dramatically changing times and amounts of storm water transported to close streams. The author also highlights that the changes in the stream level between storms, groundwater tables, and flux erosion rates and volumes are also likely to result from growing imperviousness at the watershed. Additionally, replacing the vegetation with impermeable areas lowers considerably the average annual watershed evapotranspiration.

As per the study Douglas (1983), the substitution of 25%, 50%, and 75% of the forest in the northeast United States with the impervious surface will lower annually potential evapotranspiration by 19%, 38%, and 59%, respectively.

Impervious Surface has not the only impact on the quantity of water but also impacts the quality of water due to its reduced filtering capacity of sealed soil (Bhaduri et al., 2001). The impervious surface due to urbanization of watershed has threat on water quality from both point sources pollutants such as factories and powerplant and non-point source pollutants by contaminating groundwater, infiltering water interactions with contaminants on the surface and within the soil (Barnes et al., 2000).

Conway (2007) reported that water characteristics changes such as pH and salinity are affected when as little as 2% of the surface of the soil is sealed. Pollutants build on impervious surfaces and are wiped away by rain (Hope et al., 2004) which are discharged onto contagious unsealed soil. A recent research study of changes in urban land use in Tampa Bay (27°45' N 82°31' W), USA, has shown that most pollutant loads are strongly linked with the amount of impervious surface and its extent (Xian et al., 2007).

1.2.3.2 Impacts on Food and Farming

Human Settlement and urbanization are linked to local land and water resource that could supply food and shelter and due to which prime agriculture land are frequently used near urban areas. According to Canada (1978), every year, an estimated 65,000 km^2 of agriculture is lost to urban growth for uses such as housing, industry, and infrastructure, posing a continuing threat to food and farming. In addition to the loss of land, significant agricultural activities have expanded infrastructure for farm construction and impervious areas (Allan, 2004). As the agricultural land is being captured by impervious surface area, the global estimations show that 0.43% of the world's geographical area is an impervious surface (European Commission, 2012).

According to Rose et al. (2017) study in Metro Vancouver located in the southeast corner of British Columbia, observed that as agricultural land is transformed to urban, commercial, and industrial purposes, large sections of fertile soil are lost to impervious surfaces each year, reducing the sustainability of soil-based agriculture and approximately 5260 hectares or 10% of arable agricultural soil has been covered with impervious surfaces with the highest percentage of that being for transportation (1690 ha) and residential development (960 ha).

1.2.3.3 Urban Runoff

Impervious Surface growth and especially the haphazard irregular spatial pattern is one of the major problem of waterlogging which ultimately leads to water runoff after rainfall (Yu et al., 2018).

Bhaduri et al. (2001) has found the linear relationship between the size of impervious surface area and average annual runoff. Haase & Nuissl (2007) have conducted a study in the city of Leipzig (51°20' N 12°23' E), EU and it was observed that, in the urban area between 1940 and 2003, surfaces runoff had more than doubled as impervious surfaces had increased. Similarly Leopold (1968), emphasizes the reduction in the volume of water infiltrating into soils and the amount of water lost in the air through evapotranspiration covering the soil with unproductive areas, such as towers and highways, therefore increasing the number of runoff after rainy events.

According to Elaji & Ji (2020) urban runoff simulation study in Blue River Watershed which is a fifth-order stream basin that covers about one-half of the Kansas City metropolitan area, South of the Missouri River, and has diverse LULC and development activities found that its stream tends to be frequent flooded.

A simulation study conducted in the USA by Choi & Deal (2008) confirmed that the increase in surface flow and sediment runoff under population growth scenarios and increase in impervious surface area. In Leeds (53°47' N,1°32' W), EU, Perry & Nawaz (2008) has estimated a 12% increase in surface runoff as a result of a 12.6% increase in soil paving. Similarly, in a survey carried out in Korea (36°21' N 127°23' E) the pollutant composite was impacted in the stormwater rain by the first flash following a rain event in the order: Suspended substances > organic substances > nutrients (Kim et al., 2016). Water cycle changes are associated with urbanization and urban runoff as given in Figure 1.1.

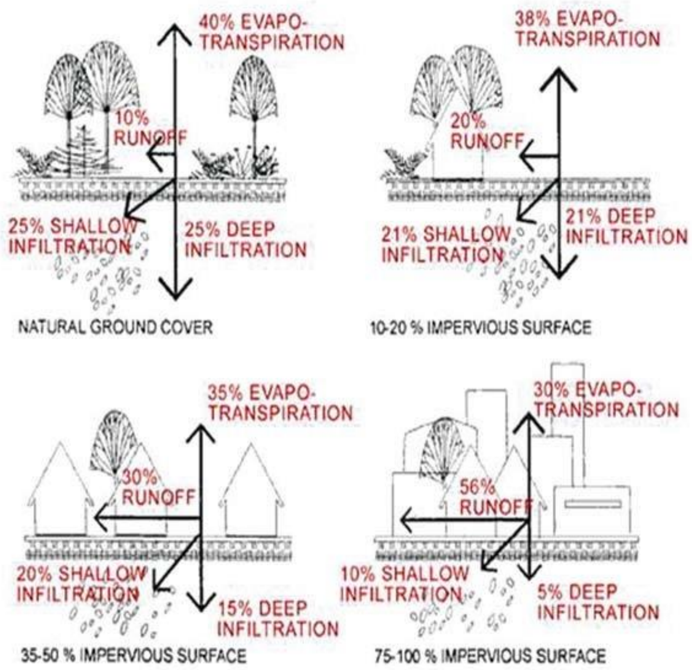

Figure 1.1: Water cycle changes associated with urbanization. Source: USEPA (1993)

1.2.3.4 Habitat Degradation, Loss and Fragmentation

The proportion of impervious surfaces in urban areas is growing, which might be a proxy for urbanization. It also influences numerous species assemblages, including bees (Fortel et al., 2014; Geslin et al., 2016) and amphibians (Parris, 2006), as well as urban ecosystem services including water supplies and flow management (Arnold & Gibbons, 1996).

According to Barnes et al. (2000), due to the increase of impervious surface in watershed lands, it has degraded and destroyed the aquatic and terrestrial habitats and is adversely impacted by water pollutants, and by a greater volume of stormwater runoff from the sealed impervious surface. The author also observed that the impervious surface covering the range between 10 to 20 percent, has significantly declined in biological integrity and habitat quality, decreased the variety of macroinvertebrates, fish, and amphibians, decreased amphibian and plant density, higher water, and sediment delivery rates and shifts in environmental sensitive organisms' populations to those that are more tolerant of deteriorating environments. Many, authors such as, Arnold & Gibbons (1996); Booth & Jackson (1997); Kennen (1999); Klein (1979), agrees that the quantity of impervious surfaces has an inverse connection with biological integrity and habitat quality.

The effect of increasing imperviousness surface has increased flood and erosion hazard following urban development because of which has caused physical degradation and loss of life. The negative effects of habitat fragmentation, on the other hand, take longer to appear and are frequently cumulative which results in changes in the biological characteristic of an area favoring edge (Adams, 1994; Soulé, 1991) and also refer to Table 1.2 for long term and short term effect on habitat degradation.

Biological homogeneity is thought to be aided by urbanization. Native ecosystems are replaced by pavement and buildings as cities are built, and what remains of the natural soil is covered with green patches that are typically dominated by non-native decorative plants which result in biodiversity loss (Pauchard et al., 2006).

1.2.3.5 Energy Balance and Microclimatic Impacts

As land is converted from pervious woods, grasslands, and croplands to impervious surfaces, the balances between solar energy intercepted at the surface (insolation) and emitted terrestrial energy have shifted. Impervious Surfaces in cities will change the local environment and lead to even greater temperatures. Increasing the temperature of the air near the sealed soil concerning air temperature outside the city is the most obvious distinction between the city climates. This phenomenon is known as Urban Heat Island (UHI) (Howard, 1833) and has medium term consequence as thermal specialization as given in Table 1.2.

According to Barnes et al. (2000), the conversion of pervious surface to impervious surface alters local energy balances through changes in the albedos of surface, the specific heat capacity, the thermal capacity, and the heat flowing from surface to atmosphere.

Similarly, according to Kamdoum Ngueuko et al. (2014), observation in Ibadan is a large city in the south-western region of Nigeria within longitudes 3°45' and 4°05' East and latitudes 7°10' and 7°30' by extracting impervious surface area from 1984 to 2006 showed the variation of surface temperature in rural and urban areas and when the mean impervious surface area increased from 67.46% to 69.61%, the surface temperature increased from 26.447°C to 33.932°C within the same period. Takebayashi & Moriyama (2007) discovered that the midday temperatures of a cement surface, a gray-painted surface, bare soil, a green surface, and a white-painted surface were in descending order. In the city of Indianapolis (39°47' N 86°8' W), USA, researchers have discovered that impervious surfaces have a greater surface temperature, indicating that unsealed soils are critical for temperature control (Weng et al., 2007).

Many authors such as Davidson & Janssens (2006); Q. Hu & Feng (2004); Sakaguchi et al. (2007); Sollins et al. (1996), agrees that increase in imperviousness of soil in an urban area has led to increasing in temperature rather than rural areas with normal temperatures and adverse effect on different species habitat.

Table 1.2: Component affected, effects, timing, and consequences of impervious surface, (Adopted From, Scalenghe & Marsan, 2009)

Components	Effect	Time	Consequence
Heat	Decreased radiation absorption	Short-Term	More Reflective surfaces
		Medium-Term	Heat Island
Water	Less Infiltration	Medium-Term	Reduced chemical reactivity
		Long-Term	Less Filtering Action
		Medium-Term	Cracking
		Short-Term	Loss of Biomass
		Long-Term	Diminishes the natural recharge of aquifers
	More Runoff	Short-Term	Increased water through adjacent areas
		Medium-Term	Increased Ponding Time
		Medium-Term	Probability of anaerobiosis
		Short-Term	Transfer of Contaminants
		Long-Term	Increased Risk of flash floods
	Barrier for perched water table	Short-Term	Increased risk of anaerobiosis
		Medium-Term	Release of contaminants
Gas	Reduced/interrupted exchanges	Long-Term	Risk of anaerobiosis
		Short-Term	Partial trapping
Biota	Loss of plant cover/biomass	Medium-Term	Reduced biodiversity
		Long-Term	Reduced carbon sink
	Urban Heat Islands	Medium-Term	Thermal specialization
Landscape	Increased wind erosion	Medium-Term	Increased air-borne particulate
	Increased water erosion	Medium-Term	Increased erosion of adjacent areas

	Uniformity	Short-Term	Reduced aesthetic appeal
		Short-Term	Reduced visual appearance
		Medium-Term	Reduced attractiveness

1.2.4 Remote Sensing Approach

Remote sensing is a technology used for measuring and monitoring changes in the earth's surface and atmosphere via electromagnetic sensor systems. This is usually done via a satellite or an aviation device. Remote Sensing integrates the art and science of earth-released sensing smoothly to the newest computerized image handling interpretive tools and methodologies (Schowengerdt, 2006). Remote sensing technology is becoming increasingly significant in the area due to the attention given to the newest public and private information, planning, and management. It is particularly beneficial in the management of natural resources, sustainable development, environmental deterioration, and disaster management (Shandilya et al., 2013).

RS offers multi-spectral, multitemporal, and multiresolution data which are useful for modeling different applications such as Agriculture, Forestry, Geology, Hydrology, Sea Ice, Air quality, and Urban area (Campbell & Wynne, 2011; Shandilya et al., 2013). One of the primary study areas in terms of global environmental change is land-use/land-cover (LULC) categorization, which is typically based on remote sensing imagery (Guan et al., 2011). In the land-use changes in all areas, anthropogenic forces play a key role (Briassoulis, 2000) which is the result of impervious surface(Slonecker et al., 2001) and LULC is generally built on urban development. GIS and Remote Sensing are suitable tools for monitoring land cover, urban/regional planning, and researching local-global space-temporal change in LULC (Dewan & Yamaguchi, 2008; Thapa & Murayama, 2012).

Kuc & Chormański (2019) conducted a study in Warsaw – the capital of Poland and largest city of Poland for mapping of imperviousness using Sentinel-2 data, the author has used NDVI (Normalized Vegetation Index) and NDBI (Normalized Built-up Index). The findings show that computed indicators and mapping urban footprints using Sentinel-2 images are appropriate for analyzing imperviousness surfaces in quickly growing cities. The author also points that NDVI is better in the mapping of impervious surface than NDBI which require further improvement.

According to Bauer et al. (2004), has used Multitemporal Landsat 5 Thematic Mapper (TM) and Lansat 7 ETM imagery for impervious surface mapping in seven-county Twin Cities Metropolitan area and discovered a strong connection between the Landsat Tasseled Cap greenness of percentage of impervious surface area. By using greenness and an impervious surface percentage as continuous variables, a regression model is used to assess each landing pixel's percent impermeable region. The comparison was done with DOQs to Landsat estimated impervious area and found that both were highly correlated with r=0.95. The author also points out the increase in impervious from 8.81% to 14.1% from 1986 to 2000 in Twin County Metropolitan Area.

Similarly, as per the study of X. Hu & Weng (2011) conducted in Indianapolis the capital of Indiana state USA has used IKONOS image with bands blue, green, and NIR (Near Infra-red) with a spatial resolution of 4 m and the panchromatic band with a spatial resolution of 1m. The author has used object-based classification technique based on image segmentation by incorporating fuzzy rules for extraction of impervious surface and found that the impervious surface area feature boundaries were properly and somewhat accurately defined with the accuracy of 95% in the residential area, similarly, roads have an accuracy of 93% and residential buildings were obtained with an accuracy of 94%. The author also highlights the advantage of object-based classification rather than pixel-based classification in the extraction of impervious surface as it includes shape, area, and elongation, and finally, the fuzzy logic has played an important role in assigning which feature belongs to which class.

According to Chen et al. (2020) has used Sentinel-2A images and extracted different indices such as NDBI (Normalized Difference Built-up Index), IBI (Index-based Built-up Index), BCI (Biophysical Composition Index), CBCI (Combinational Biophysical Composition Index), and ENDISI (Enhanced Normalized Difference Impervious Surface Index) and found that ENDISI, IBI, and NDBI were less affected by other parameters and shows more information of impervious surface. The author also highlights that these all six indices are capable of extracting impervious surface and the author also point that these all indices were affected by bare soil. The author also used the same indices in different areas such as Fuxian Lake Basin, Shenzen City, and Nanjing City to map impervious surfaces and observed that overall accuracy varied from 83.9 to 94.68 and kappa coefficients varied from 0.5735 to 0.7584.

Similarly, Lu et al. (2011) conducted the study in two urban sites of Brazil by using Quickbird imagery which has blue, green, red, and NIR bands at 2.4m, and used wavelet merging technique with the panchromatic band to new multispectral image with 0.6m spatial resolution. The author has used three different techniques such as hybrid technique which includes thresholding, unsupervised classification, and manual editing, maximum likelihood classification which includes per pixel-based automatic classification, and segmentation-based method for impervious surface mapping and observed that the hybrid method has the best performance than other two methods. The author also highlights that the segmentation-based method has the almost same accuracy as MLC because of difficulties in distinguishing impervious surfaces from bare soils, shadows, and wetlands due to spectral confusion.

1.2.5 Machine Learning Approach

As we all know that Machine Learning is a subset of Computer Science and Artificial Intelligence. McCarthy (2007), described artificial intelligence as the “science and engineering of making intelligent machines, especially intelligent computer programs”. The author also points out the AI applications in gaming, speech recognition, natural language comprehension, computer vision, expert systems, and heuristic classification. The evolution from Artificial Intelligence to Deep Learning is given in Figure 1.2.

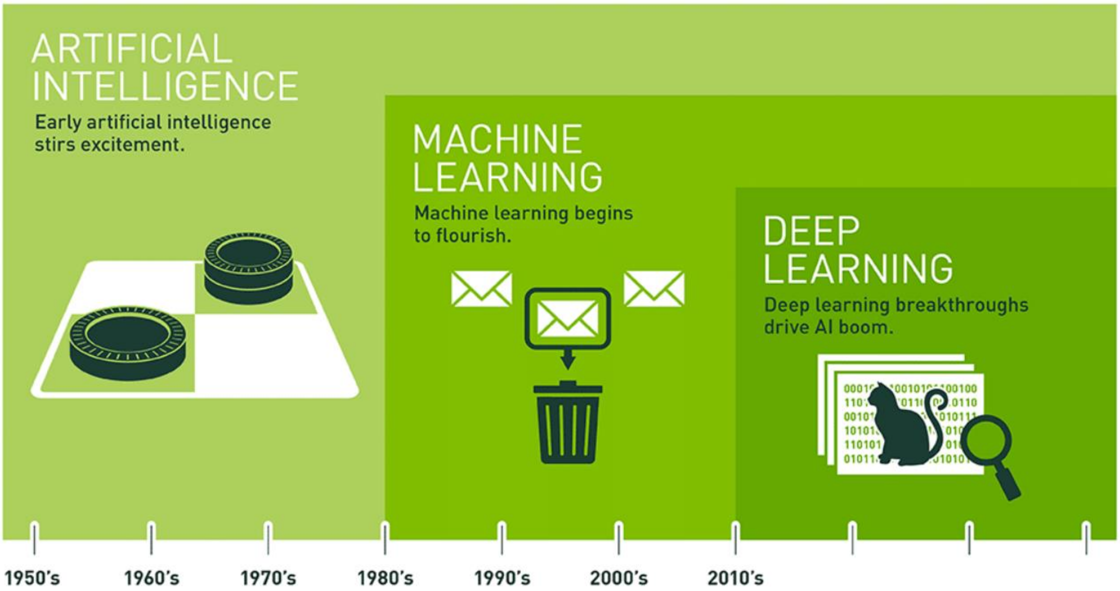

Figure 1.2: Evolution of Artificial Intelligence, Machine Learning, and Deep Learning (Adopted From, COPELAND, 2016)

Ongsulee (2017) defined machine learning as the strong relation with computational statistics which focuses on making predictions and similarly Machine learning is a technique used in data analytics to create sophisticated models and algorithms that can be used in prediction. The author also points out some widely adopted machine learning algorithms as are supervised learning, unsupervised learning, semi-supervised learning, and reinforcement learning. Supervised learning covers about 70% of total applications whereas other including unsupervised learning falls between 10% to 30%. El Naqa & Murphy, (2015) defined machine learning as an emerging area of computer algorithms intended to imitate human intelligence via learning from the environment and in the new era of so-called Big Data they are regarded as the working horse. The algorithms of machine learning differ considerably in part by the way they express applicant programs such as decision-making tree, mathematical functions, generalized programming language (Jordan & Mitchell, 2015).

Spatial as well as biological science are rapidly adopting a strong kind of machine learning that allows computers to handle perceptual issues like image and speech is known as deep learning (Rusk, 2016). Deep learning has computer models which are composed of many processing layers to learn data representations of various abstract degrees. These approaches have significantly advanced the state-of-the-art in voice recognition, visual object identification, object detection, and a variety of other fields such as drug development and genomics, and many deep learning applications are based on feedforward neural networks as well backpropagation architecture (LeCun et al., 2015). Some of the deep learning methods are Restricted Boltzmann Machine (RBM), Auto-Encoder, Convolution Neural Network (CNN), and Recurrent Neural Network (RNN) are given Figure 1.3.

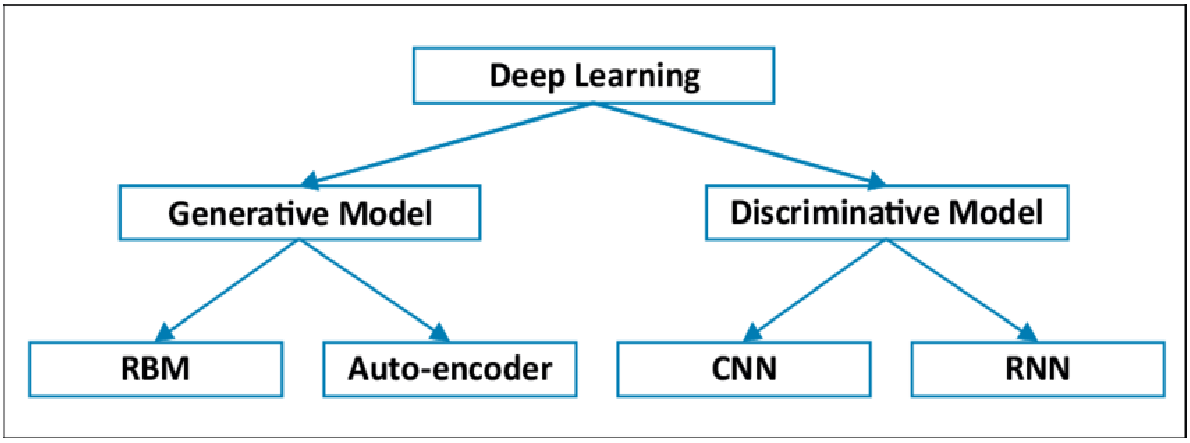

Figure 1.3 : Deep Learning methods (Adopted From, Ganapathy et al., 2018)

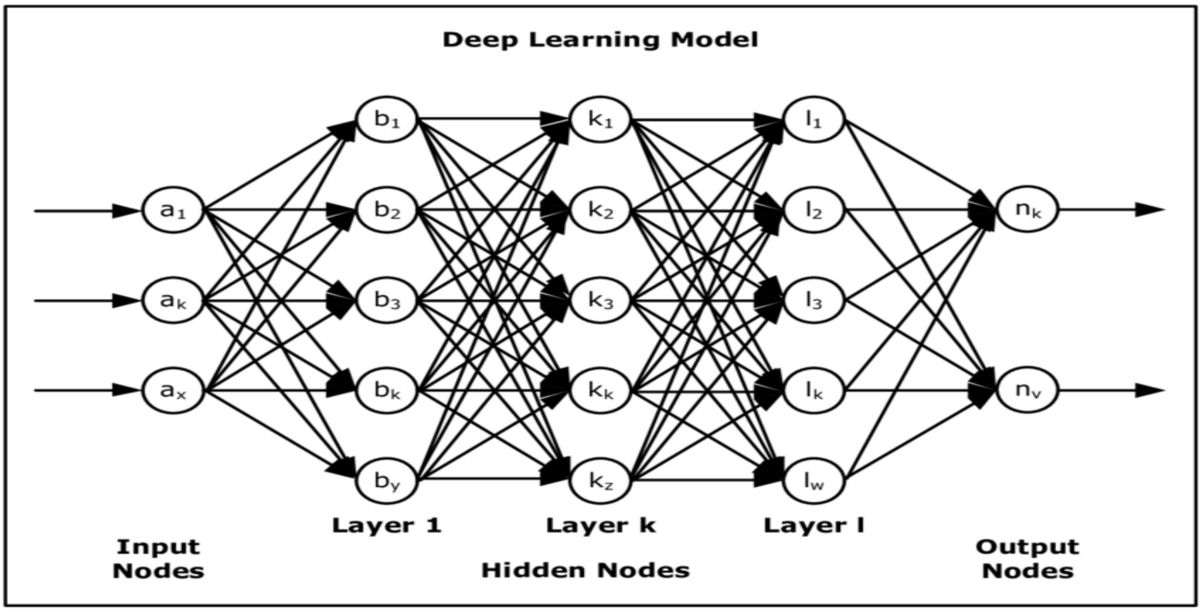

Figure 1.4: Artificial Neural Network Deep Learning Model (Adopted From, Serrano, 2017)

Machine learning (ML), which includes Artificial Neural Networks (ANN) as given in Figure 1.4 of various architectures and Support Vector Machines (SVM), has become one of the most significant technologies for intelligent geospatial data analysis, processing, and visualization in recent years (Kanevski et al., 2008). Due to diverse combinations of surface materials and the many forms of size, form, and positioning, and reflectivity of the items making up a typical picture scene, extracting information from remote sensing data on the built environment is a complicated process (Wieland & Pittore, 2014) and thus machine learning, as well as its different methods, come into play for analyzing Geospatial Analysis.

Misra et al. (2020) conducted a study to extract Built-up impervious surface in Delhi, India using Sentinel-2 Datasets with Blue, Green, Red, and Near Infrared (NIR) Bands with 10m resolution by accessing supervised based classification of machine learning such as Spectral Angle Mapper (SAM), Support Vector Machine (SVM) and Neural Network (NN) and found that NN performs better than other two machine learning algorithms. The author also highlights the performance of NN is better due to its backpropagation algorithm which helped to decrease the error and enabled the trained class in the appropriate domain of each data source to be accurately recognized.

According to Wieland & Pittore (2014) observation in which author tends to classify and perform the evaluation of urban pattern recognition to find the potential of a machine learning algorithm in the context of object-based image analysis using medium Resolution Landsat and Very High Resolution such as WorldView-2, QuickBird, and IKONOS. The author has used 4 (Four) machine learning classifications algorithm such as Normal Bayes, K Nearest Neighbor (KNN), Random Trees (RT), and SVM and concludes that SVM and RT seemed to be the top-performing classifiers on all image types, similarly KNN and NB performed well in specific settings but could not generalize exhibited erratic behavior in a variety of training-testing settings.

Similarly, Corbane et al. (2020) used the Sentinel-2 layer for Global Human Settlement mapping. The author has used data such as Global Human Settlement of built-up Areas, European Settlement, Facebook High-Resolution settlement data, and Microsoft building footprint data. Using these data, the author has proposed Convolution Neural Network (CNN) model names as GHS-S2Net to perform the pixel-wise classification. The author has also used transfer learning and after training and hyperparameter tuning, they have obtained an accuracy of 61% to 83%. The author conducted an independent validation of results using the trained model in different sites of the world and successfully concludes the model robustness against different variable conditions of urban areas. The author also highlights exceptional learning potential despite the absence of precise training data that may restrict the application of CNN models in a genuine remote-sensing context.

Similarly McGlinchy et al. (2019) use the FCNN UNet model of deep learning to segment Urban Environment from High-Resolution data of WorldView-2 which contains 8 bands coastal blue, blue, green, yellow, red, red edge, and two near-infrared channels at 2 m resolution. The author trained the model by varying the bands and with the different number of epochs to get the final accuracy. The highest accuracy the author got is 98% by using blue, green, red, and NIR1 of batch size 32 and epochs 52. The author also points out that the UNet produce the cleaner result of roads and residential areas rather than other LULC result.

1.3 Aims and Objectives

1.3.1 Aims

Kathmandu Valley is quite possibly the most urbanized place. The urbanization cycle has created and divided heterogeneous land use mixes in the valley by not supplementing the natural environment conditions (Rana & Marwasta, 2015). So, a proper study is required for mapping the impervious surface of Kathmandu Valley. The significant point of this study is to use the enormous storehouse of Open Street Map (OSM) information and prepare a profound deep learning model for impervious surface mapping utilizing distributed computing assets.

1.3.2 Objectives

The major objective of this thesis entitled "*Impervious Surface Probability Distribution Mapping of Kathmandu Valley"* are as follows:

- To develop a deep learning model for impervious surface prediction.
- To find the probability distribution of the impervious surface of Kathmandu Valley of 2020.

1.4 Study Area

Kathmandu Valley is a historical place and located in the central part of Nepal. It consists of the Capital City of Nepal known as Kathmandu. The Kathmandu Valley is situated between 27°56' and 27°80' N and 85°20' and 85°50' E. Kathmandu Valley is made up of parts of three districts, Kathmandu, Bhaktapur, and Lalitpur of Bagmati Province and these districts are the most populated and developed districts of Nepal. Kathmandu Valley has an area of 718 sq km. The flat land of bowl-shaped Kathmandu Valley at central part stands at 1425 m from sea level and is surrounded by mountain ranges that go up to 2732 m elevation. The Newars are the valley's indigenous people and the builders of its historic civilization.

The Kathmandu valley serves as both an administrative center and a significant tourism destination. Because of its strategic position, it is the center of the most important economic activity (Rana & Marwasta, 2015).

Kathmandu Valley is the center of Nepal's Urbanization growth. Kathmandu is the only city with millions of population and the level of urbanization of Kathmandu Valley, including three districts Kathmandu, Lalitpur, and Bhaktapur is around 96.97% (MoUD, 2017). According to the Central Bureau of Statistics(CBS), Kathmandu Valley has 40% of the total urban Population (Rana & Marwasta, 2015). In several places of Kathmandu, the average urban population density is 10,000 People per square kilometers as per census 2011.

The study area is extracted from these three districts which are highly populated and bowl-shaped area known as Kathmandu Valley using DEM.

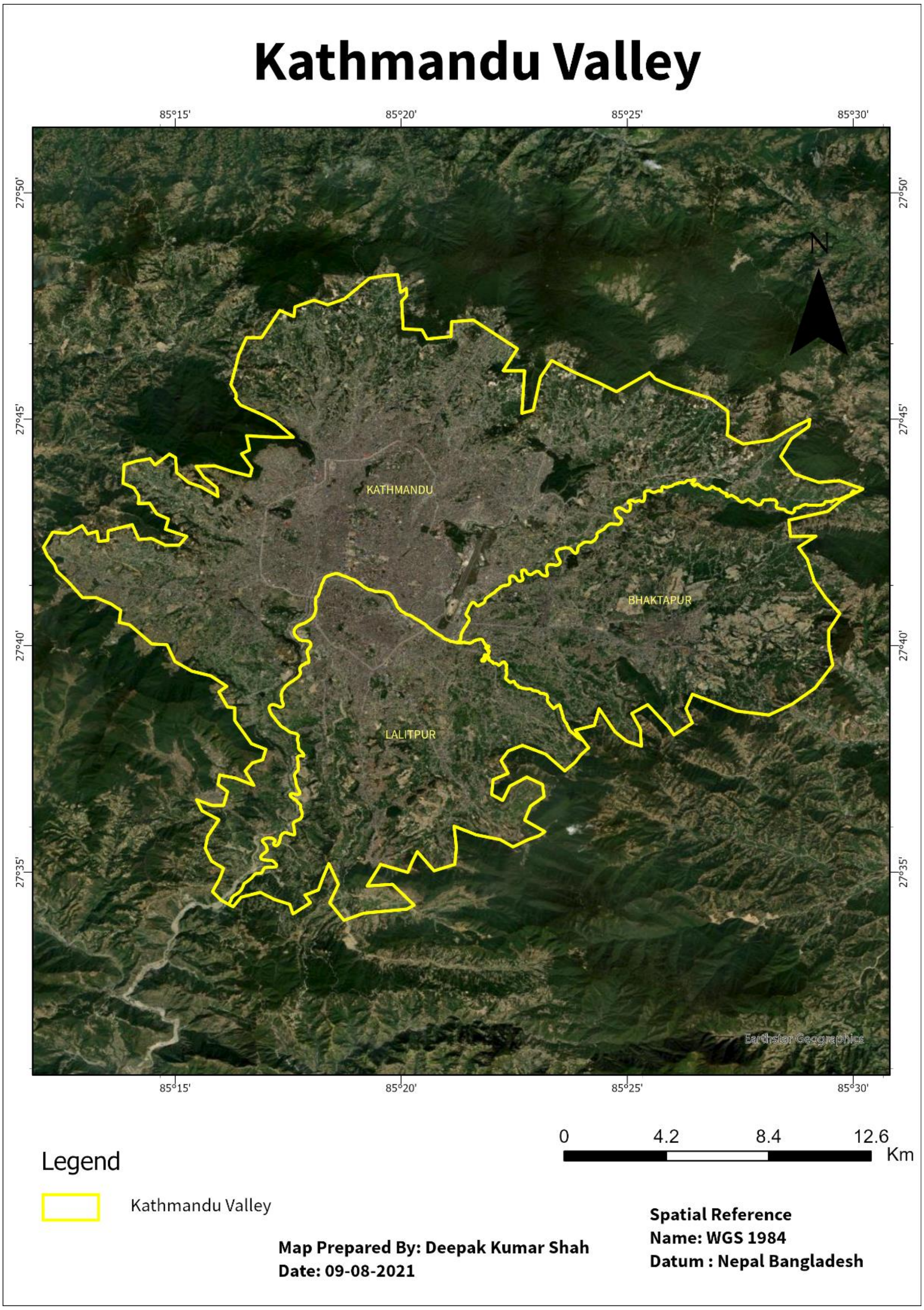

Map 1.1: Map Showing Study Area

1.5 Rationale

Impervious surface is the cover of soils with impenetrable materials like concrete, metal, and glass (Scalenghe & Marsan, 2009). IS have adverse effects on a different element of the environment such as decreased radiation absorption, less infiltration, increased in the runoff, loss of plant cover biomass, lead to urban heat island, habitat degradation, increased water, and wind erosion (Elaji & Ji, 2020; Haase & Nuissl, 2007; Pauchard et al., 2006; Scalenghe & Marsan, 2009). Kathmandu Valley is the center of Nepal's Urbanization growth and has 40% of the total urban population living in this area (Rana & Marwasta, 2015).

The consequence of the impervious surface observed is that in recent years Kathmandu Valley has been the hub for flash floods (Suardiwerianto, Yogi, 2017). Similarly Lamichhane & Shakya (2019) have presented that minimum temperature, maximum temperature, and precipitation in the Kathmandu watershed are projected to increase by 0.66 C, 0.6 C, and 23% respectively RCP4.5 scenarios. Thapa & Murayama (2009) observed that urbanization is one of the major reasons for encroachment of agricultural land in rural hills and mountains peripheries.

As from the different study, we found that impervious surface has a different impact on the environment and most of the study, focused on some indices of Sentinel Imagery to map impervious area using threshold method, classifications, and some use deep learning method (Chen et al., 2003; X. Hu & Weng, 2011; Kuc & Chormański, 2019). So, I felt a proper study is required on impervious surfaces identification of Kathmandu valley and proposing to find the “Impervious Surface Probability Distribution Mapping of Kathmandu Valley” using the deep learning method.

Mapping impervious surfaces are useful in the sustainable planning of urban areas and the mitigation of the UHIs effect (Hua et al., 2020). The probability layer of impervious surface can be fed in water runoff modeling to find flash floods and urban flooding (Canters et al., 2006).

Chapter-2: Methodology

Artificial Intelligence(AI) based on different machine learning algorithms is quickly developing processing in every industry to gains benefits from efficiency and cost reductions (Hassani et al., 2020). Machine learning is dependent on the possibility that frameworks can learn from information, recognize patterns, and settle on choices with negligible human mediation. In this study, we will be using the deep learning method which is a subset of machine learning to map impervious surfaces by using the data from Open Street Map as impervious surface and Sentinel-2A bands.

This chapter deals with a detailed explanation of different software, tools, and data used in this study. And at last, the explanation of Methodological Flow to map the impervious surface of Kathmandu Valley.

2.1 Software and Tools

The different software, tools, and packages used in the development and analysis of this study are as follows:

2.1.1 ArcGIS Pro

ArcGIS Pro is a sophisticated desktop GIS program that may be used for data visualization, advanced analysis, and data maintenance in 2D, 3D, and 4D. This tool is used to make the study area and the resulting map. ArcGIS is a universal GIS application for all GIS-related works.

2.1.2 Google Earth Engine

Google Earth Engine is a cloud-based huge analytic platform that enables Google to address a range of social challenges, including deforestation, droughts, disasters, diseases, food safety, water management, climate monitoring, and the preservation of the environment, in a variety of ways. Earth Engine comprises a multi-performance, parallel computing service and analysis-ready data catalog (Gorelick et al., 2017). GEE provides its API for both JavaScript as well as Python. It has a dedicated scripting code editor for JavaScript know as Earth Engine Code Editor. The code editor is divided into four sections the first section contains script file, API document, and assets, the second section is the part where code is written, the third section contains the debugging tools such as Inspector, console, and tasks and at last the fourth section contain the map where the result is displayed either in form of vector or raster data. Google Earth Engine code Editor looks a like as given in Figure 2.1.

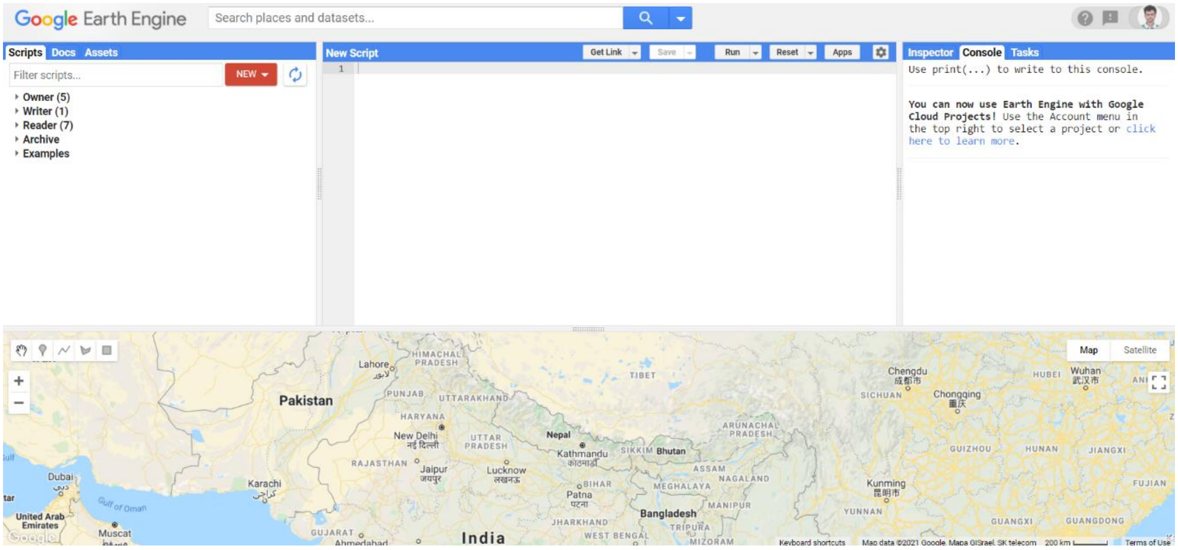

Use print(...) to write to this console.

You can now use Earth Engine with Google Cloud Projects! Use the Account menu in the top right to select a project or click here to learn more.

Figure 2.1: Google Earth Engine Code Editor

In this study, we have used Sentinel-2A multispectral data and Sentinel-2 Cloud Probability data provided by GEE. Most of the data preparation part is done in GEE using its massive computation power.

2.1.3 Google Colab

Google Colab is a product of Google for education and research purpose. Google Colab is a cloud-based service providing machine learning and research-based on Jupyter

Notebooks (Carneiro et al., 2018). Jupyter is a browser-based and open-source application that blends interpreted languages, libraries, and visualization tools (Perez & Granger, 2007). Google Colab is integrated with the Google services environment, and we can use and integrate services such as Google Cloud Service (GCS), Google Drive, GEE, and others. The language we use in Google Colab is python. And we can also use pip as a package management system to install and manage different python packages. It provides CPU processing, high-power Graphical Processing Unit (GPU), and Tensor Processing Unit (TPU) to use in our machine learning or deep learning while training the model.

In this study Google Colab platform is used to code the training model and train the model using GPU. After training the model we are also using it to predict the probability of the impervious surface of Kathmandu Valley.

2.1.4 Python Programming Language

Python is an open-source high-level, object-oriented, programming language developed for development speed optimization. Python is interpreted general-purpose programming language which is designed on the philosophy of natural language code readability (Lutz, 2001). Python is the most wanted programming language and a great tool for Data Science (VanderPlas, 2016). Python has many components or packages for Data Science such as Pandas, Numpy, and Scipy for data exploration, Matplotlib and Seaborn for Data Visualization, sci-kit-learn for Machine Learning, and similarly Kera, Tensorflow, and PyTorch for Deep Learning.

In this study, we are using Python Programming language to code our UNet Deep Learning algorithm in Google Colab which involves training and prediction.

2.1.5 JavaScript

JavaScript is the major Web browser scripting language and is crucial for contemporary Web applications (Jensen et al., 2009). JavaScript is also abbreviated as JS. According to Mozilla Developer Network, JavaScript (JS) is a compiled programming language with first-class functions that are lightweight, interpreted, or just-in-time. Javascript is one of the most powerful scripting languages which run on the client-side of the Web and is responsible for the behavior of web pages of occurrence of an event.

Here we are using JavaScript as scripting language in Earth Engine Code editor for analysis as well as data preparation and manipulation of planetary imagery. Mostly the JavaScript in the code editor is vanilla JavaScript with GEE API.

2.1.6 TensorFlow

TensorFlow is a complete, free, and open-source machine learning platform and is a powerful tool for managing all elements of a machine learning system. TensorFlow is a large-scale machine learning system in diverse contexts. TensorFlow utilizes a dataflow graph to show computation, shared state, and transactions that change that state (Abadi, 2016). TensorFlow covers a wide range of applications, although it focuses on deep neural network training and inference in particular and it provides a framework for the study and deployment of Machine Learning in various fields such as voice identification, computer vision, robotics, information retrieval, and processing of natural languages (Abadi, 2016).

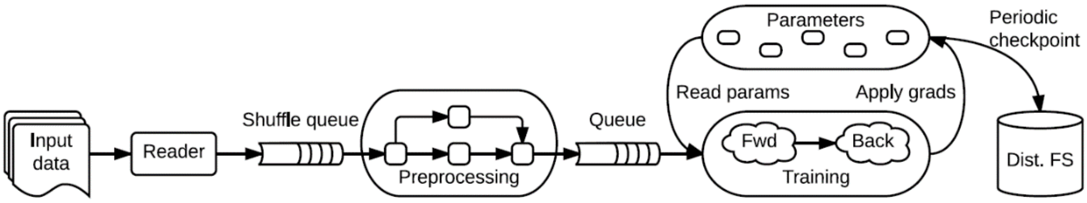

Figure 2.2: A schematic TensorFlow dataflow graph for a training pipeline (*Adopted from Abadi, 2016)*)

Refer to Figure 2.2 on Tensorflow dataflow works. It is the basic framework for model development, training, and inference. Keras is a TensorFlow wrapper that makes it more accessible, easier to use, and cleaner to work with which comes in TensorFlow Package. In our study, we are using TensorFlow python API for model development, training, and prediction of impervious surfaces. Tensorflow can run on multiple platform such as CPU, GPU and TPU as given in Figure 2.3.

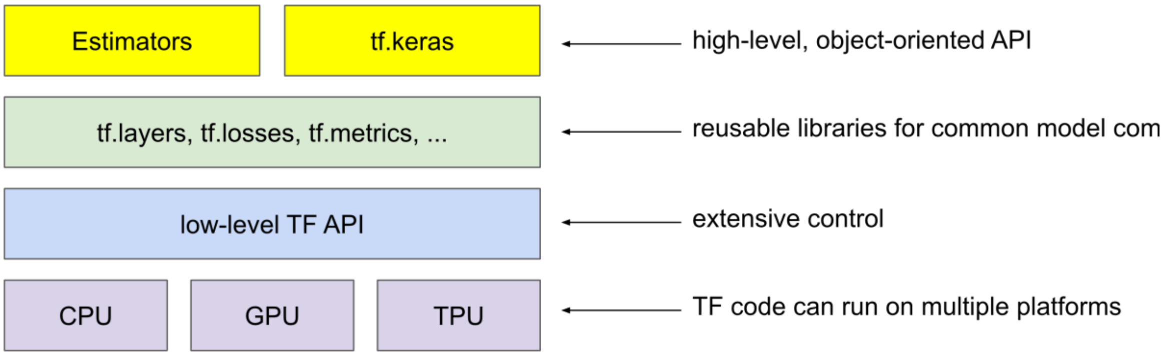

Figure 2.3: TensorFlow Toolkit Hierarchy (Google, 2021)

2.2 Data Used

Data used in the mapping probability distribution of the impervious surface of Kathmandu valley are Sentinel-2A and Open Street Map.

2.2.1 Sentinel-2A

According, ESA, Sentinel-2 is a multi-spectral imagery mission in Europe with a high-resolution broad swath. Two satellites Sentinel-2A and Sentinel-2B in the same orbit but phased at 180, have the complete mission requirements to provide the equator a high return frequency of 5 days. The revisit time of a single satellite is 10 days. Sentinel-2A was launched on 23rd June 2015 and Sentinel-2B was launched on 7th March 2017.

For this study, we will be using Sentinel-2A available in the GEE catalog by filtering data for 2020. Bottom Of Atmosphere (BOA) reflectance images are provided by the Sentinel Level-2A product, which is derived from the related Level-1C products.

The bands that are provided by the Sentinel-2A GEE catalog are given in Table 2.1 and the bands that we are going to select for our study are given in Table 2.2.

Table 2.1 : Bands of Sentinel-2A From GEE Catalog

Bands	Pixel Size	Wavelength	Description
B1	60 meters	443.9nm-442.3nm	Aerosols
B2	10 meters	496.6nm - 492.1nm	Blue
B3	10 meters	560nm - 559nm	Green
B4	10 meters	664.5nm - 665nm	Red
B5	20 meters	703.9nm - 703.8nm	Red Edge 1
B6	20 meters	740.2nm - 739.1nm	Red Edge 2
B7	20 meters	782.5nm - 779.7nm	Red Edge 3
B8	10 meters	835.1nm - 833nm	NIR
B8A	20 meters	864.8nm - 864nm	Red Edge 4
B9	60 meters	945nm - 943.2nm	Water Vapor
B11	20 meters	1613.7nm - 1610.4nm	SWIR 1
B12	20 meters	2202.4nm - 2185.7nm	SWIR 2
AOT	10 meters		Aerosol Optical Thickness
WVP	10 meters		Water Vapor Pressure
SCL	20 meters		Scene Classification Map
TCI_R	10 meters		Red Channel, TCI
TCI_G	10 meters		Green Channel, TCI
TCI_B	10 meters		Blue Channel, TCI
MSK_CLDPRB	20 meters		Cloud Probability Map

MSK_SNWPRB	10 meters		Snow Probability Map
QA60	60 meters		Cloud Mask

Table 2.2: Selected Sentinel-2A Bands and resolution for impervious surface study

Sentinel-2A			
Acquisition Date: 01/01/2020 to 31/12/2020			
Bands	Pixel Size	Wavelength	Description
B2	10 meters	496.6nm - 492.1nm	Blue
B3	10 meters	560nm - 559nm	Green
B4	10 meters	664.5nm - 665nm	Red
B5	20 meters	703.9nm - 703.8nm	Red Edge 1
B6	20 meters	740.2nm - 739.1nm	Red Edge 2
B7	20 meters	782.5nm - 779.7nm	Red Edge 3
B8	10 meters	835.1nm - 833nm	NIR
B8A	20 meters	864.8nm - 864nm	Red Edge 4
B11	20 meters	1613.7nm - 1610.4nm	SWIR 1
B12	20 meters	2202.4nm - 2185.7nm	SWIR 2

2.2.2 Sentinel 2 Cloud Probability

Sentinel 2 Cloud Probability is derived from Sentinel 2 data with sentinel2-cloud-detector library by using LightGBM a gradient boost base algorithm. The resulting data is from 0 to 1 which is scaled from 1 to 100. This higher the number, then there is a high probability of cloud. Probability calculated by up sampling all the bands to 10-meter resolution using bilinear interpolation. Sentinel 2 Cloud Probability is an image collection of with probability of cloud of Sentinel 2 Surface Reflectance Imagery as given in Table 2.3.

Table 2.3: Sentinel 2 Cloud Probability Bands and resolution

Sentinel-2 Cloud Probability Data Acquisition Date: 01/01/2020 to 31/12/2020				
Name	Min	Max	Pixel Size	Description
Probability	0	100	10 meters	Cloud Probability per pixel

This data is used for masking cloud from Sentinel-2A data to extract surface reflectance data of different bands.

2.2.3 Open Street Map

Open Street Map (OSM) has acquired free access to a vast amount of mapped geographic data from all around the world. OSM is volunteered Geographic Information (VGI) from all around the world which are responsible for mapping data by using mapping systems available on the internet by non-professional (Jokar Arsanjani et al., 2015). OSM data has a lot of features such as road, building, park, and others, we are going to extract the data which are mostly concrete such as roads, buildings, and some land use for impervious surface mapping. The country-level data is available on the [GEOFABRIK download]() website. Geofabrik extracts the country-level data from OSM and puts it in their server according to a different continent.

The data that was extracted from the Open Street Map are building and road which falls under the impervious surface. The type of buildings and roads, extracted from Open Street Map are given in Figure 2.4.

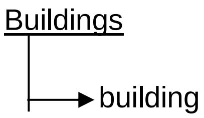

Roads

- motorway
- motorway_link
- primary
- primary_link
- trunk
- trunk_link
- residential
- secondary
- secondary_link
- tertiary
- tertiary_link
- track
- track_grade1

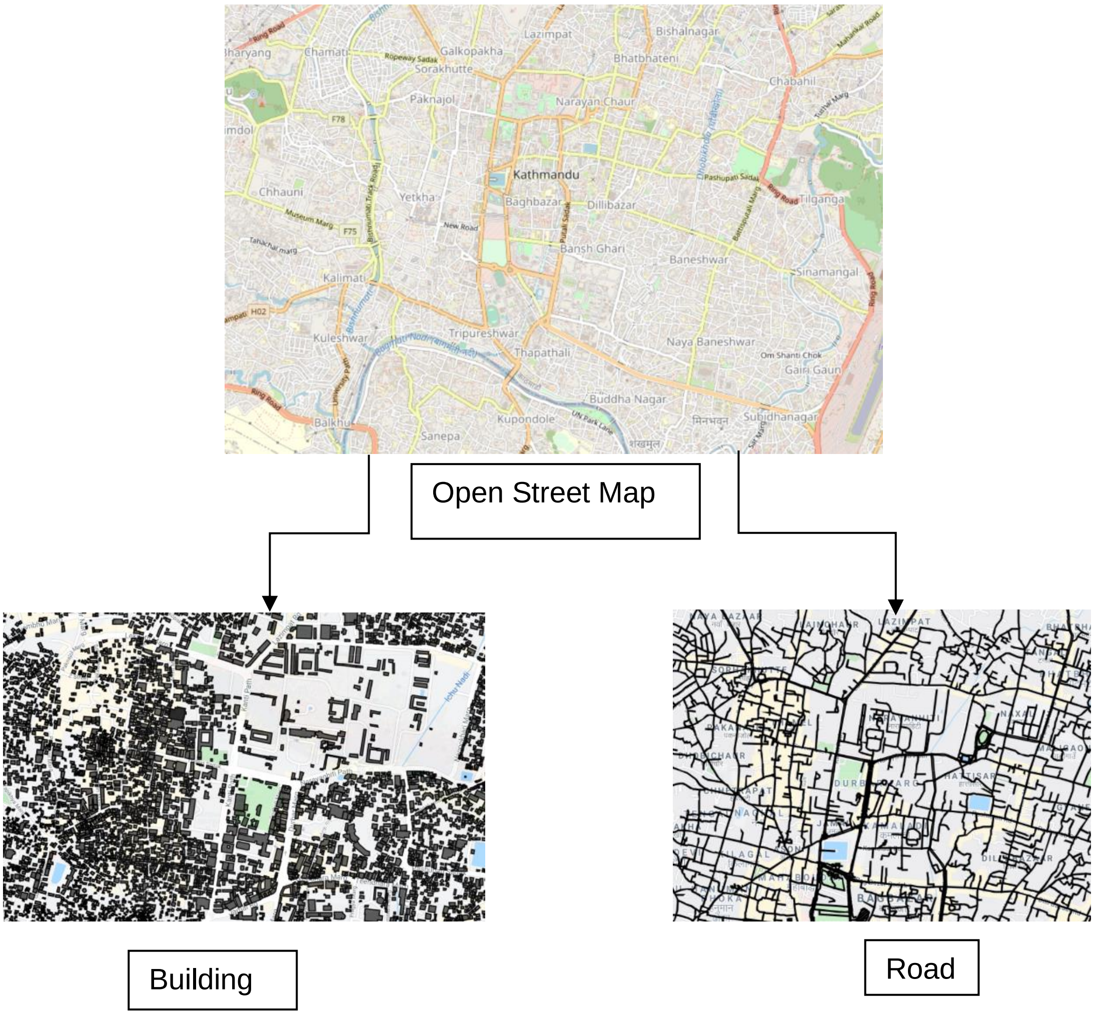

Figure 2.4 : Buildings, Road and Land Use Data Extraction from Open Street Map

2.3 Methodological Flow

The whole methodological flow chart is divided into three parts, preprocessing, processing and finally predictions. The preprocessing parts contains the data preparations sections. The preprocessing of data is mostly done using GEE and its massive catalog of image collection. Similarly, the processing which includes the fitting the model and finally the predictions to find the probability distribution of impervious surface are done using Google Colab.

- The vector data roads and buildings are extracted from OSM which has the characteristics of impervious surface are merged and rasterized at 10m resolution.
- Sample polygons are collected where the impervious surface mapping is high in OSM.
- Similarly, the Sentinel-2A image collection of 2020 dated from 01/01/2020 to 31/12/2020 is extracted and filtered according to our collected sample data.
- Cloud is removed and masked from filtered image collection by using Sentinel Cloud Probability.
- The bands which are at 20 meters resolution are resampled and sharpened to 10 meters on the base of the remaining high-resolution bands which is 10 meters.
- Then a composite is created by taking the median of all filtered and cloud masked image collection of 2020.
- Here the OSM acts as target value which in this study is regarded as impervious surface and the data such as bands and indices from Sentinel-2A is taken as the predictor.

- The dataset is divided into three parts training, evaluation, and testing of data. The training dataset is used to construct the prediction model and the evaluation dataset is used to assess the performance of the model, fine-tuning, and selecting the best parameter for the model while training the model.

- FCNN UNet model is created using TensorFlow and training and evaluation data is fed to the model to fit the data. The model is trained using Adam optimizers and a combination of different bands and indices to get the best results and accuracy.

- After the model is trained with an acceptable root mean square error (RMSE), the Sentinel-2A image including bands and indices are provided to the model, for prediction as result. The result will contain the probability of impervious surface from 0 to 1.

Refer the schematic diagram of methodological flow chart given in Figure 2.5 for more detail flow of this study.

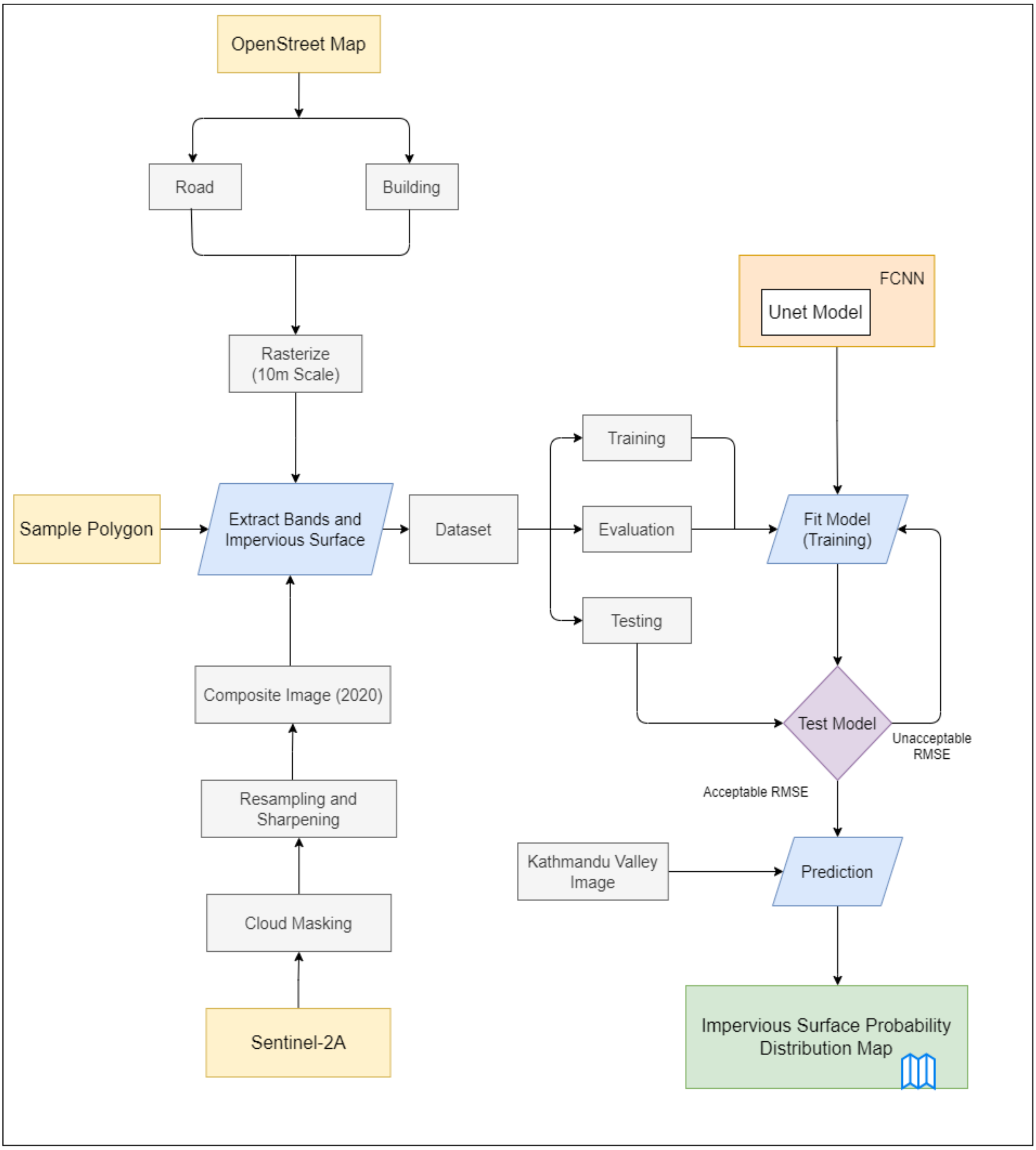

Figure 2.5: Methodological Flow Chart

Chapter-3: Process and Results

This chapter discusses the process and result of impervious surface mapping using Sentinel-2A and OSM. The process involves the data preparation part, developing the FCNN UNet model, training the model, and finally predicting the impervious surface of Kathmandu Valley.

3.1 Data Preprocessing

Data pre-processing may frequently have a substantial influence on machine learning generalization (Kotsiantis et al., 2006). The preprocessing of data is a method to prepare raw data for a machine-learning model. It is a very crucial step before the data is fed to the Machine Learning model since the data quality and valuable information obtained from it influence the learning capacity of the model. While data pre-processing is a useful tool that may allow the user to analyze and process complicated data but it can take a long time to preprocess the data (García et al., 2016).

So, the data preprocessing involves cleaning and formatting the data which is required a machine learning model to train. Here the data preprocessing involves rasterization of Open Street Map features, Image processing, cloud cover masking, resampling of bands, layering, and mosaicking, and finally exporting the data to the required format.

3.1.1 Open Street Map Rasterization

The Open Street Map contains the mapped data of different features such as roads, buildings, parks, industries, rivers, forests, and many more, but mostly the OSM is famous for its huge amount mapped roads network around the world. All the data are in vector format containing different polygons, lines, and points for each building, road, or place, and others.

The data that are used to rasterized are roads and buildings which is given in Table 3.1.

Table 3.1 : Features and Geometry Type of OSM Data

Features	Features Type	Feature Class	Geometry Type
Buildings	Building	building	Polygon
Roads	Primary	motorway	Line
		motor_link	Line
		primary	Line
		primary_link	Line
		trunk	Line
		trunk_link	Line
	Secondary	residential	Line
		secondary	Line
		secondary_link	Line
		tertiary	Line
		tertiary_link	Line
		track	Line
		track_grade1	Line

These feature classes of roads were selected according to the observation of roads and finding if the roads that were taken are paved or not. The buildings are fine with polygon, but roads have linear geometry type as line string which needs to convert into a polygon with a proper buffer around the line string. The buffer size of roads are listed in Table 3.2.

Table 3.2: Buffer Size of Roads

	Features Type	Buffer Size
Roads	Primary	5 meters
	Secondary	2 meters

The primary and secondary road buffer sizes are given according to OSM documentation and Nepal Road Standard 2070. According to Nepal Road Standard 2070, the paved road size varies from a minimum of 3.5 meters to 5.5 meters (MoDOR, 2013) as given in below Figure 3.1.

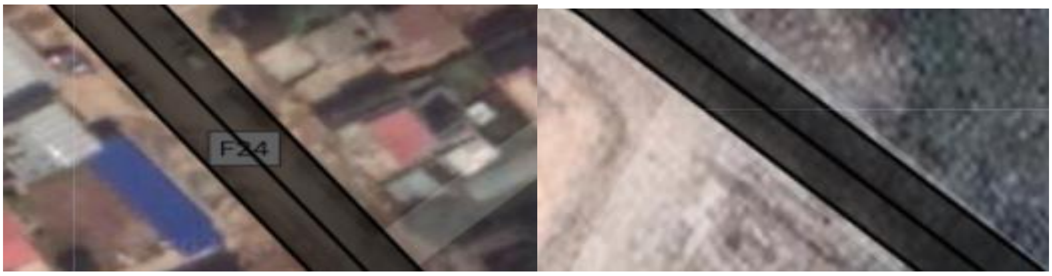

Figure 3.1: Buffer with the primary road of 5 meters and the secondary road of 2 meter

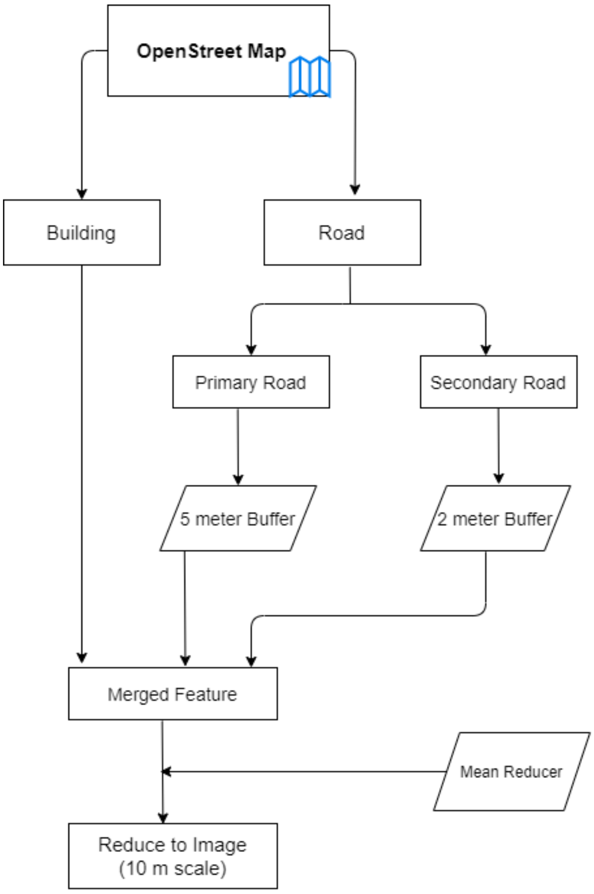

Figure 3.2: Rasterization process

After the data is extracted and roads are buffered then all the features are merged into one feature collection. Initially, the merged feature collection is converted to an image with a scale of 1 meter using the sum reducer. And then the converted image resolution is decreased to 10 meters using mean reducer and it contains the band name as ‘impervious’ which will have a value between 0 and 1. This image will act as the target value for impervious surfaces while training the model.

Impervious = [0,1]

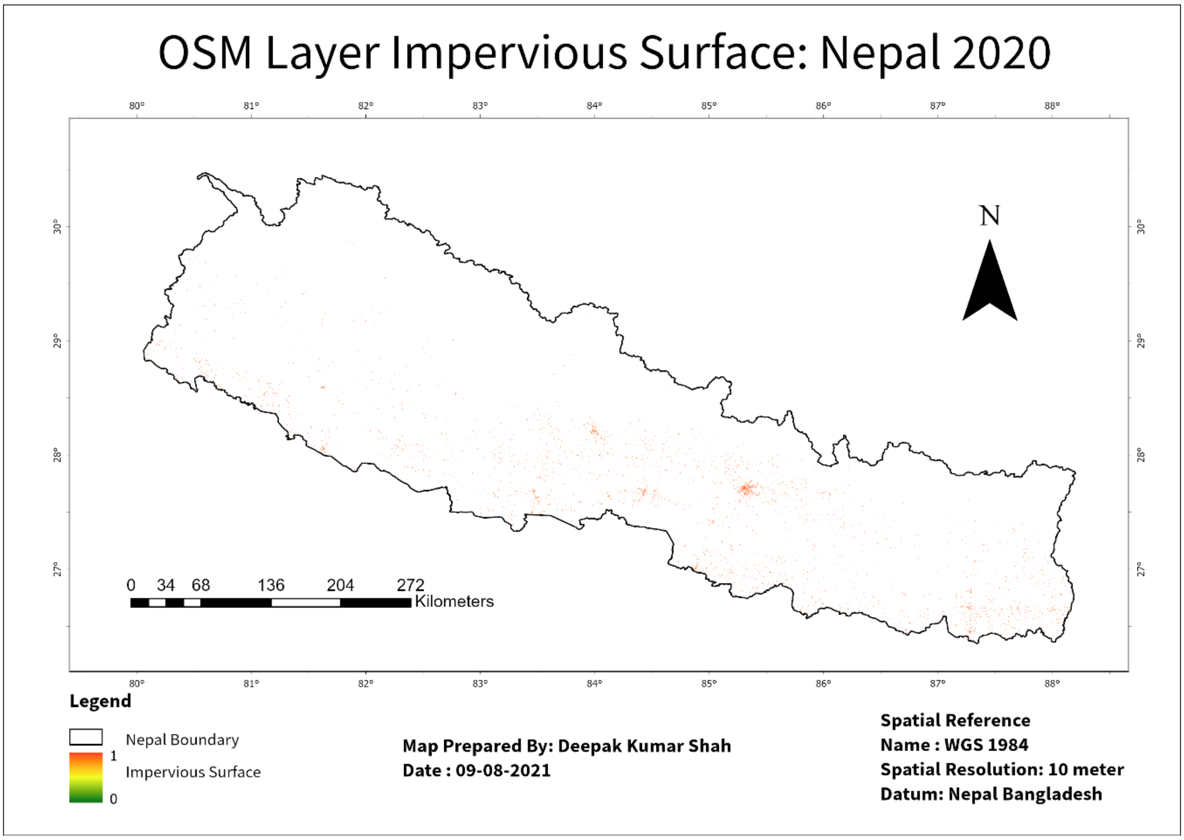

Map 3.1: OSM Layer Impervious Surface of Nepal 2020

From the rasterization process, which is given above in Figure 3.2, the Impervious Layer of whole Nepal is rasterized as given in Map 3.1. And according to our study area of Kathmandu Valley, the impervious layer is extracted from whole Nepal as given in Map 3.2 of OSM Layer.

Here, Kathmandu Valley is selected as study area because it is highly urbanized than any other cities or place in Nepal. Although, the trained model can be used to find the impervious layer of other cities.

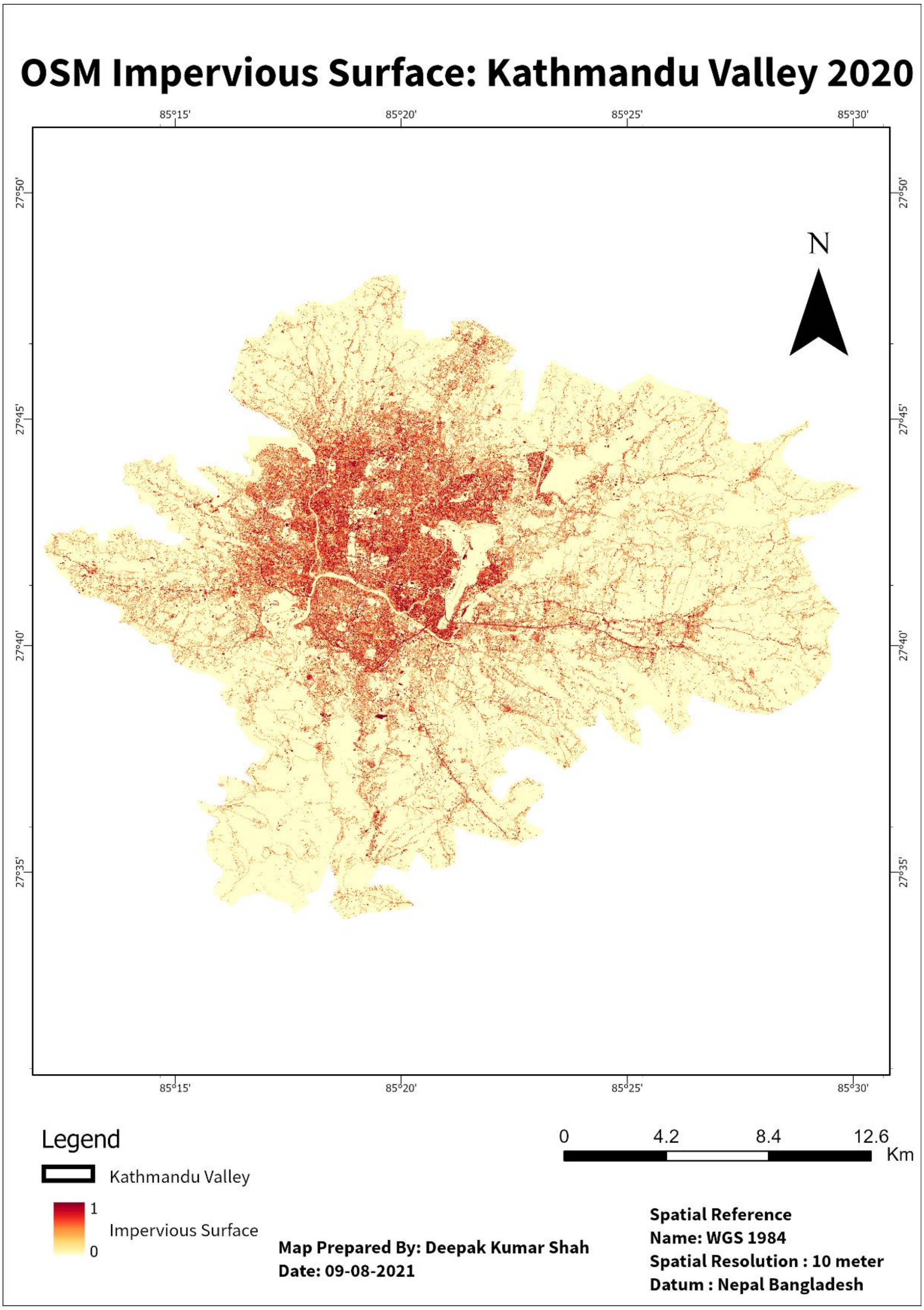

Map 3.2: OSM Layer of Impervious Surface of Kathmandu Valley

3.1.2 Image Processing

There is a growing number of image data obtained from satellites. For instance, NASA satellites send over 3 terabytes of data to the Earth daily (Aksoy, 2008; Durbha & King, 2004). These terabytes of images are in raw format which needs to be processed to extract the data and information from it in a usable format. The goal of pre-processing and processing of an image is to improve the image data by suppressing unwanted distortions or enhancing specific visual characteristics that are relevant for further processing (Sonka et al., 2015). Image processing is also considered to enhance the raster image for further analysis.

In this study, we are using Sentinel-2A provided by Copernicus mission for different Land monitoring applications. Sentinel Level-2A is orthorectified atmospherically corrected surface reflectance which means no need for further atmospheric correction of data. This study uses the Sentinel-2A data provided by the GEE catalog. It provides more than 13 bands of 10m, 20m, and 60m resolutions. In this study, we will be using 10 bands such as B2, B3, B4, B5, B6, B7, B8, B8A, B11, and B12 which are of 10m and 20m bands. These bands and their reflectance act as a predictor for impervious surfaces for training the model.

For impervious surfaces, we will be using Sentinel-2A image collection data from 01-01-2020 and 31-12-2020. Image processing sections includes the cloud masking, resampling, calculation of indices and finally taking the median of all filtered image and converting it to composite image. The advantage of Composite image is the existence of contamination, as well as the highly varying quantity of missing data in different portions of the time series, might provide significant challenges in analyzing long-term behavior (Flood, 2013).

3.1.2.1 Cloud Masking

Cloud masking is the process of detecting and removing cloud and shadow by comparing the reflectance values of clean pixels with the pixels that are contaminated by clouds

(Candra et al., 2016). Clouds and cloud shadow considerably impair the capacity of our satellite sensors to automatically identify, map, and monitor earth surface information. And due to this, it hinders in analysis and classification of land cover (Candra et al., 2016, 2020).

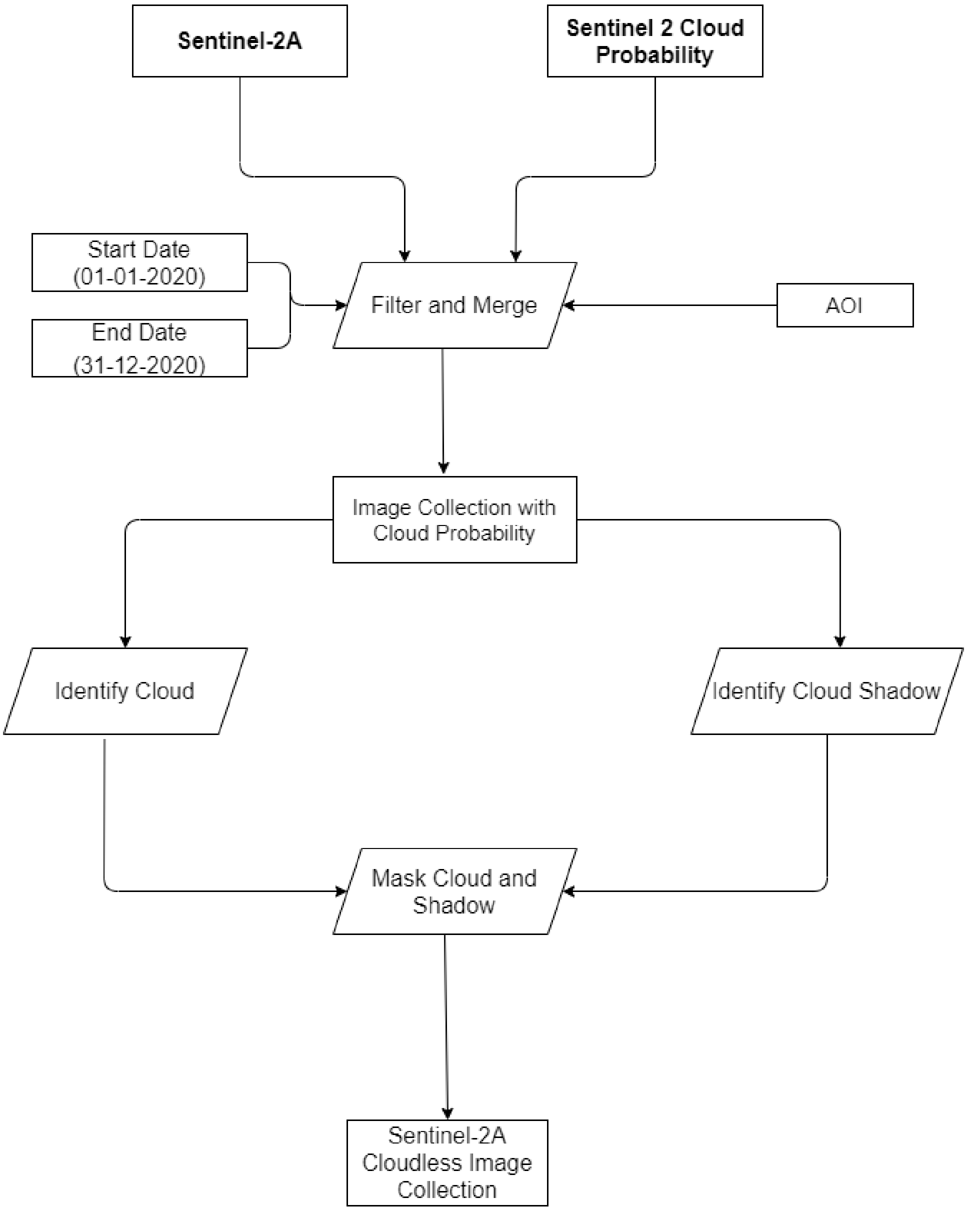

Figure 3.3: Cloud Masking Process

In Figure 3.3 cloud masking process is explained which is used in this study to prepare Sentinel-2A data. The Cloud Masking process of Sentinel-2A is done using Cloud Probability of Sentinel 2 Image Collection Provided in GEE Catalog.

Sentinel-2A image collection comes with a property called *CLOUDY_PIXEL_PERCENTAGE* which gives the percentage of cloud cover in a single image. So Initially the Sentinel-2A image collection is filtered according to start date, end date, and area of interest (AOI). After filtering the image collection, it is again filtered with a cloud pixel percentage less than 60% (Miceli & Braaten, 2021). The different threshold of the cloud property are given in Table 3.3 which are used in Cloud Masking Process explained in Figure 3.3.

Table 3.3: Cloud Masking property and threshold

Property	Threshold
CLOUD_FILTER	60
CLD_PRB_THRESH	50
NIR_DRK_THRESH	0.15

In a similar manner Sentinel, 2 Cloud Probability image collection is also filtered with start date, end date, and AOI. After that, the filtered Sentinel-2A image collection and Sentinel 2 Cloud Probability are merged according to the system index provided in each image.

The cloud is identified per image and per pixel using the cloud probability threshold which is greater than 50%. And then it is added as the band which contains the value either 0 or 1. Similarly, the cloud shadow is identified using the mean solar azimuth angle of the cloud and dark pixels which are not water are considered as cloud shadows.

Not water = (SCL != 6)
Dark Pixels = (B8 < (NIR_DARK * 1e4)*(Not water))
Shadow Azimuth = (90 - MEAN_SOLAR_AZIMUTH_ANGLE)
Cloud Shadow = (dark Pixels && Shadow Azimuth)

After identifying the cloud and cloud shadow both are merged in a single band called cloud which has a value of either 0 or 1, where 0 indicates the pixel doesn’t have cloud and 1 indicates that pixel has either cloud or shadow. The using cloud band the Sentinel-2A images are masked where the value is 1 and after masking, we get the Sentinel-2A cloudless image collection. An example of how the cloud and shadow masking is done is given in below Figure 3.4

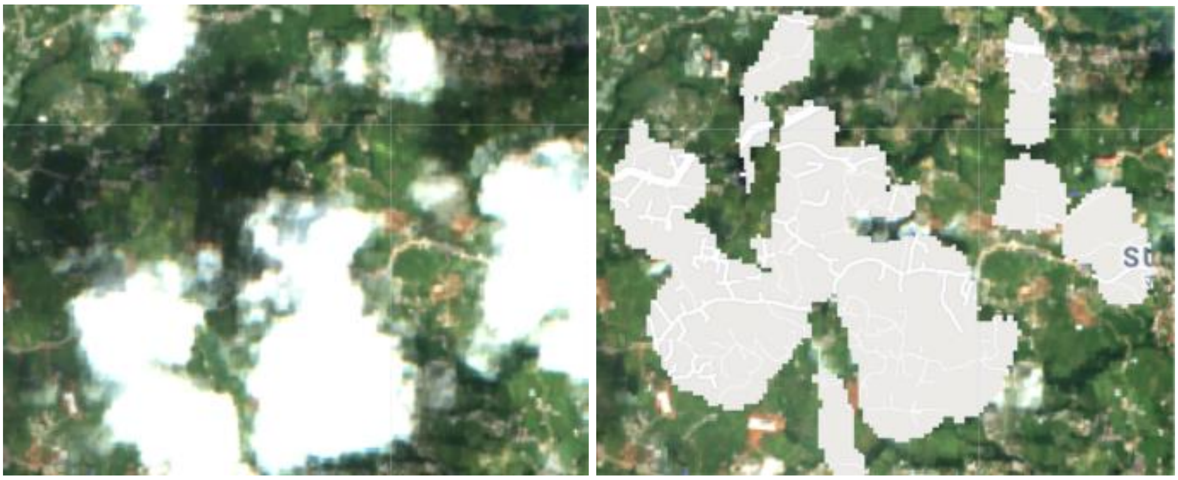

Figure 3.4: Zoomed Image with cloud and shadow on the left and masked image on the right

3.1.2.2 Layering and Composite

After removing the cloud and cloud shadow, the image collection, which is already filtered according to the start date, end date, and AOI are converted to a composite image by taking the median of all the images. Layering is the process of stacking an image on top of another and composite is making up a single element by combining different elements, in this case by combining all the images and their bands. As a measure of central tendency, the median is superior to the mean as outliers and skewed data have less impact on the median (Rousselet & Wilcox, 2020). A schematic diagram of layering and composite is highlighted in Figure in 3.5. Figure 3.6 is an example of Sentinel-2A True color composite. Similarly, Map 3.3 is the extracted True Color composite Map of Kathmandu Valley.

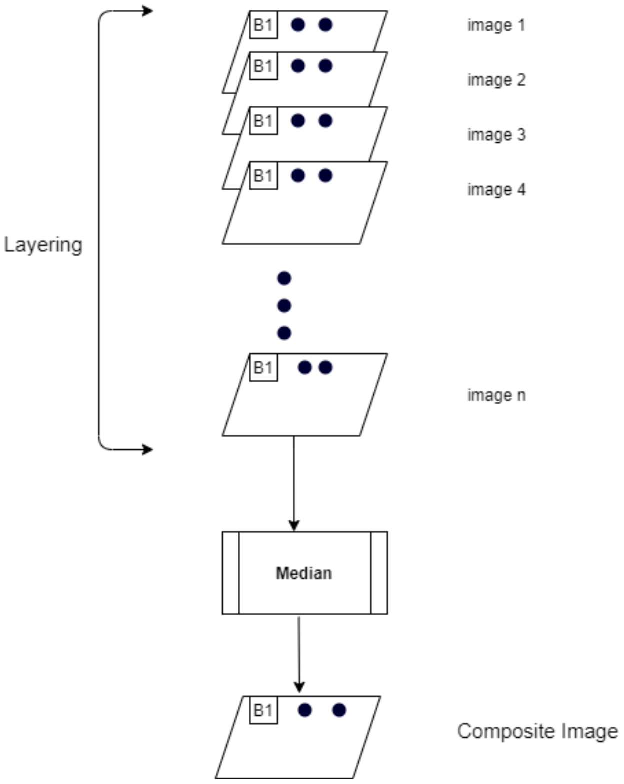

Figure 3.5: Layering and Composite of Image Collection

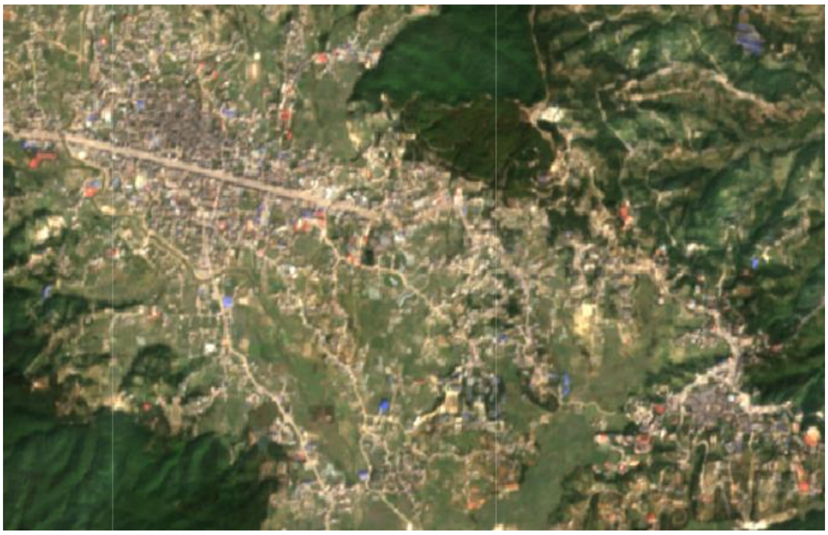

Figure 3.6: Sentinel-2A True Color (B4, B3 and B2 Bands) Cloudless Composite Image

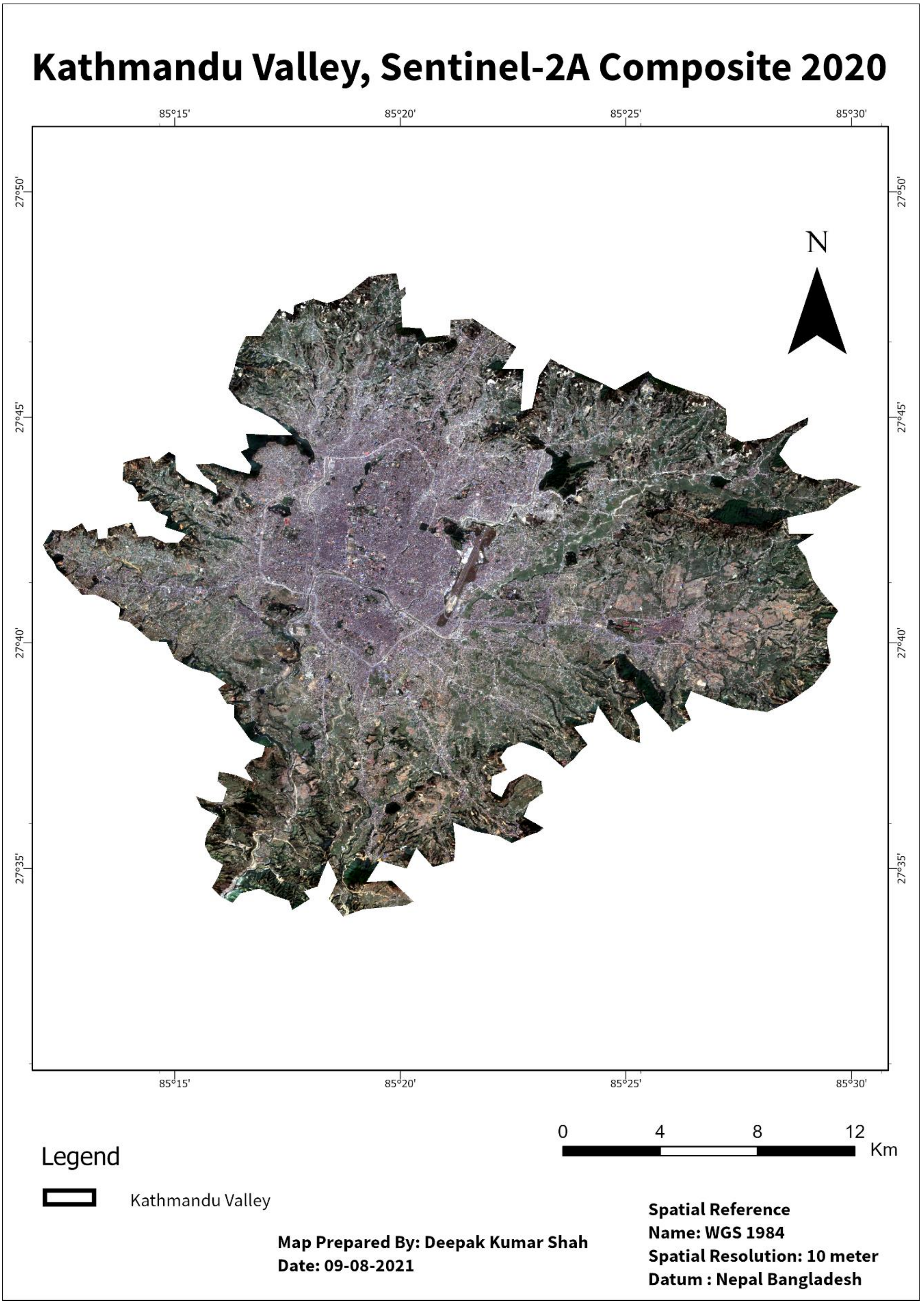

Map 3.3: Sentinel-2A True Color Composite Imagery of Kathmandu Valley, 2020

3.1.2.3 Resampling and Sharpening

According to Baboo & Devi (2010), resampling is a part of satellite imagery preprocessing which repairs the original deformed image, and this technique is used to determine the value of the new pixel of the corrected or new image from the original image. So, it involves finding the DN value of the output image matrix. Resampling is mostly used when, either we want to up-sample an image or down-sample an image. An image can be resampled to a finer matrix to improve its look for image display and eliminate artifacts caused by the border between image parts (Parker et al., 1983). Many aspects must be addressed when pan-sharpening a collection of pictures, and the resampling method is one of them since it works to rebuild an image's edges (Jawak & Luis, 2013).

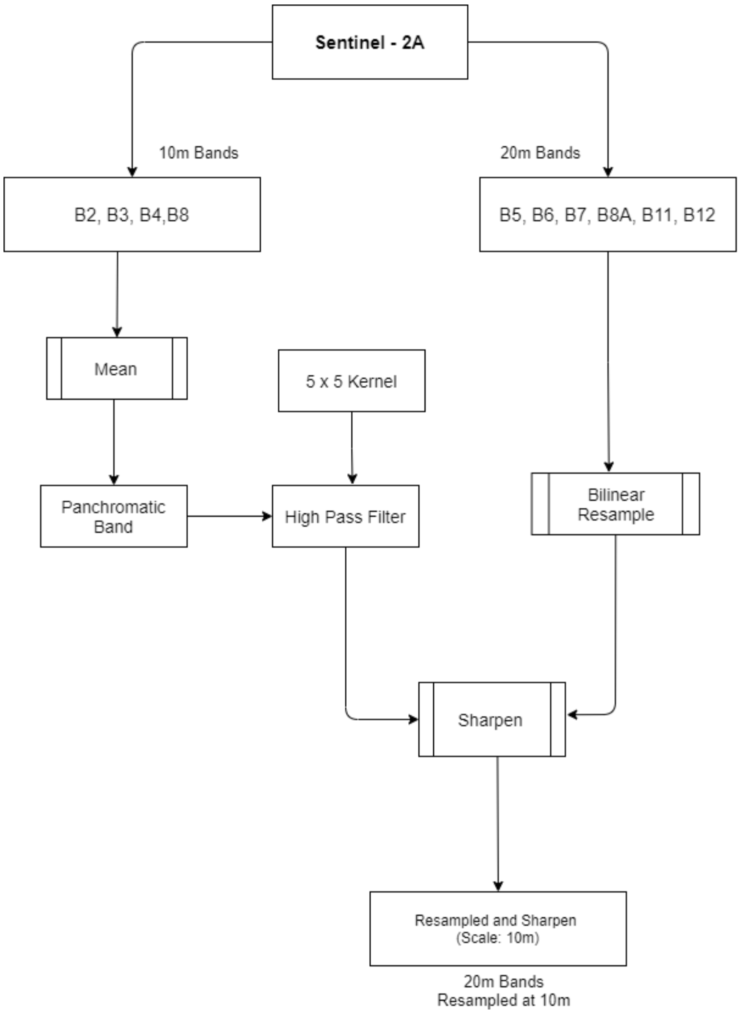

Figure 3.7: Resampling of 20m Bands to 10m Bands Process

Refer to Figure 3.7 for detail resampling process. In this study, we are using the resampling method for 20m bands to increase the spatial resolution up to 10m bands so that there will be consistent for all 10m bands. Initially, the 10-meter bands which are B2, B3, B4, and B8, and similarly 20-meter bands such as B5, B6, B7, B8, B8A, B11, and B12 are separated where the average of 10m bands act as the panchromatic band (Kaplan, 2018) and the 20m meter band are resampled using Bilinear Interpolation Resampling method. Due to its simplicity in image-driven applications, bilinear interpolation is the most preferred technique. The bilinear interpolation method uses a weighted average of its four surrounding pixels to interpolate high-resolution pixels (Kim et al., 2009).

Figure 3.8: Average of 10m Bands as Panchromatic Band

Then 5X5 kernel is created to make High Pass Filter (HPF) given in Figure 3.9 from Panchromatic bands which is given in Figure 3.8. The High Pass Filter is those filters that are not affected by high frequencies while reducing the low frequency and are used for sharpening the image (Dogra & Bhalla, 2014). In terms of spectrum accuracy of real color composite representation, the PCA technique produces poor results than HPF (Luciano et al., 2004). Finally, the high pass filter is used with resampled bands to increase the spatial resolution of 20-meter bands to 10-meter bands.

Figure 3.9: High Pass Filter

Given below in Figure 3.10 and Figure 3.11 are the RGB combination of different 20 m bands which are resampled and sharpen at 10m bands.

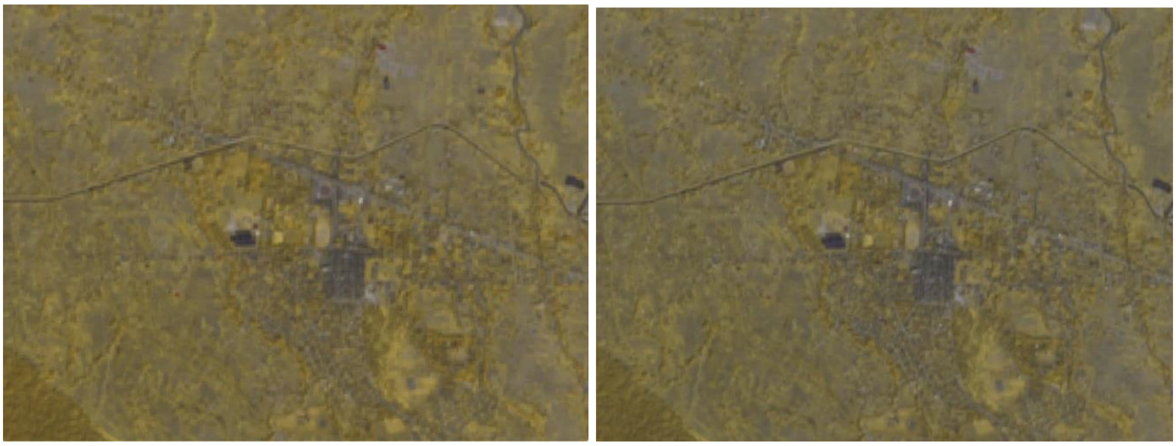

Figure 3.10: B7, B6, B5 Bands Combination with Original on left and Resampled on Right

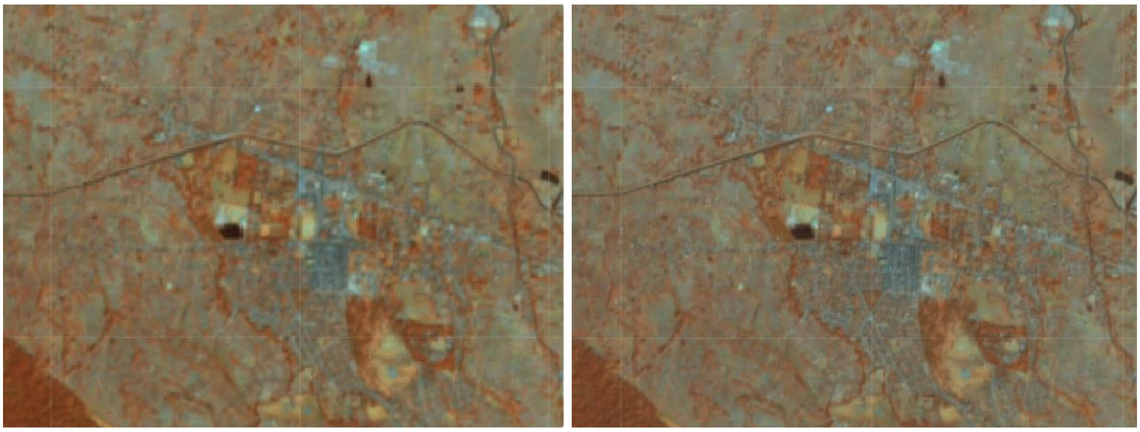

Figure 3.11: B8A, B11, B12 Bands Combination with Original on left and Resampled on Right

3.1.2.4 Sentinel-2 Indices

Over the year the scientific community has created various spectral indices to tackle complicated environmental challenges. So Normalized Indices are the combination of different bands to produce meaningful results towards target data in this case is impervious surface. Similarly, Indices can be also regarded as data engineering for machine learning work. Data engineering refers to a collection of processes necessary to identify which data are important and to establish how the data should be accessible, safe, and updated in a way that fulfills scientific, technical, institutional, and regulatory criteria that sometimes are quite complicated (Cui et al., 2019). It is also observed that the longer composite time period have less effect on NDVI (Chen et al., 2003)

These combinations of bands and data engineering processes are referred to as Feature Engineering. New features from the included feature set are extremely frequent practice. Such designed functionality will either increase the current vector or it will replace sections. These functions are mostly computed fields depending on the values of the other functionalities. Now all the bands have the same spatial resolution as 10m. Some of the popular indices that are prepared from the combination of these different bands which will be useful for impervious surface probability mapping are as follows:

3.1.2.4.1 Normalized Difference Vegetation Index (NDVI)

NDVI is the normalized difference ratio between NIR which is near Infrared radiation and the visible Red light band of Sentinel-2A. NDVI is a measure of a green area and an explicit spatial measure of vegetation production (Goward & Prince, 1995). Vegetation health and density are measured by the standardized vegetation difference index (NDVI) utilizing satellite-screen images of plant reflection (Kinyanjui, 2011)

$$NDVI = \frac{\mathrm{B8} + \mathrm{B4}}{\mathrm{B8} - \mathrm{B4}} \tag{1}$$

Sentinel-2 NDVI is calculated by the ratio of NIR and RED different and NIR and RED difference. The value of NDVI range from -1 to 1 where the higher value of NDVI represents healthy vegetation (Kinyanjui, 2011) and a visualized example is given in Figure 3.12.

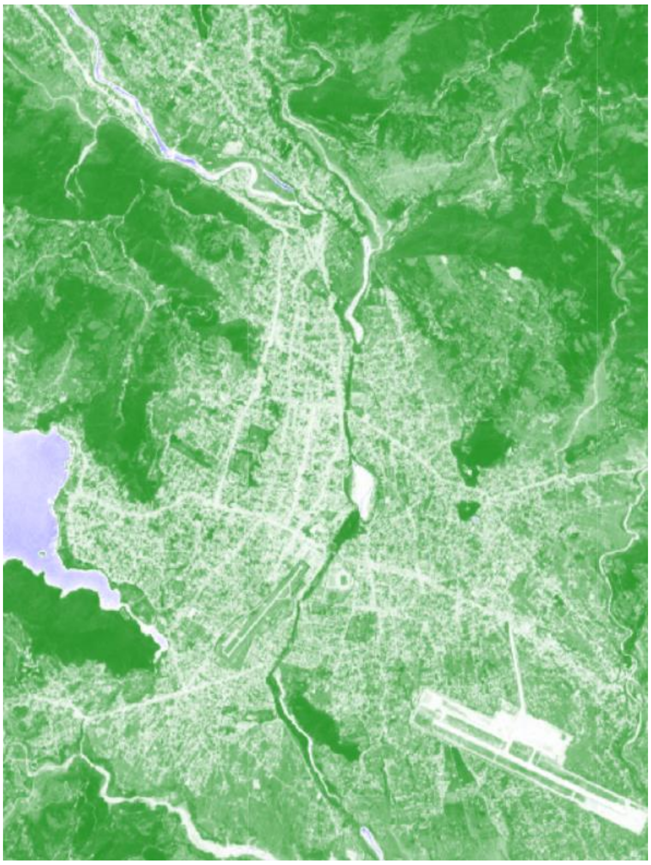

Figure 3.12: Visualization of NDVI

3.1.2.4.2 Normalized Difference Water Index (NDWI)

The NDWI is a novel approach created for delineating open water characteristics and improved their appearance in the digital image of a distant sensor. This method has been developed, to improve the presence of these characteristics and to eliminate the presence of land and terrestrial plants with the help of near-infrared radiation and visible green light (McFEETERS, 1996; H. Xu, 2006).

$$NDWI = \frac{B8 + B3}{B8 - B3} \tag{2}$$

Sentinel-2 NDWI is calculated by the ratio of addition of NIR and GREEN to the difference of NIR and RED. The value of NDWI range from -1 to 1 and a visualized example is given in Figure 3.13.

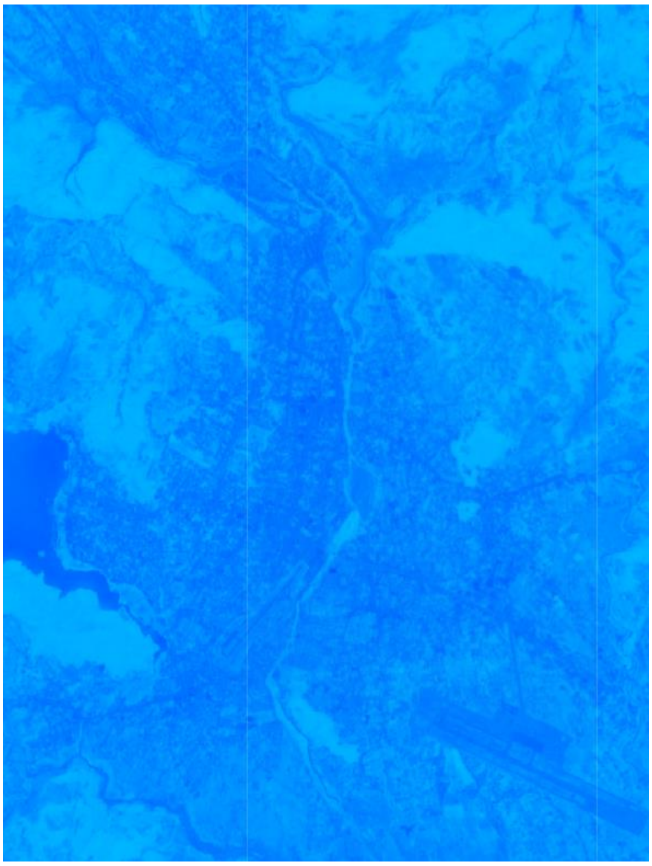

Figure 3.13: Visualization of NDWI

3.1.2.4.3 Normalized Difference Built-up Index (NDBI)

NDBI is an index to map and monitor urban areas. It distinguishes urban areas from dark rural background areas (Li & Chen, 2018). It is calculated by the normalized difference between SWIR which is short wave infrared radiation and NIR which is near-infrared radiation band (Xu et al., 2018).

Since Sentinel-2 have two SWIR band as SWIR1 which is B11 and SWIR2 which is B12. So the average of SWIR1 and SWIR2 is taken to get SWIR12.

$$SWIR_{12} = \frac{B11 + B12}{2} \tag{3}$$

$$NDBI = \frac{SWIR_{12} - B8}{SWIR_{12} + B8} \tag{4}$$

A visualized example of NDBI is given in Figure 3.14.

Figure 3.14: Visualization of NDBI

3.1.2.4.4 Soil Adjusted Vegetation Index (SAVI)

The SAVI is an essential step in developing simple "global" models, which explain dynamic soil vegetation systems using remotely sensed data. SAVI tries to reduce the brightness of the soil by applying a correction factor for soil brightness. The band that is involved in the calculation of SAVI are visible band RED and Near-infrared radiation NIR and a constant factor L which is taken under circumstance and presence of vegetation (Huete, 1988).

$$SAVI = \frac{B8 - B4}{B8 + B4 + L} * (1 + L) \tag{5}$$

The value SAVI range from -1 to 1 and a visualized example is given in Figure 3.15.

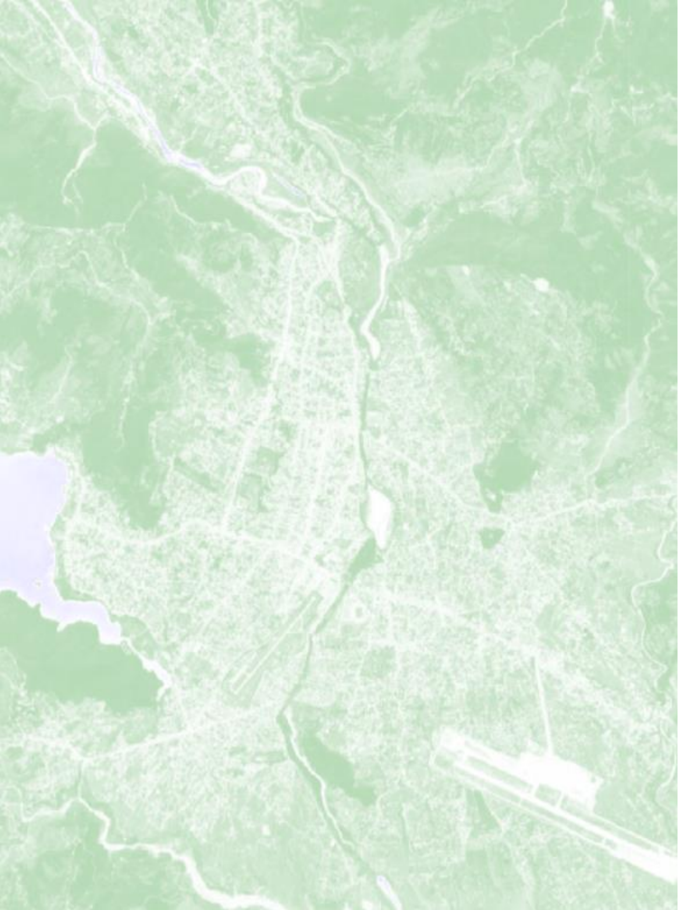

Figure 3.15: Visualization of SAVI

3.1.2.4.5 Modified Normalized Difference Water Index (MNDWI)

H. Xu (2006) observed that in the SWIR band the water body is more absorbed than that of the NIR band, and in the SWIR band, the built-up class is more radiated. The MNDWI was proposed based on this discovery as follows:

So MNDWI is the normalized difference between visible light GREEN and Short-wave infrared radiation. Since in Sentinel-2A have two SWIR band B11 and B12 so the average is taken to calculate MNDWI.

$$MNDWI = \frac{B3 - SWIR_{12}}{B3 + SWIR_{12}} \qquad (6)$$

A visualized example of MNDWI is given in Figure 3.16.

Figure 3.16: Visualization of MNDWI

3.1.2.4.6 Index-Based Built-up Index (IBI)

Xu (2008) presented the IBI method for rapid extraction of built-up land characteristics from satellite imagery. The author used SAVI, MNDWI, and NDBI to calculate IBI as follows:

$$IBI = \frac{NDBI - (SAVI + MNDWI)/2}{NDBI + (SAVI + MNDWI)/2} \tag{7}$$

The NDBI is calculated in equation 4, SAVI is calculated in 5, and MNDWI is calculated in 6. A visualized example of IBI is given in Figure 3.17.

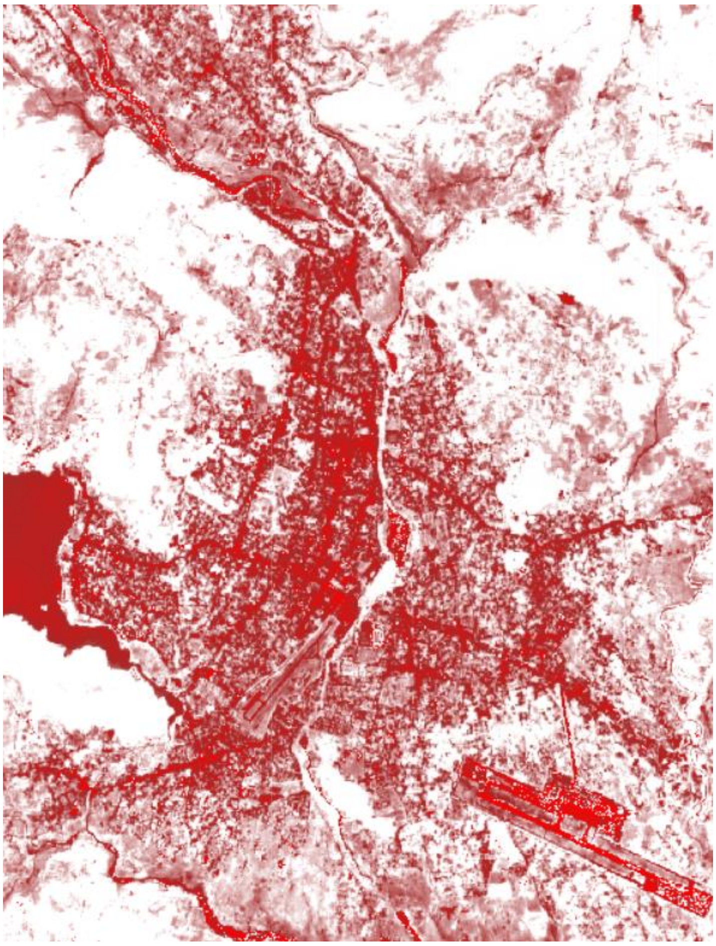

Figure 3.17: Visualization of IBI

3.2 Dataset Preparation

Data extraction is the process of extracting predictor data and target that is the impervious surface in this case to train the Machine Learning model which is explained in Figure 3.18. The data that is required for the data extraction process is Sentinel-2A image which is explained in 3.1.2, Rasterized OSM which is explained in 3.1.1, and Sample Polygon. Sample Polygon is the feature collection of collected polygons where there is high impervious surface area which is mapped using buildings and roads from OSM.

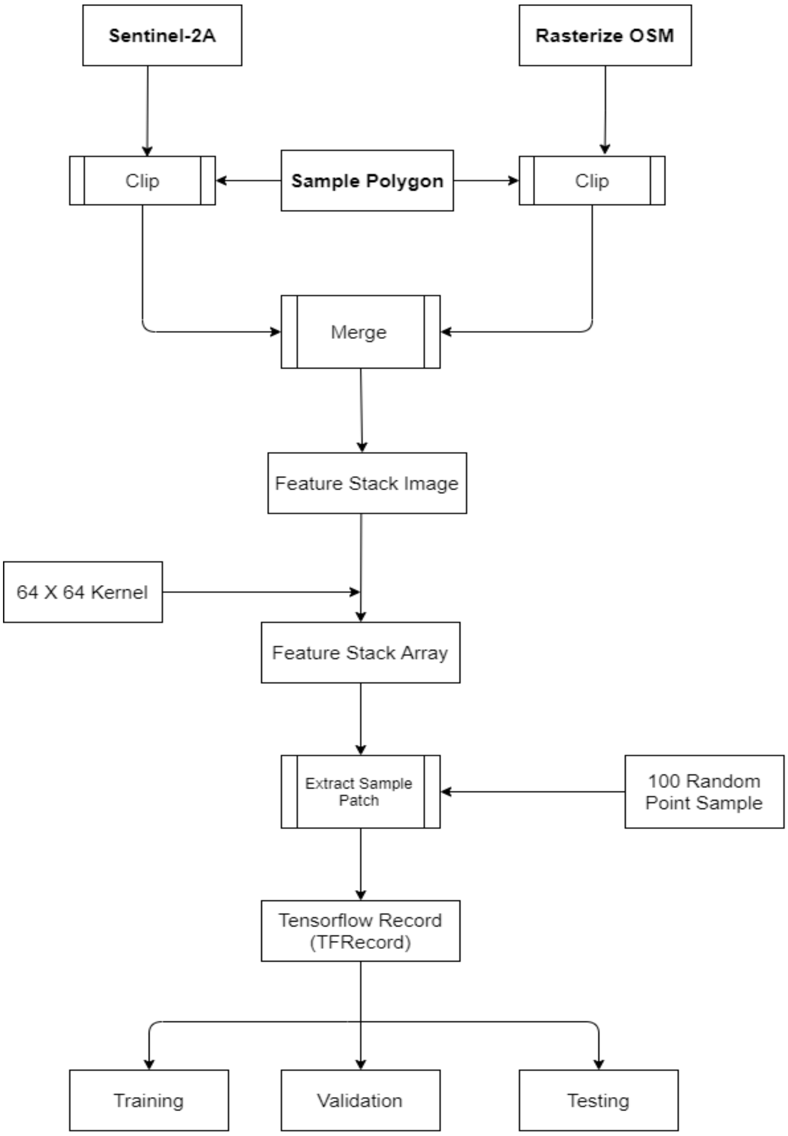

Figure 3.18: Data Extraction Process

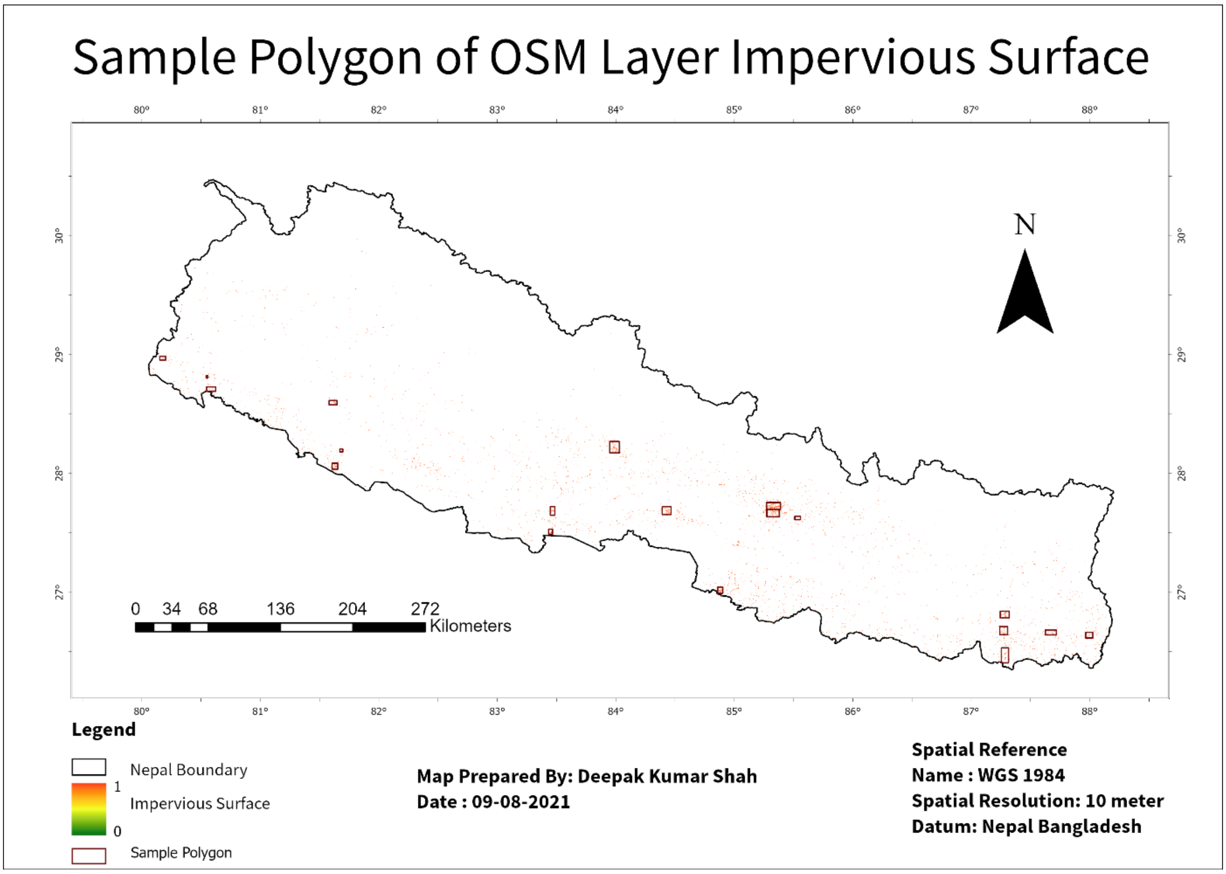

Map 3.4: Collected Sample Polygon of OSM Layer

These 19 samples polygons given in Map 3.4 are selected according to the place which are highly are urbanized in Nepal and have more feature such as roads and buildings are mapped in OSM. Since, this study focus from the data of Nepal but as the impervious surface are quite similar in other countries, the sample polygon can be also taken from other places which highly urbanized and more mapped features in OSM.

Sentinel-2A image and OSM Rasterized data are clipped according to Sample Polygon and then merged to produce feature stacked image.

The features that are collected from Sentinel-2A and Rasterized OSM are as follows:

Bands = [“B2”, “B3”, “B4”, “B5”, “B6”, “B7”, “B8”, “B8A”, “B11”, “B12”]

Indices = [“NDVI”, “NDWI”, ”NDBI”, “SAVI”, “MNDWI”, “IBI”]

Sentinel-2A = Bands + Indices

= [“B2”, “B3”, “B4”, “B5”, “B6”, “B7”, “B8”, “B8A”, “B11”, “B12”, “NDVI”, “NDWI”, ”NDBI”, “SAVI”, “MNDWI”, “IBI”]

OSM = [“impervious”]

Feature Stacked Image = Sentinel-2A + OSM

= [“B2”, “B3”, “B4”, “B5”, “B6”, “B7”, “B8”, “B8A”, “B11”, “B12”, “NDVI”, “NDWI”, ”NDBI”, “SAVI”, “MNDWI”, “IBI”, ”impervious”]

Kernel Size = [64 X 64]

1	2	...	…	64
2				
…				
…				
64				

Now, the Feature Stacked image is converted into Feature Stack Array using 64 X 64 Kernel. 100 random sample point is taken and according to that sample point, 100 sample Patch is extracted from Feature Stack Array. Each Sample Patch will have a size of 64X64 with a height of 16 as the total number of features is 16. Then these sample patches are merged and converted to Tensorflow Record File with a tfrecord. Custom TFRecord data format from TensorFlow is quite handy. The blazing-fast tf.data API, distributed data sets, and parallel I/O use native support of the files. These files are ingested as data to the deep learning model for training, testing, and validation. After that, each tfrecord file is randomly transferred to either training, validation, or testing folder.

Patch Size = [64 X 64]

Training Dataset = 80%

Testing Dataset= 20%

Validation Dataset= 10%

Training data are those data that are used for fitting the model. Similarly, validation data are datasets used to give an impartial evaluation of model fit on the training dataset while tweaking the hyperparameters. Finally, after fitting the model with the training and validation dataset, the testing dataset is used to evaluate the fit model.

3.3 Model Development

The Model Development section deals with deep learning model development and different parameter selection for further training, testing, and prediction purpose.

3.3.1 Optimizers

Optimizers are techniques or strategies used to modify characteristics like weights and learning rates of your neural network to reduce losses. Optimizers are responsible for minimizing the error and maximizing the efficiency of the model. In this study, we are using Adam Optimizer. Adam Stands for Adaptive momentum estimation introduced by Kingma & Ba (2017). For the gradient optimization of stochastic objective functions, Adam is a simple and computer-efficient technique. Adam has the advantage in solving large databases with a higher dimension. Adam combines the benefits of two algorithms AdaGrad and RMSProp (Kingma & Ba, 2017). The default parameters of Adam used from Tensorflow API in this study, and are as follows:

learning_rate = 0.001, beta1 = 0.9, beta2 = 0.999 and epsilon = 1e-08

3.3.2 Loss Function

The loss function calculates the gap between the actual data and the predicted output. It is the technique to find the efficiency of the model. The cost or loss function reduces to a unique scalar value, a value that allows candidates' solutions to be classified and compared, the numerous excellent and poor characteristics of a possible complicated system (Reed & MarksII, 1999).

Since this study deals with regression problems we will be using “Mean Squared Error (MSE)” as a loss function. Mean Squared Error function is the squared difference between predicted output y_pred and actual output y_actual divided by the total number of outputs.

$$L(y, y') = \frac{1}{N}\sum_{i=0}^{N}(y - y_i')^2 \tag{8}$$

Loss Function = Mean Squared Error

3.3.3 Metrics

Metrics are the function that is important for finding the performance of the Regression Model. The metrics show how your model is converging towards minima. In this study, the “RMSE” Root Mean Squared Error function is used as a Metric. RMSE is an extension of MSE. RMSE is a quadratic rule for measuring the average size of the error. It's the square root of average squares of prediction and real observation difference.

Metric = RMSE

$$RMSE = \sqrt{\frac{1}{N}\sum_{i=0}^{N}\left(y - y_i'\right)^2} \tag{9}$$

3.3.4 Activation Function

In Neural Network, Activation Functions are used to calculate the weighted number of inputs and biases, which decides whether a neuron may be activated or not. The data given is manipulated by gradient processing which generally leads to a gradient descent to generate a NN output including the parameters of the data (Nwankpa et al., 2020). It is used to assess whether a neural network's output is yes or no. It converts the resultant values from 0 to 1 or -1 to 1, and so on (Sharma, 2021).

3.3.4.1 Sigmoid

The activation function in the artificial neural network is useful for transforming an input into a specific output when determining the outcome in the form of a prediction model. The activation function utilized in this investigation is sigmoid (Pratiwi et al., 2020). Sigmoid is mostly used in Deep Neural networks and is non-linear. Sigmoid is easy to use than other activation functions (Nwankpa et al., 2020).

$$f(\mathrm{x}) = \frac{1}{(1 + e^{-x})} \tag{10}$$

3.3.4.2 ReLU

ReLU stands for Rectified Linear Units and was first proposed by Nair & Hinton (2010). ReLus is one of the widely used Deep Learning Activations Function. The ReLU AF conducts a threshold operation with values less than zero are set to zero for each input item (Nwankpa et al., 2020). ReLu is given by:

$$f(x) = \max(0, x) = \begin{pmatrix} x_{i,} & if\ x_i \geq 0 \\ 0, & if\ x_i < 0 \end{pmatrix} \tag{11}$$

3.3.5 FCNN UNet Model

As, Impervious Surface consists of very complex material which requires the investigation done at pixel level from Sentinel-2A imagery utilizing fully convolution neural network (FCNN) specially UNet model (McGlinchy et al., 2019). UNet is a Computer Vision Semantic Segmentation algorithm and was first introduced by Ronneberger et al. (2015) for

Biomedical Image Segmentation. Here in this study the same configuration of UNet is implemented to find the impervious layer as given Figure 3.19.

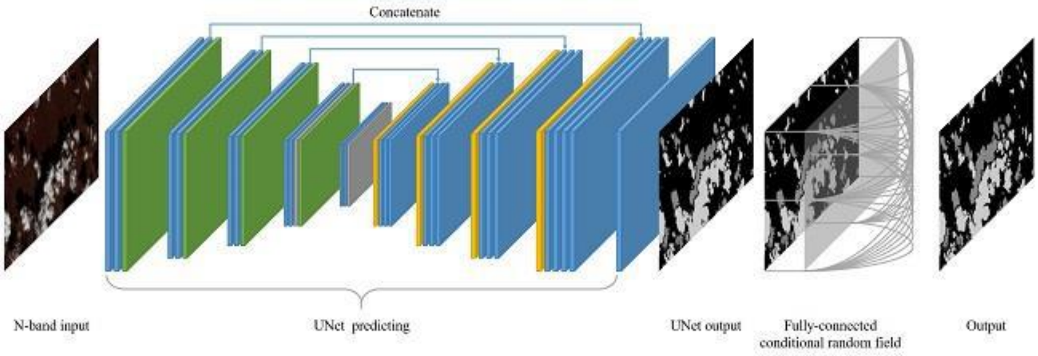

Figure 3.19: Representation UNet Model (Adapted From, Jiao et al., 2020)

There are two ways to architecture. The first path is the path (also known as the encoder) to record the image context. The encoder is only a standard set of convolutionary and max-pooling layers. The second approach is the symmetric expansion path (also known as the decoder) that allows for accurate localization using transposed convolutions. And thus, it is also called FCNN because of its end-to-end convolution layer (Lamba, 2019).

The UNet architecture is explained in figure 31 below. It consists of two parts as explained above one is called encoder and another decoder. The encoder consists of a convolution network with 3X3 unpadded convolution which is followed by the ReLU activation function and 2x2 max-pooling layer. In each step of the encoder, the number of channels is doubled. Similarly, the decoder consists of 2X2 up-sampling convolution which cuts the number of channels into half and is concatenated with cropped feature map from an encoder. The decoder also has a 3x3 convolution with a ReLU activation function. At last, the 1x1 convolution layer is followed by tanh activation function to produce a probability layer of impervious surface.

The schematic diagram of UNet architecture for this study is given below in Figure 3.20 and snapshot of implementation of UNet mode in Python using Tensorflow library is given in Figure 3.21.

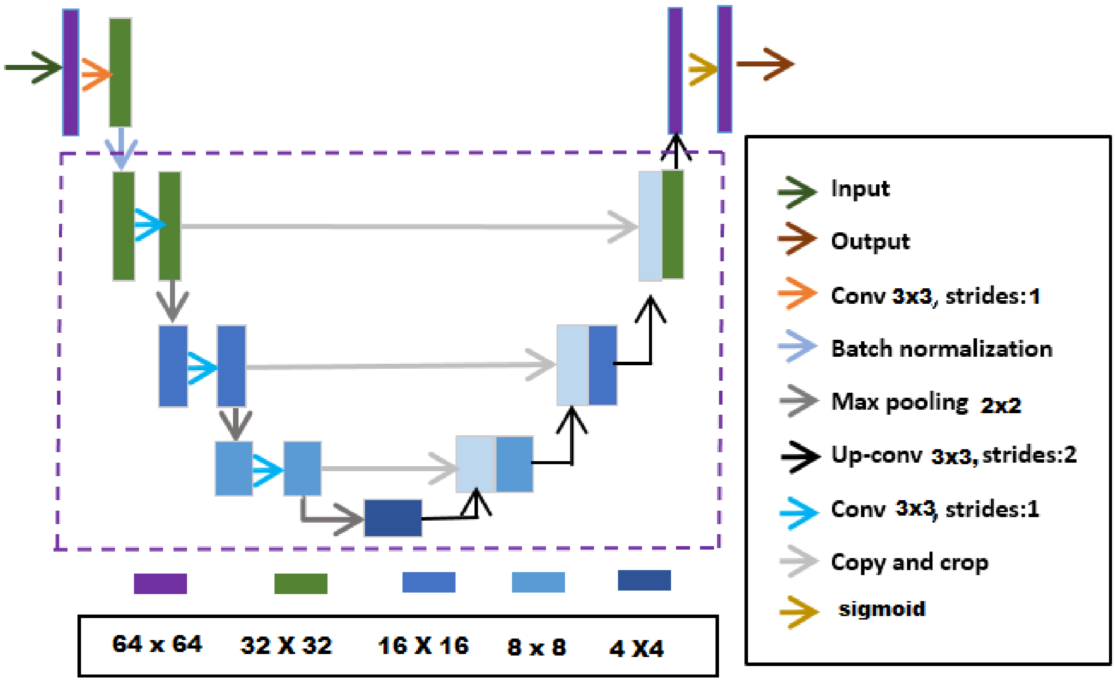

Figure 3.20: Architecture of UNet Model (Adapted From, Ding et al., **2019)**

The implementation of UNet is given below using TensorFlow API.

```
from tensorflow.python.keras import layers
from tensorflow.python.keras import losses
from tensorflow.python.keras import models
from tensorflow.python.keras import metrics
from tensorflow.python.keras import optimizers

def conv_block(input_tensor, num_filters):
        encoder = layers.Conv2D(num_filters, (3, 3), padding='same')(input_tensor)
        encoder = layers.BatchNormalization()(encoder)
        encoder = layers.Activation('relu')(encoder)
        encoder = layers.Conv2D(num_filters, (3, 3), padding='same')(encoder)
        encoder = layers.BatchNormalization()(encoder)
        encoder = layers.Activation('relu')(encoder)
        return encoder

def encoder_block(input_tensor, num_filters):
        encoder = conv_block(input_tensor, num_filters)
        encoder_pool = layers.MaxPooling2D((2, 2), strides=(2, 2))(encoder)
        return encoder_pool, encoder

def decoder_block(input_tensor, concat_tensor, num_filters):
        decoder = layers.Conv2DTranspose(num_filters, (2, 2), strides=(2, 2), padding='same')(input_tensor)
        decoder = layers.concatenate([concat_tensor, decoder], axis=-1)
        decoder = layers.BatchNormalization()(decoder)
        decoder = layers.Activation('relu')(decoder)
        decoder = layers.Conv2D(num_filters, (3, 3), padding='same')(decoder)
        decoder = layers.BatchNormalization()(decoder)
        decoder = layers.Activation('relu')(decoder)
        decoder = layers.Conv2D(num_filters, (3, 3), padding='same')(decoder)
        decoder = layers.BatchNormalization()(decoder)
        decoder = layers.Activation('relu')(decoder)
        return decoder

def get_model():
        inputs = layers.Input(shape=[None, None, len(BANDS)]) # 64
        encoder0_pool, encoder0 = encoder_block(inputs, 8) # 32
        encoder1_pool, encoder1 = encoder_block(encoder0_pool, 16) # 16
        encoder2_pool, encoder2 = encoder_block(encoder1_pool, 32) # 8
        encoder3_pool, encoder3 = encoder_block(encoder2_pool, 64) # 4
        encoder4_pool, encoder4 = encoder_block(encoder3_pool, 128) # 2
        center = conv_block(encoder4_pool, 256) # center
        decoder4 = decoder_block(center, encoder4, 128) # 4
        decoder3 = decoder_block(decoder4, encoder3, 64) # 8
        decoder2 = decoder_block(decoder3, encoder2, 32) # 16
        decoder1 = decoder_block(decoder2, encoder1, 16) # 32
        decoder0 = decoder_block(decoder1, encoder0, 8) # 64
        outputs = layers.Conv2D(1, (1, 1), activation='sigmoid')(decoder0)

        model = models.Model(inputs=[inputs], outputs=[outputs])

        model.compile(
                optimizer=optimizers.get(OPTIMIZER),
                loss=losses.get(LOSS),
                metrics=[metrics.get(metric) for metric in METRICS])

        return model
```

Figure 3.21: Implementation of UNet using TensorFlow API

3.4 Feature Exploration

Before fitting the data or feeding the machine learning model, it is very important to understand how features are behaving towards target value. Simple linear regression analysis is used to determine the linear connection between a predictor and an outcome variable (Zou et al., 2003). Given below in Figure 3.22 is a simple linear regression plot between Features and target value which is impervious.

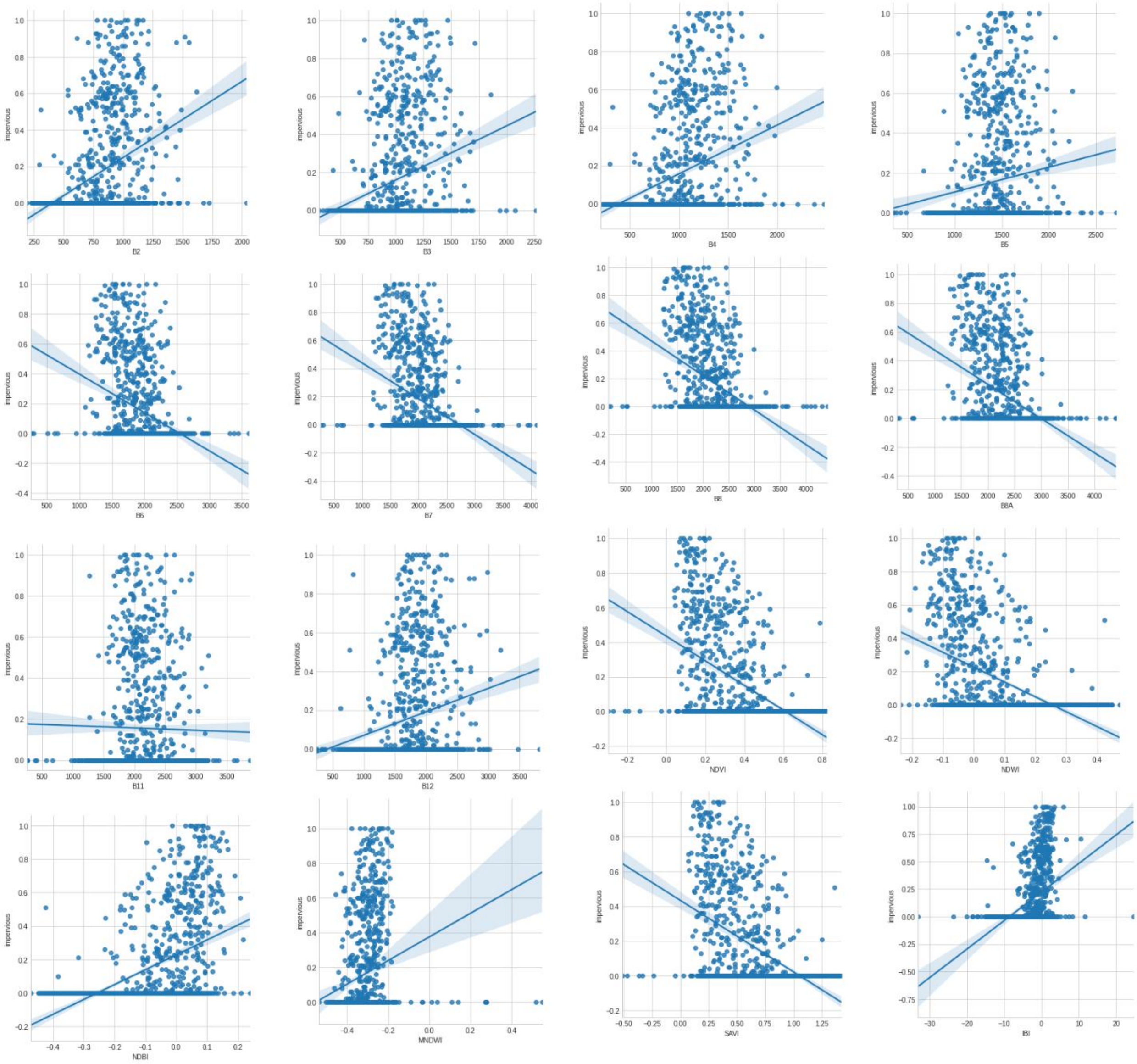

Figure 3.22:Feature Relationship with impervious surface

The above plots are between B2, B3, B4, B5, B6, B7, B8, B8A, B11, B12, NDVI, NDWI, NDBI, MNDWI, SAVI, and IBI with impervious data. From the above plot B2, B3, B4, B5, B12, NDBI, MNDWI, and IBI have positive relationship, similarly B6, B7, B8, B8A, NDVI, NDWI, and SAVI have a negative relationship and B11 show no relationship as it has an almost flat line.

Similarly, another important analysis in the exploration of data is to find the mutual information scores. Mutual Information plays an important role in selecting the features which are playing an important role in predicting the target variables (Liu et al., 2009). Mutual information can detect linear as well as non-linear relations between target and predictor. Given below in Figure 3.23 is the plot of mutual information score and we can see that B5, B11, and B12 have very less scores whereas NDVI and SAVI have a high score towards predicting impervious surface.

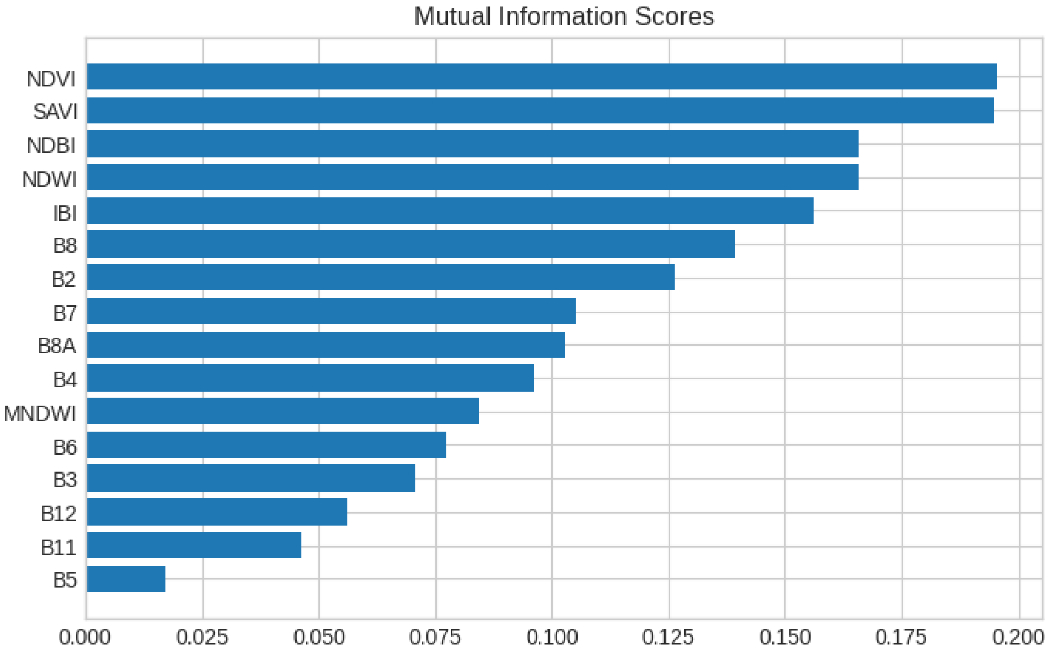

Figure 3.23: Mutual Information Score of Features

3.5 Model Fitting and Inferencing

Model fitting denotes the statistical process through which the theoretical predictions are compared to current data in one specific population (Neale & Maes, 2004). If the model fails, the theory, or at least a portion of it, should be rewritten. If the model fits, it does not necessarily indicate that it is "correct" in a broad sense; nonetheless, it may be useful in future studies that extend the scope of the model (Maas et al., 2020). Mostly algebraic and statistical components are involved while fitting the model. A well-fitted model gives precise results. Sometimes model gives overfitted or under fitted results in the case of overfitting of the model or underfitting of the model. When a machine learning or deep learning model's performance on unseen test data deviates from the performance seen during training, this is referred to as overfitting (Yeom et al., 2018).

While fitting the model early stopping has been used. Early stopping is a way that enables you to specify and stop training for arbitrary numbers as soon as the performance of the model stops improving with a validation dataset. The parameters used for early stopping are given in Figure 3.24.

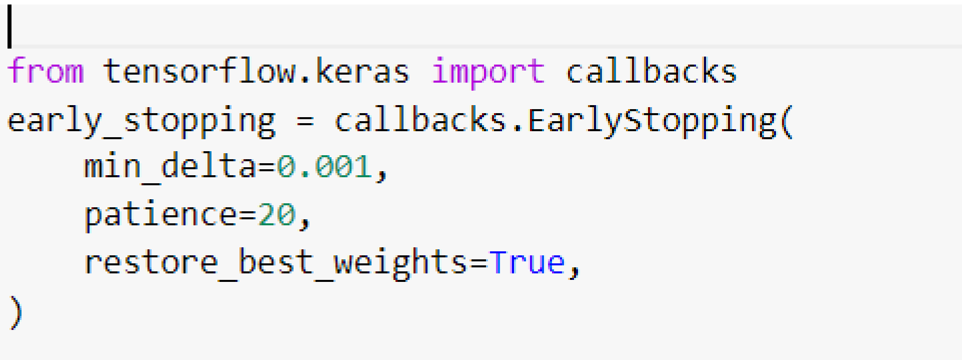

```
from tensorflow.keras import callbacks
early_stopping = callbacks.EarlyStopping(
    min_delta=0.001,
    patience=20,
    restore_best_weights=True,
)
```

Figure 3.24: Code Snippets of Early Stopping

So according to early stopping our model training will wait for 20 epochs and if the error is not decreasing more than 0.001 even after 20 epochs then it will stop and it will restore the best weights which will give the best output among the result.

Similarly, code snippets of the parameters used in fitting the model is given in Figure 3.25.

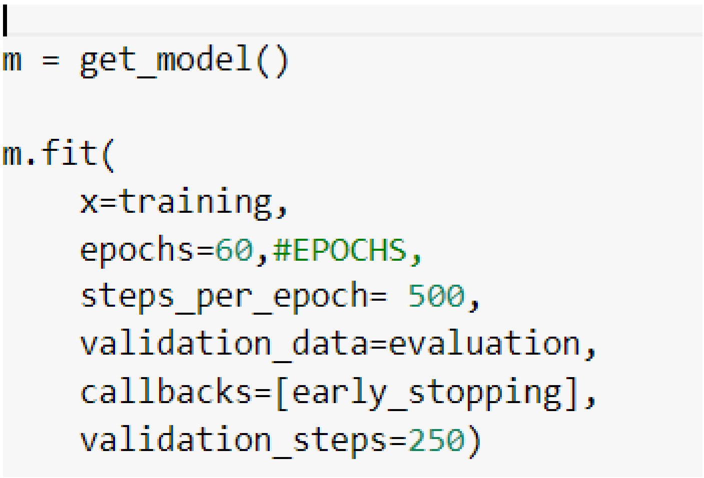

```
m = get_model()

m.fit(
    x=training,
    epochs=60,#EPOCHS,
    steps_per_epoch= 500,
    validation_data=evaluation,
    callbacks=[early_stopping],
    validation_steps=250)
```

Figure 3.25: Code Snippets for Model Fitting

The model fit takes the parameter x which is training data, an epoch which is the number of times it will be going through whole training data, steps_per_epoch is 500, validation_data will take evaluation data to tune the model, callbacks take the early stopping parameter and the validation_steps take the number for validation data.

After getting the appropriate trained model, it can be used to find the impervious surface probability layer of study area which is Kathmandu Valley. It can be also used to find the impervious layer of other places and cities which are highly urbanized.

For the fitting, the model three combinations of features are used and they are as follows:

3.5.1 Optical Bands

At first, the model is fitted with Optical band features. The optical band features are as follows.

Features = Optical Bands = [‘B2’, ‘B3’, ‘B4’, ‘B5’, ‘B6’, ‘B7’, ‘B8A’, ‘B8’, ‘B11’, ‘B12’]

The total number of features used in this training is 9.

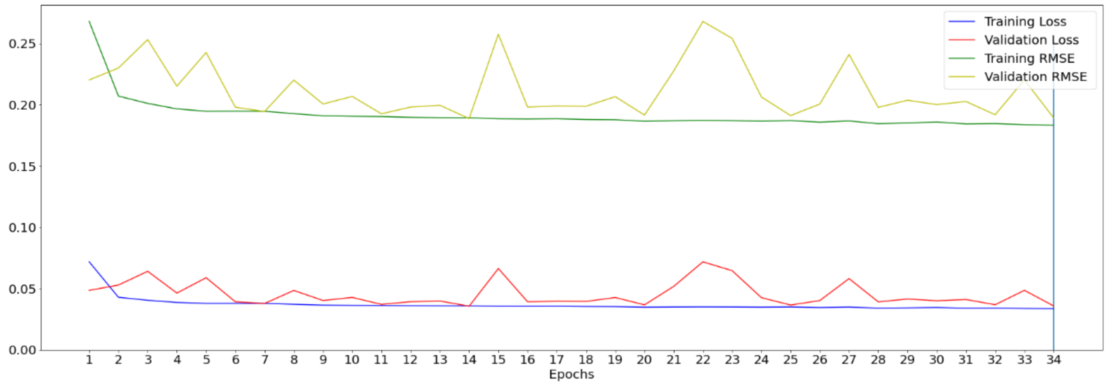

Figure 3.26: Loss and RMSE chart using Optical Bands as Features

Training RMSE	0.18333
Test RMSE	0.1991

When the model is trained using optical bands it ran for 34 epochs with a minimum training RMSE is 0.18333 given in Figure 3.26. The inference is done using the same model to find out the probability distribution of the impervious surface of Kathmandu Valley and is given in the below Map 3.5.

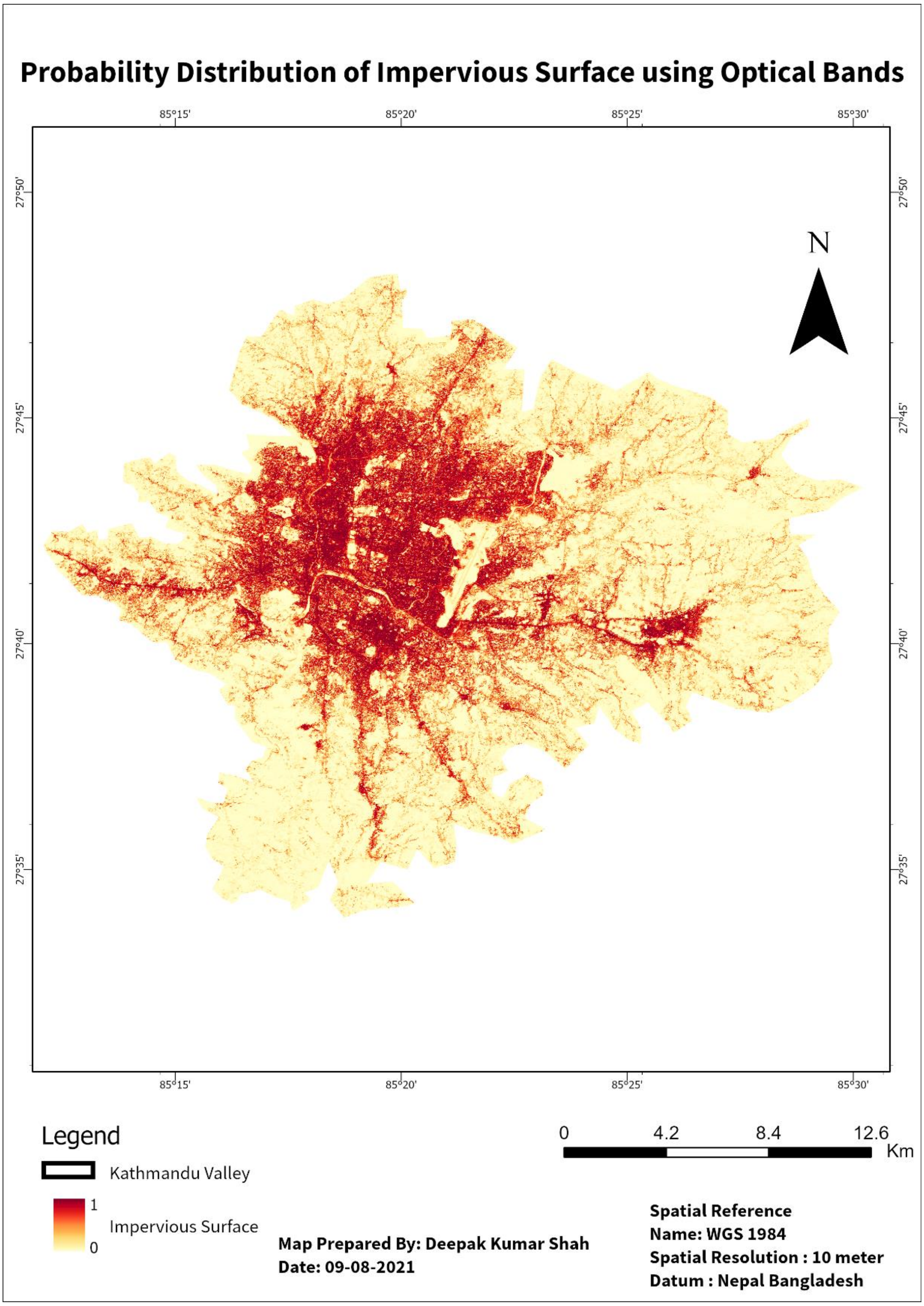

Map 3.5: Probability Distribution of Impervious Surface using Optical Bands

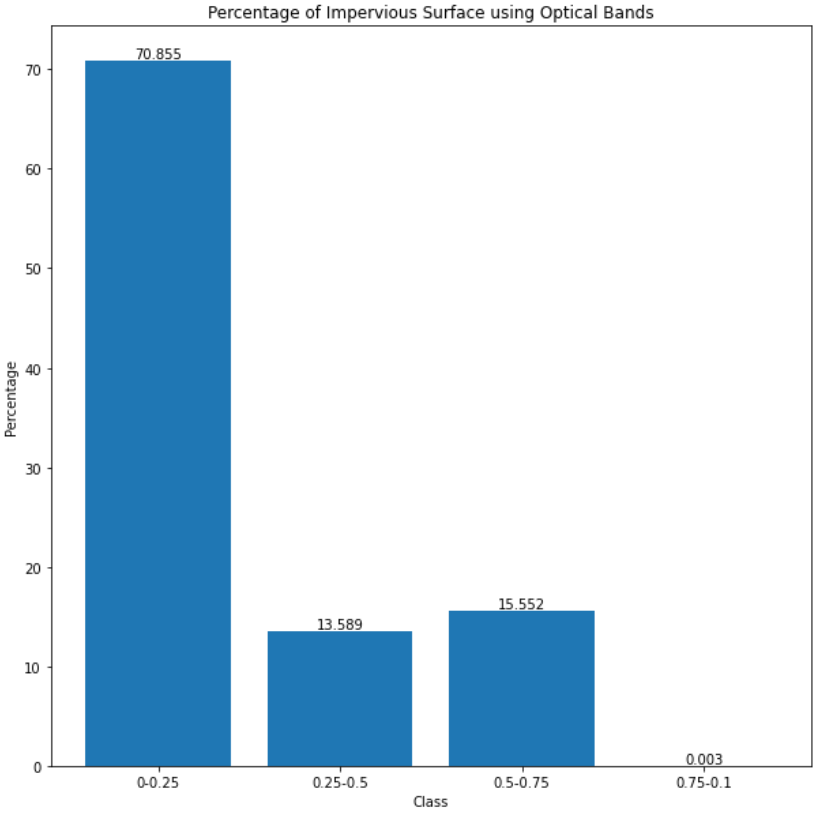

Figure 3.27: Percentage of Impervious Surface using Optical Bands

The percentage of impervious that are predicted using optical bands is higher in less than 25%, similarly between 25% to 50% which is like 50% to 75%. It has also predicted some impervious surfaces which are greater than 75% which is given in above graph Figure 3.27.

3.5.2 Optical Bands and Indices

I this section the model has trained again by adding the indices feature with optical bands.

Features = Optical Bands + Indices

= [‘B2’, ‘B3’, ‘B4’, ‘B5’, ‘B6’, ‘B7’, ‘B8A’, ‘B8’, ‘B11’, ‘B12’, ‘NDVI’, ‘NDWI’, ‘NDBI’, ‘MNDWI’, ‘SAVI’, ‘IBI’]

The total number of features used here is 16.

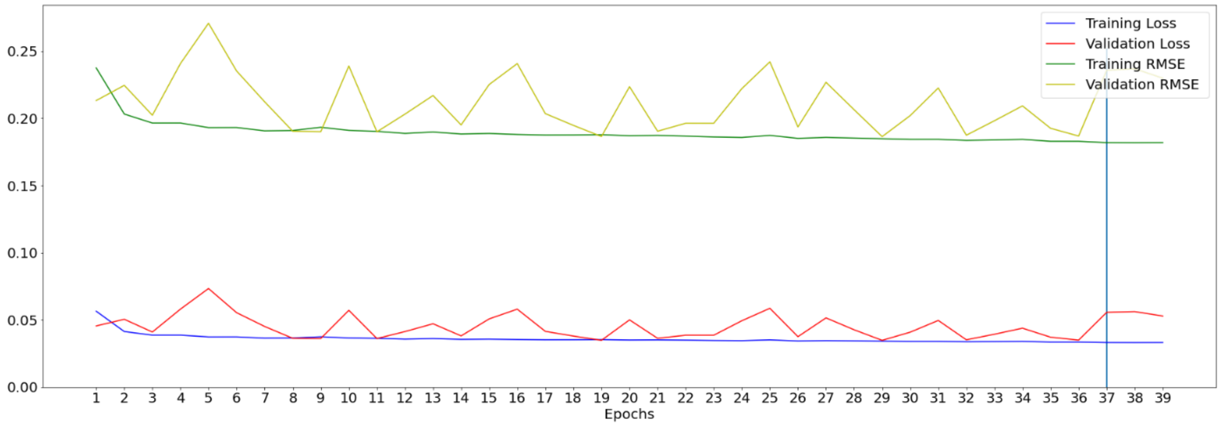

Figure 3.28: Loss and RMSE chart using Optical Bands and Indices as Features

Training RMSE	0.18185
Test RMSE	0.1976

When the model is trained using optical bands and some indices it ran for 39 epochs with minimum training RMSE is 0.18185 which is at 37 epochs due to early stopping as given in 3.28. The inference is done using the same model to find out the probability distribution of the impervious surface of Kathmandu Valley and is given in the below Map 3.6.

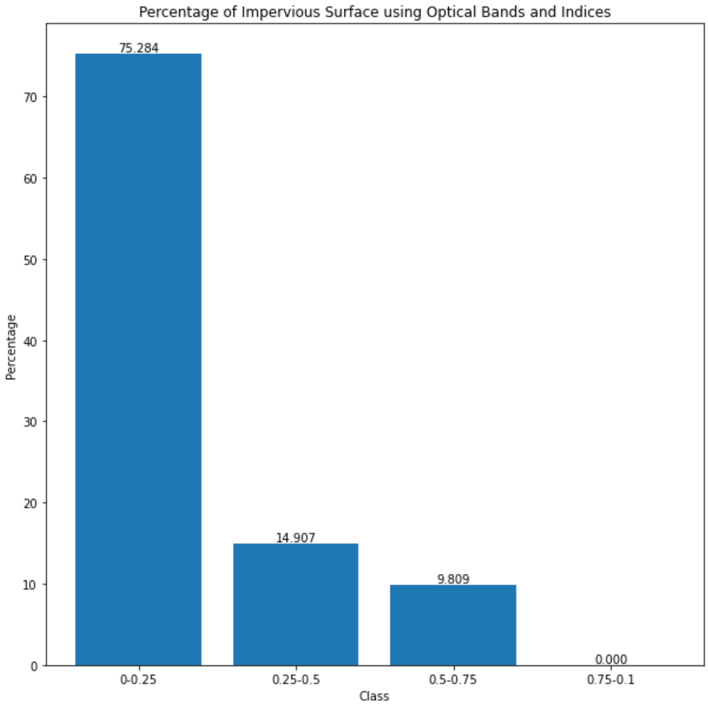

Figure 3.29: Percentage of Impervious Surface using Optical Bands and Indices

The percentage of impervious that are predicted using optical bands is higher in less than 25% which is 75.28%, similarly between 25% to 50% which is higher than 50% to 75%. It has also not predicted any impervious surface greater than 75% which is given in Figure 3.29.

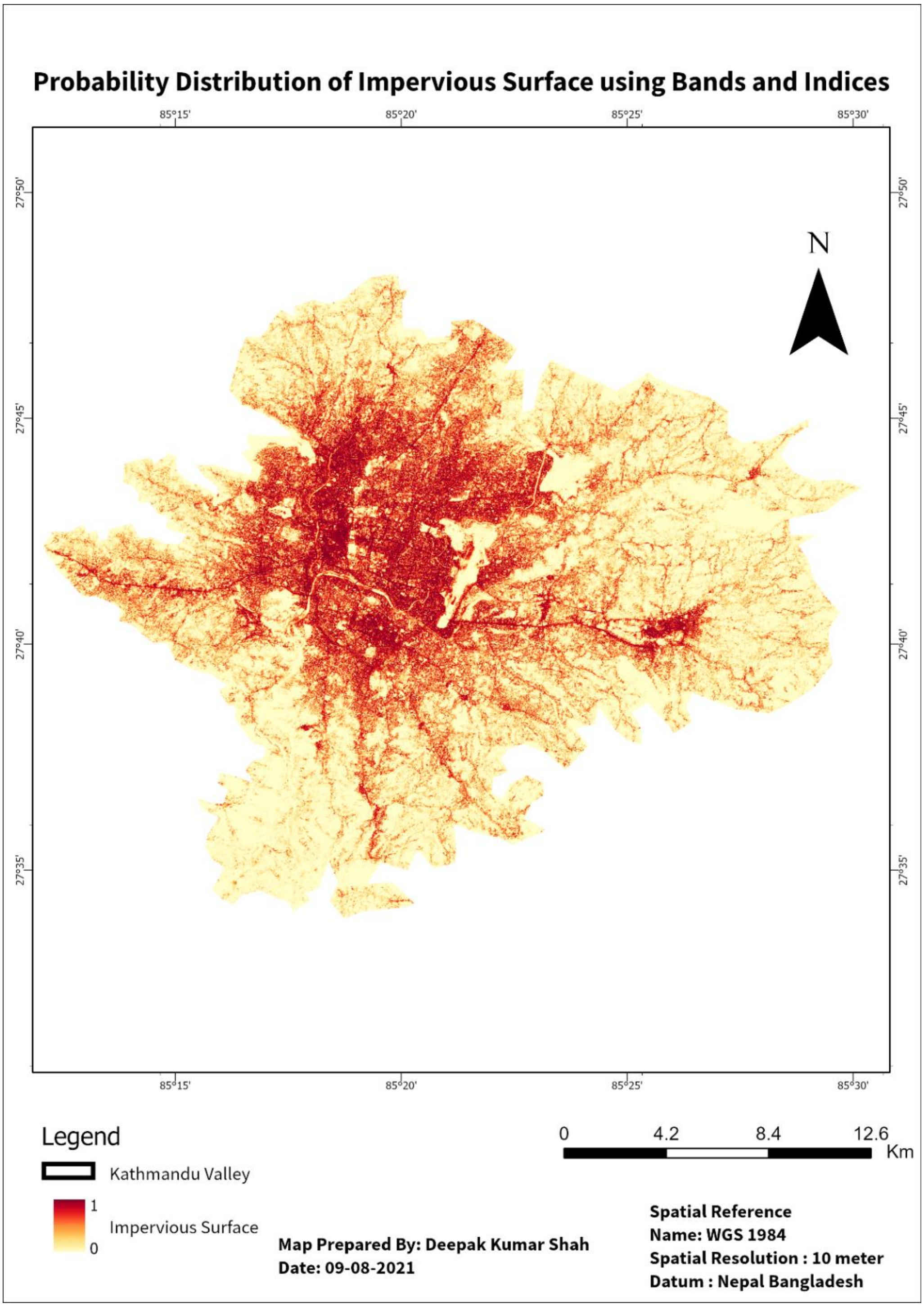

Map 3.6: Probability Distribution of Impervious Surface using Optical Bands and Indices

3.5.3 Selected Features

From the feature exploration section, we can find that not all the features are contributing to the impervious surface. The feature which has a low score in mutual information and does not show a positive or negative relationship can be eliminated from the features (H. Zou et al., 2003). So features that have a low score and do not show good relationships are B5, B11, and B12.

Selected Features = [‘B2’, ‘B3’, ‘B4’, ‘B6’, ‘B7’, ‘B8A’, ‘B8’, ‘NDVI’, ‘NDWI’, ‘NDBI’,
‘MNDWI’, ‘SAVI’, ‘IBI’]

Now all together we have 13 features for training.

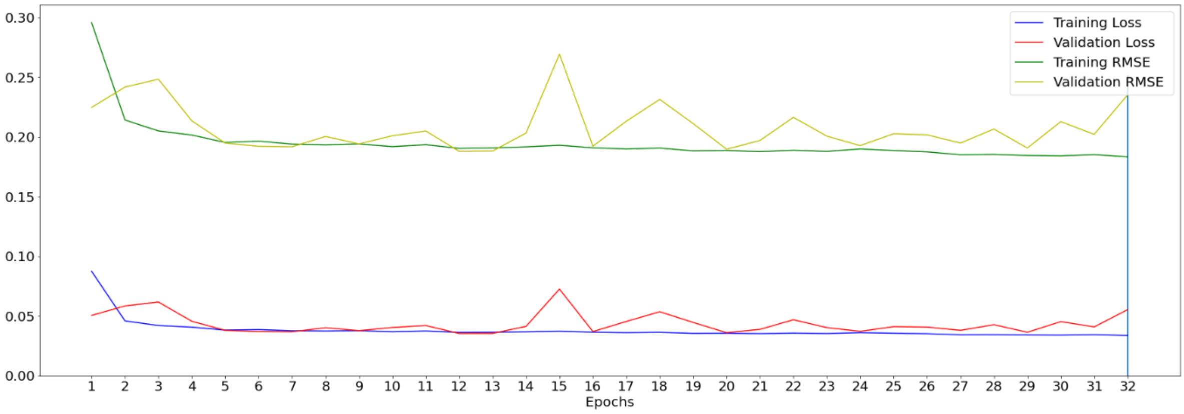

Figure 3.30: Loss and RMSE chart using Selected Bands and Indices

Training RMSE	0.18331
Test RMSE	0.1985

When the model is trained using selected bands and indices it ran for 32 epochs with minimum training RMSE is 0.18331 which is at 32 epochs due to early stopping as given in Figure 3.30. The inference is done using the same model to find out the probability distribution of the impervious surface of Kathmandu Valley and is given in the below Map 3.7.

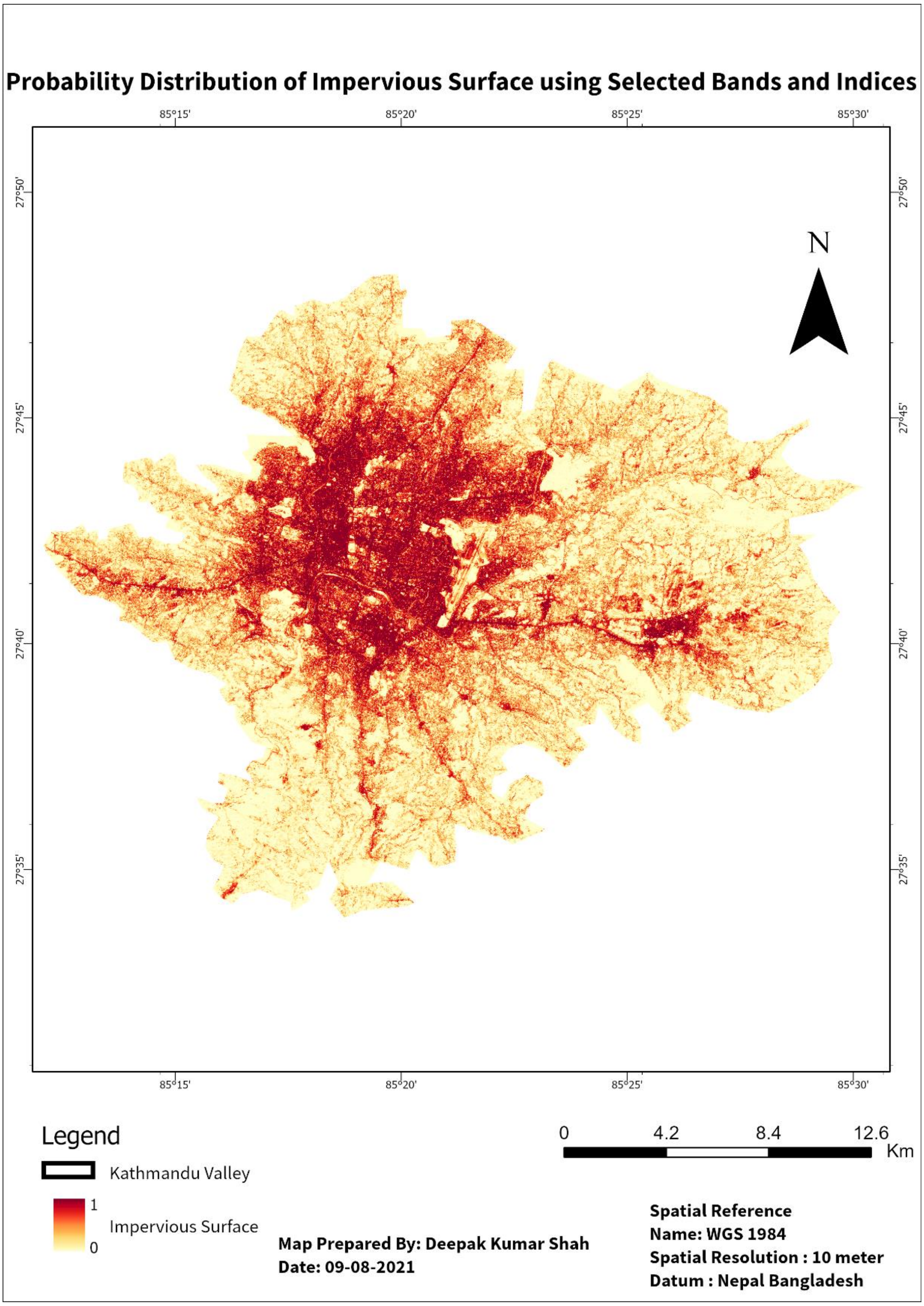

Map 3.7: Probability Distribution of Impervious Surface using Selected Optical Bands and Indices

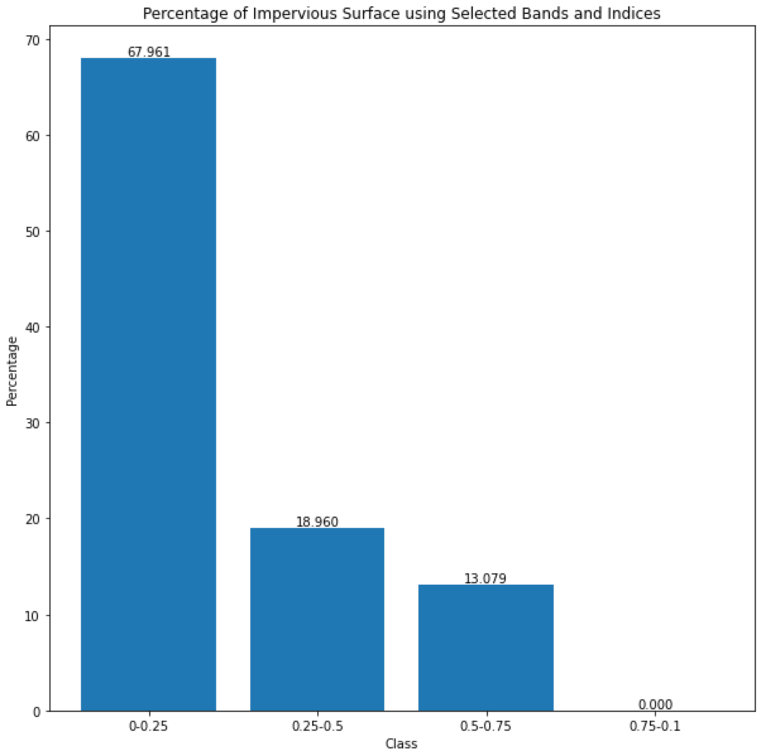

Figure 3.31: Percentage of Impervious Surface using Selected Bands and Indices

The percentage of impervious that are predicted using selected optical bands is higher in less than 25% which is 67.96%, similarly between 25% to 50% which is higher than 50% to 75%. It has also not predicted any impervious surface greater than 75% which is given in Figure 3.31.

3.6 Result Comparison

The UNet model was trained with parameters such as Adam as an optimizer, Mean Squared Error as Loss, and Root Mean Squared Error as the metric. It uses the ReLU as an activation function in the convolution layer and the sigmoid as the final activation function to produce the probability layer of the impervious surface.1

Table 3.4: Training and Test RMSE

	Optical Bands	Optical Bands and Indices	Selected Bands and Indices
Training RMSE	0.18333	0.18185	0.18331
Test RMSE	0.1991	0.1976	0.1985

Training and Test RMSE for each model using different features are given above. The training RMSE and Test RMSE is lower in the model using Bands and Indices and higher in the model using only Optical Bands as given in Table 3.4.

Similarly, from Figure 3.32 we can see all three predicted probability layers of impervious surface. The OSM layer is sparse as all the buildings, as well as other impervious surfaces, are not mapped well. The impervious surface layer using only optical bands of Sentinel-2A of 10m does pretty much a good job in the inferencing probability distribution, but it has some drawbacks as it failed to recognize the runway of the airport. It does a good job in separating the previous layer from impervious like river and forest tree areas. Similarly using optical bands and indices also does a good job in finding the impervious surface, but it also fails to generalize the airport runway. It has predicted impervious surface layer and separated pervious surface better than only using optical bands. It has also the lowest RMSE score in both training and testing datasets. The probability distribution of impervious surface using selected bands and indices has been predicted very well for impervious surface but in some cases, it fails to separate the pervious surface from impervious.

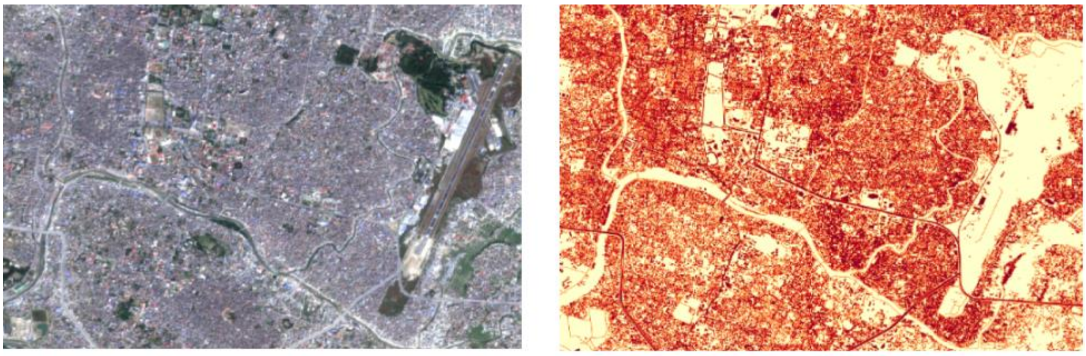

(a) Sentinel-2A Composite

(b) OSM Impervious Layer

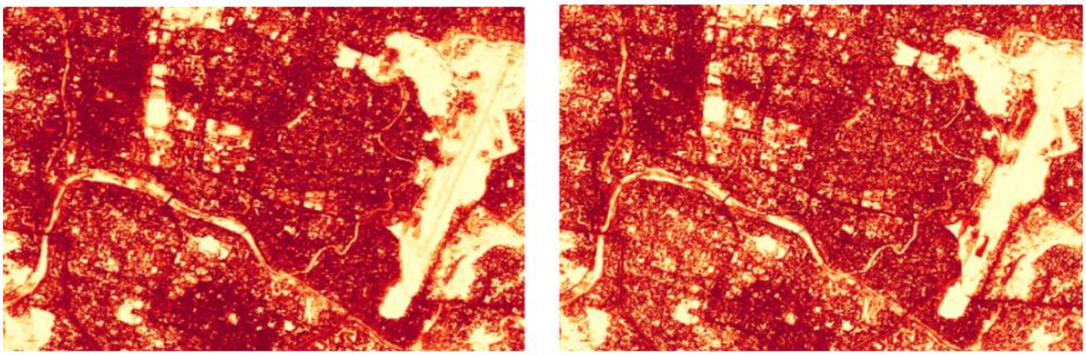

(c) Impervious Layer using Optical Bands

(d) Impervious Layer using Optical Bands and Indices

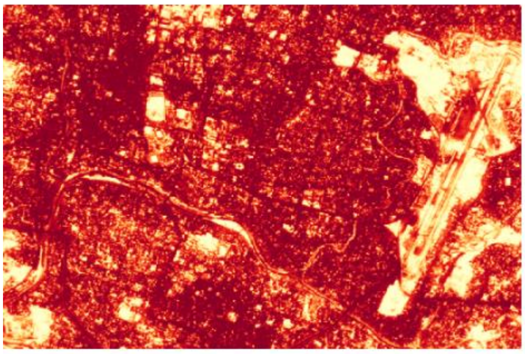

(d) Impervious Layer using Selected Bands and Indices

Figure 3.32: Probability Distribution Impervious Surface Comparison

Roads and buildings are well predicted in all three probability distribution model layers. There are also not many differences in the RMSE score of all three models.

Impervious layer between 0 to 0.25 class is higher using optical bands and indices which is 75.28%, similarly between 0.25 to 0.5 is higher in using selected indices which is 18.96%, between 0.5 to 0.75 is higher using optical bands which is 15.552% and above 0.75 has only been predicted using optical bands which 0.002862% which are given in below Figure 3.33.

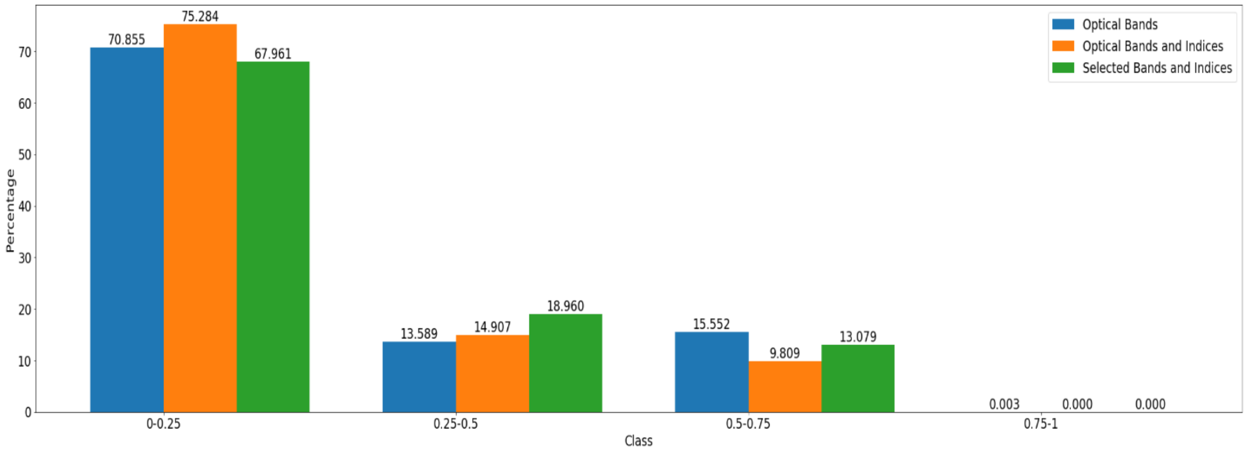

Figure 3.33: Comparison of Percentage of Impervious Layer from all three models

Chapter- 4: Discussion and Conclusion

4.1 Discussion

The UNet model is trained with same configuration by varying the number of features. From Table 3.4 of RMSE score matrix it is observed that optical bands with all the indices shows the better score in comparison of other two in RMSE. As model comparison with techniques given in literature review is difficult to compare with the proposed method as most of the result is based on some indices to identify impervious surface using remote sensing approach or even if it is the case with machine learning there is difference region, model configuration and time period.

Bauer et al. (2004) presented impervious surface classification using Landsat with R^2 values of 0.86. Similarly Corbane et al. (2020) obtained 61% to 83% accuracy using Facebook and Microsoft built-up areas with CNN model. McGlinchy et al. (2019) got 98% accuracy using 2m bands of WorldView-2. These all methods are difficult to compare with the presented study as model is trained using the data is Sentinel-2A as predictor and OSM patches as target from value for impervious surface probability distribution from Nepal only which have 0.181 as Training RMSE and 0.1976 as Testing RMSE score.

4.2 Conclusion

In this study, we have presented a *Deep Learning* method to find the probability distribution of impervious surfaces using the CNN UNet Model. Deep Learning is a powerful method that has advantages such as features are automatically inferred, appropriate adjustment of feature, and maximum utilization of unstructured data to get the high-quality desired result over other Machine Learning methods.

This study utilizes the mapped Volunteered Geographic Information (VGI) data storehouse of OSM for labeling as impervious surface and Sentinel-2A data with 10-meter resolutions band were regarded as a predictor for the impervious surface. And the combination of these features which includes bands and indices were made to train three different models. The Test dataset RMSE scores of these models are 0.1991, 0.1976, and 0.1985. These different models are successful in identifying the impervious surface of Kathmandu Valley districts. The visual debugging of these three different models has a good impression in predicting impervious surface layer.

Since *Deep Learning* methods are data-hungry models and they require a huge amount of data for training. In this study, we have taken 19 amount sample polygons among these polygons 12 polygon patches were fed to the training of impervious surface. To get a better and finer result the training data should be accurately mapped and should cover the whole impervious area for training purposes.

Chapter- 5: Limitations

Some limitations of this study using the data from OSM mapped layer and models output of impervious layer are as follows:

- Not all the buildings are mapped in the OSM layer which gives the wrong impression of impervious layer and is regarded as pervious area as given in Figure 5.1. And in this case, the value is given 0 even if the area is impervious surface.

Figure 5.1: Not mapped building

- Some roads which are in line geometry in the OSM layer are mapped on the side of the road rather than the center and as given in Figure 5.2, if we put buffer then there is a high probability that some pervious surface is also regarded as the impervious surface in training data as given value 1 rather than 0.

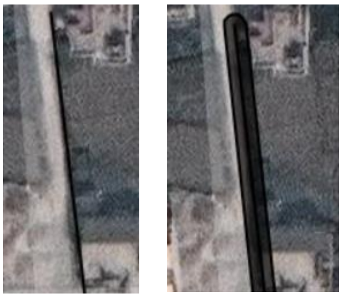

Figure 5.2: Linear roads and roads with buffer

- Buildings roofs are of different material compositions, some are of the thatched roof, some are of cement and sand, some are of steel (Wieland & Pittore, 2014) which have different surface reflectance and add some noise in data.

- Dry rivers which are also predicted as an impervious layer in some cases and an example of such case is given in Figure 5.3.

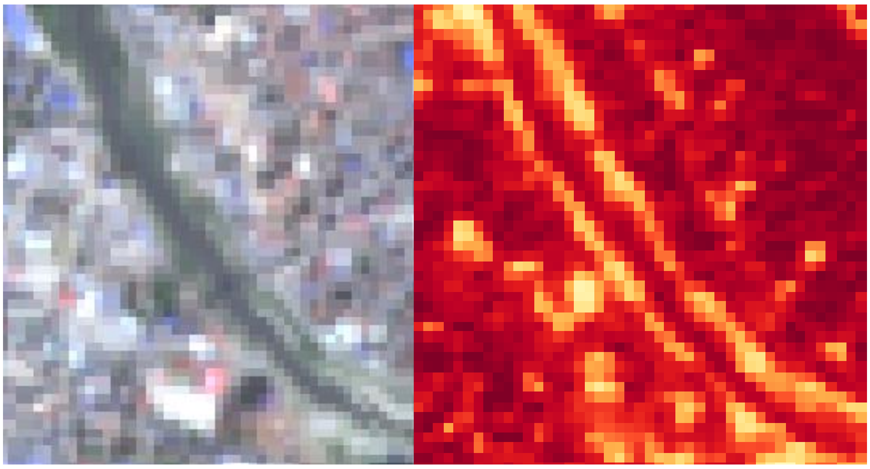

Figure 5.3: Dry River as Impervious Surface

- Since the deep learning model, such UNet models are data-hungry models which required a lot of data but the data that is mapped in OSM of Nepal is less than what is required.

References

Abadi, M. (2016). TensorFlow: Learning functions at scale. *Proceedings of the 21st ACM SIGPLAN International Conference on Functional Programming*, 1. https://doi.org/10.1145/2951913.2976746

Adams, L. W. (1994). *Urban Wildlife Habitats: A Landscape Perspective*. U of Minnesota Press.

Aksoy, S. (2008). Spatial Techniques for Image Classification. *Image Processing for Remote Sensing*. https://doi.org/10.1201/9781420003130.ch22

Allan, J. D. (2004). Landscapes and Riverscapes: The Influence of Land Use on Stream Ecosystems. *Annual Review of Ecology, Evolution, and Systematics*, *35*(1), 257–284. https://doi.org/10.1146/annurev.ecolsys.35.120202.110122

Arnold, C. L., & Gibbons, C. J. (1996). Impervious Surface Coverage: The Emergence of a Key Environmental Indicator. *Journal of the American Planning Association*, *62*(2), 243–258. https://doi.org/10.1080/01944369608975688

Assouline, S. (2004). Rainfall-Induced Soil Surface SealingContribution of the Agricultural Research Organization, Institute of Soil, Water and Environmental Sciences, Bet Dagan, Israel, No. 617/03.A Critical Review of Observations, Conceptual Models, and Solutions. *Vadose Zone Journal*, *3*(2), 570–591. https://doi.org/10.2113/3.2.570

Baboo, D. S. S., & Devi, M. R. (2010). An Analysis of Different Resampling Methods in Coimbatore, District. *Global Journal of Computer Science and Technology*. https://computerresearch.org/index.php/computer/article/view/670

Barnes, K., Morgan, J., & Roberge, M. (2000). *IMPERVIOUS SURFACES AND THE QUALITY OF NATURAL AND BUILT ENVIRONMENTS*.

Bauer, M. E., Heinert, N. J., Doyle, J. K., & Yuan, F. (2004). *Impervious Surface Mapping and Change Monitoring Using Landsat Remote Sensing*. 10.

Baumhardt, R. L., Römkens, M. J. M., Whisler, F. D., & Parlange, J.-Y. (1990). Modeling infiltration into a sealing soil. *Water Resources Research*, *26*(10), 2497–2505. https://doi.org/10.1029/WR026i010p02497

Bhaduri, B., Minner, M., Tatalovich, S., & Harbor, J. (2001). Long-Term Hydrologic Impact of Urbanization: A Tale of Two Models. *Journal of Water Resources Planning and Management*, *127*(1), 13–19. https://doi.org/10.1061/(ASCE)0733-9496(2001)127:1(13)

Bodo, T. (2019). Rapid Urbanisation: Theories, Causes, Consequences and Coping Strategies. *Sryahwa*, *2*(3), 32–35.

Bonsu, M. (1992). A physically based model for surface sealing of soil. *Journal of Soil Science*, *43*(2), 229–235. https://doi.org/10.1111/j.1365-2389.1992.tb00131.x

Booth, D. B., & Jackson, C. R. (1997). Urbanization of Aquatic Systems: Degradation Thresholds, Stormwater Detection, and the Limits of Mitigation1. *JAWRA Journal of the American Water Resources Association*, *33*(5), 1077–1090. https://doi.org/10.1111/j.1752-1688.1997.tb04126.x

Briassoulis, H. (2020). Analysis of Land Use Change: Theoretical and Modeling Approaches. 2nd edn. Edited by Scott Loveridge and Randall Jackson. WVU Research Repository, 2020.

Campbell, J. B., & Wynne, R. H. (2011). *Introduction to Remote Sensing, Fifth Edition*. Guilford Press.

Canada, S. (1978). Human Activity and the Environment. *Canadian Public Policy / Analyse de Politiques*, *4*(4), 587. https://doi.org/10.2307/3549992

Candra, D. S., Phinn, S., & Scarth, P. (2016). CLOUD AND CLOUD SHADOW MASKING USING MULTI-TEMPORAL CLOUD MASKING ALGORITHM IN TROPICAL ENVIRONMENTAL. *ISPRS - International Archives of the Photogrammetry, Remote Sensing and Spatial Information Sciences*, *XLI-B2*, 95–100. https://doi.org/10.5194/isprsarchives-XLI-B2-95-2016

Candra, D. S., Phinn, S., & Scarth, P. (2020). Cloud and cloud shadow masking for Sentinel-2 using multitemporal images in global area. *International Journal of Remote Sensing*, *41*(8), 2877–2904. https://doi.org/10.1080/01431161.2019.1697006

Canters, F., Chormanski, J., Van De Voorde, T., & Batelaan, O. (2006). Effects of different methods for estimating impervious surface cover on runoff estimation at catchment level. *Proceedings of Accuracy 2006, 7th International Symposium on Spatial Accuracy Assessment in Natural Resources and Environmental Sciences, Lisbon, Portugal, Proceedings of Accuracy 2006, 7th International Symposium on Spatial Accuracy Assessment in Natural Resources and Environmental Sciences, July 5-7, Lisbon, Portugal, July 5-7, 2006*, 557–566.

Carneiro, T., Medeiros Da NóBrega, R. V., Nepomuceno, T., Bian, G.-B., De Albuquerque, V. H. C., & Filho, P. P. R. (2018). Performance Analysis of Google Colaboratory as a Tool for Accelerating Deep Learning Applications. *IEEE Access*, *6*, 61677–61685. https://doi.org/10.1109/ACCESS.2018.2874767

CBS. (2012). *National Population and Housing Census 2011*. https://unstats.un.org/unsd/demographic-social/census/documents/Nepal/Nepal-Census-2011-Vol1.pdf

Chen, P.-Y., Srinivasan, R., Fedosejevs, G., & Kiniry, J. R. (2003). Evaluating different NDVI composite techniques using NOAA-14 AVHRR data. *International Journal of Remote Sensing*, *24*(17), 3403–3412. https://doi.org/10.1080/0143116021000021279

Choi, W., & Deal, B. M. (2008). Assessing hydrological impact of potential land use change through hydrological and land use change modeling for the Kishwaukee River basin (USA). *Journal of Environmental Management*, *88*(4), 1119–1130. https://doi.org/10.1016/j.jenvman.2007.06.001

Conway, T. M. (2007). Impervious surface as an indicator of pH and specific conductance in the urbanizing coastal zone of New Jersey, USA. *Journal of Environmental Management*, *85*(2), 308–316. https://doi.org/10.1016/j.jenvman.2006.09.023

Corbane, C., Syrris, V., Sabo, F., Politis, P., Melchiorri, M., Pesaresi, M., Soille, P., & Kemper, T. (2020). Convolutional neural networks for global human settlements mapping from Sentinel-2 satellite imagery. *Neural Computing and Applications*. https://doi.org/10.1007/s00521-020-05449-7

Cui, C., Chou, S.-H. S., Brattain, L., Lehman, C. D., & Samir, A. E. (2019). Data Engineering for Machine Learning in Women's Imaging and Beyond. *American Journal of Roentgenology*, *213*(1), 216–226. https://doi.org/10.2214/AJR.18.20464

Davidson, E. A., & Janssens, I. A. (2006). Temperature sensitivity of soil carbon decomposition and feedbacks to climate change. *Nature*, *440*(7081), 165–173. https://doi.org/10.1038/nature04514

Devkota, K. (2012). *Dynamics of Urbanization in Nepal:* 23.

Dewan, A. M., & Yamaguchi, Y. (2008). Using remote sensing and GIS to detect and monitor land use and land cover change in Dhaka Metropolitan of Bangladesh during 1960–2005. *Environmental Monitoring and Assessment*, *150*(1), 237. https://doi.org/10.1007/s10661-008-0226-5

Dogra, A., & Bhalla, P. (2014). Image Sharpening By Gaussian And Butterworth High Pass Filter. *Biomedical and Pharmacology Journal*, *7*(2), 707–713. https://doi.org/10.13005/bpj/545

Douglas, I. (1983). *The urban environment*. https://www.osti.gov/biblio/6147133

Duley, F. L. (1940). Surface factors affecting the rate of intake of water by soils. *Proceedings. Soil Science Society of America, 1939*, *4*, 60–64.

Durbha, S. S., & King, R. L. (2004). Knowledge mining in Earth observation data archives: A domain ontology perspective. *IGARSS 2004. 2004 IEEE International Geoscience and Remote Sensing Symposium*, *1*, 13b. https://doi.org/10.1109/IGARSS.2004.1368973

El Naqa, I., & Murphy, M. J. (2015). What Is Machine Learning? In I. El Naqa, R. Li, & M. J. Murphy (Eds.), *Machine Learning in Radiation Oncology: Theory and Applications* (pp. 3–11). Springer International Publishing. https://doi.org/10.1007/978-3-319-18305-3_1

Elaji, A., & Ji, W. (2020). Urban Runoff Simulation: How Do Land Use/Cover Change Patterning and Geospatial Data Quality Impact Model Outcome? *Water*, *12*(10), 2715. https://doi.org/10.3390/w12102715

European Commission. (2012). *In-Depth Report: Soil Sealing. Science for Environmental Policy*.

Flood, N. (2013). Seasonal Composite Landsat TM/ETM+ Images Using the Medoid (a Multi-Dimensional Median). *Remote Sensing*, *5*(12), 6481–6500. https://doi.org/10.3390/rs5126481

Fortel, L., Henry, M., Guilbaud, L., Guirao, A. L., Kuhlmann, M., Mouret, H., Rollin, O., & Vaissière, B. E. (2014). Decreasing Abundance, Increasing Diversity and Changing Structure of the Wild Bee Community (Hymenoptera: Anthophila) along an Urbanization Gradient. *PLOS ONE*, *9*(8), e104679. https://doi.org/10.1371/journal.pone.0104679

Ganapathy, N., Swaminathan, R., & Deserno, T. (2018). Deep Learning on 1-D Biosignals: A Taxonomy-based Survey. *Yearbook of Medical Informatics*, *27*, 098–109. https://doi.org/10.1055/s-0038-1667083

García, S., Ramírez-Gallego, S., Luengo, J., Benítez, J. M., & Herrera, F. (2016). Big data preprocessing: Methods and prospects. *Big Data Analytics*, *1*(1), 9. https://doi.org/10.1186/s41044-016-0014-0

Geslin, B., Féon, V. L., Folschweiller, M., Flacher, F., Carmignac, D., Motard, E., Perret, S., & Dajoz, I. (2016). The proportion of impervious surfaces at the landscape scale structures wild bee assemblages in a densely populated region. *Ecology and Evolution*, *6*(18), 6599–6615. https://doi.org/10.1002/ece3.2374

Google. (2021). *Introduction to TensorFlow | Machine Learning Crash Course*. Google Developers. https://developers.google.com/machine-learning/crash-course/first-steps-with-tensorflow/toolkit

Gorelick, N., Hancher, M., Dixon, M., Ilyushchenko, S., Thau, D., & Moore, R. (2017). Google Earth Engine: Planetary-scale geospatial analysis for everyone. *Remote Sensing of Environment*, *202*, 18–27. https://doi.org/10.1016/j.rse.2017.06.031

Goward, S. N., & Prince, S. D. (1995). Transient Effects of Climate on Vegetation Dynamics: Satellite Observations. *Journal of Biogeography*, *22*(2/3), 549–564. https://doi.org/10.2307/2845953

Guan, D., Li, H., Inohae, T., Su, W., Nagaie, T., & Hokao, K. (2011). Modeling urban land use change by the integration of cellular automaton and Markov model. *Ecological Modelling*, *222*(20), 3761–3772. https://doi.org/10.1016/j.ecolmodel.2011.09.009

H. Zou, K., Tuncali, K., & G. Silverman, S. (2003, June 1). *Correlation and Simple Linear Regression | Radiology*. https://doi.org/10.1148/radiol.2273011499

Haase, D., & Nuissl, H. (2007). Does urban sprawl drive changes in the water balance and policy?: The case of Leipzig (Germany) 1870–2003. *Landscape and Urban Planning*, *80*(1), 1–13. https://doi.org/10.1016/j.landurbplan.2006.03.011

Hassani, H., Silva, E. S., Unger, S., TajMazinani, M., & Mac Feely, S. (2020). Artificial Intelligence (AI) or Intelligence Augmentation (IA): What Is the Future? *AI*, *1*(2), 143–155. https://doi.org/10.3390/ai1020008

Hope, D., Naegeli, M. W., Chan, A. H., & Grimm, N. B. (2004). Nutrients on Asphalt Parking Surfaces in an Urban Environment. *Water, Air and Soil Pollution: Focus*, *4*(2), 371–390. https://doi.org/10.1023/B:WAFO.0000028366.61260.9b

Howard, L. (1833). *The Climate of London: Deduced from Meteorological Observations Made in the Metropolis and at Various Places Around it*. Harvey and Darton, J. and A. Arch, Longman, Hatchard, S. Highley [and] R. Hunter.

Hu, Q., & Feng, S. (2004). U.S. SOIL TEMPERATURE AND ITS VARIATION: A New Dataset. *Bulletin of the American Meteorological Society*, *85*(1), 29–31.

Hu, X., & Weng, Q. (2011). Impervious surface area extraction from IKONOS imagery using an object-based fuzzy method. *Geocarto International*, *26*(1), 3–20. https://doi.org/10.1080/10106049.2010.535616

Hua, L., Zhang, X., Nie, Q., Sun, F., & Tang, L. (2020). The Impacts of the Expansion of Urban Impervious Surfaces on Urban Heat Islands in a Coastal City in China. *Sustainability*, *12*(2), 475. https://doi.org/10.3390/su12020475

Huete, A. R. (1988). A soil-adjusted vegetation index (SAVI). *Remote Sensing of Environment*, *25*(3), 295–309. https://doi.org/10.1016/0034-4257(88)90106-X

Jawak, S. D., & Luis, A. J. (2013). A Comprehensive Evaluation of PAN-Sharpening Algorithms Coupled with Resampling Methods for Image Synthesis of Very High Resolution Remotely Sensed Satellite Data. *Advances in Remote Sensing*, *2013*. https://doi.org/10.4236/ars.2013.24036

Jensen, S. H., Møller, A., & Thiemann, P. (2009). Type Analysis for JavaScript. In J. Palsberg & Z. Su (Eds.), *Static Analysis* (pp. 238–255). Springer. https://doi.org/10.1007/978-3-642-03237-0_17

Jokar Arsanjani, J., Zipf, A., Mooney, P., & Helbich, M. (2015). An Introduction to OpenStreetMap in Geographic Information Science: Experiences, Research, and Applications. In *Lecture Notes in Geoinformation and Cartography* (pp. 1–15). https://doi.org/10.1007/978-3-319-14280-7_1

Jordan, M. I., & Mitchell, T. M. (2015). Machine learning: Trends, perspectives, and prospects. *Science*, *349*(6245), 255–260. https://doi.org/10.1126/science.aaa8415

Kamdoum Ngueuko, J., Adepoju, K., & Akinyede, J. (2014). Assessment of impervious surface area and surface urban heat island: A case study. *International Journal of Ecological Economics and Statistics*, *35*, 48–64.

Kanevski, M., Pozdnukhov, A., & Timonin, V. (2008). Machine Learning Algorithms for GeoSpatial Data. Applications and Software Tools. *International Congress on Environmental Modelling and Software*. https://scholarsarchive.byu.edu/iemssconference/2008/all/53

Kaplan, G. (2018). Sentinel-2 Pan Sharpening—Comparative Analysis. *Proceedings*, *2*(7), 345. https://doi.org/10.3390/ecrs-2-05158

Kennen, J. G. (1999). Relation of Macroinvertebrate Community Impairment to Catchment Characteristics in New Jersey Streams1. *JAWRA Journal of the American Water Resources Association*, *35*(4), 939–955. https://doi.org/10.1111/j.1752-1688.1999.tb04186.x

Kim, H., Jeong, H., Jeon, J., & Bae, S. (2016). The Impact of Impervious Surface on Water Quality and Its Threshold in Korea. *Water*, *8*(4), 111. https://doi.org/10.3390/w8040111

Kim, H., Park, S., Wang, J., Kim, Y., & Jeong, J. (2009). Advanced Bilinear Image Interpolation Based on Edge Features. *2009 First International Conference on Advances in Multimedia*, 33–36. https://doi.org/10.1109/MMEDIA.2009.14

Kingma, D. P., & Ba, J. (2017). Adam: A Method for Stochastic Optimization. *ArXiv:1412.6980 [Cs]*. http://arxiv.org/abs/1412.6980

Kinyanjui, M. J. (2011). NDVI-based vegetation monitoring in Mau forest complex, Kenya. *African Journal of Ecology*, *49*(2), 165–174. https://doi.org/10.1111/j.1365-2028.2010.01251.x

Klein, R. D. (1979). Urbanization and Stream Quality Impairment1. *JAWRA Journal of the American Water Resources Association*, *15*(4), 948–963. https://doi.org/10.1111/j.1752-1688.1979.tb01074.x

Kotsiantis, S. B., Kanellopoulos, D., & Pintelas, P. E. (2006). *Data Preprocessing for Supervised Leaning Abstract—Many factors affect the success of*.

Kuc, G., & Chormański, J. (2019). SENTINEL-2 IMAGERY FOR MAPPING AND MONITORING IMPERVIOUSNESS IN URBAN AREAS. *ISPRS - International Archives of the Photogrammetry, Remote Sensing and Spatial Information Sciences*, *XLII-1/W2*, 43–47. https://doi.org/10.5194/isprs-archives-XLII-1-W2-43-2019

Lamba, H. (2019, February 17). *Understanding Semantic Segmentation with UNET*. Medium. https://towardsdatascience.com/understanding-semantic-segmentation-with-unet-6be4f42d4b47

Lamichhane, S., & Shakya, N. M. (2019). Integrated Assessment of Climate Change and Land Use Change Impacts on Hydrology in the Kathmandu Valley Watershed, Central Nepal. *Water*, *11*(10), 2059. https://doi.org/10.3390/w11102059

LeCun, Y., Bengio, Y., & Hinton, G. (2015). Deep learning. *Nature*, *521*(7553), 436–444. https://doi.org/10.1038/nature14539

Leopold, L. B. (1968). *Hydrology for Urban Land Planning: A Guidebook on the Hydrologic Effects of Urban Land Use*. U.S. Geolgoical Survey.

Li, K., & Chen, Y. (2018). A Genetic Algorithm-Based Urban Cluster Automatic Threshold Method by Combining VIIRS DNB, NDVI, and NDBI to Monitor Urbanization. *Remote Sensing*, *10*(2), 277. https://doi.org/10.3390/rs10020277

Liu, F., Zhao, Y., Muhammad, R., Liu, X., & Chen, M. (2020). Impervious Surface Expansion: A Key Indicator for Environment and Urban Agglomeration—A Case Study of Guangdong-Hong Kong-Macao Greater Bay Area by Using Landsat Data. *Journal of Sensors*, *2020*, e3896589. https://doi.org/10.1155/2020/3896589

Liu, H., Sun, J., Liu, L., & Zhang, H. (2009). Feature selection with dynamic mutual information. *Pattern Recognition*, *42*(7), 1330–1339. https://doi.org/10.1016/j.patcog.2008.10.028

Lu, D., Hetrick, S., & Moran, E. (2011). Impervious surface mapping with Quickbird imagery. *International Journal of Remote Sensing*, *32*(9), 2519–2533. https://doi.org/10.1080/01431161003698393

Luciano, B. A., Alparone, L., Baronti, S., Garzelli, A., & Selva, M. (2004). *Spectral Information Extraction By Means Of Ms+pan Fusion*.

Lutz, M. (2001). *Programming Python*. O'Reilly Media, Inc.

Maas, H., Carducci, B., Nave, C., Mio, J., & Riggio, R. (2020). *Model Fitting*. 409–414. https://doi.org/10.1002/9781119547167.ch138

McCarthy, J. (2007). *WHAT IS ARTIFICIAL INTELLIGENCE?* 14.

McFEETERS, S. K. (1996). The use of the Normalized Difference Water Index (NDWI) in the delineation of open water features. *International Journal of Remote Sensing*, *17*(7), 1425–1432. https://doi.org/10.1080/01431169608948714

McGlinchy, J., Johnson, B., Muller, B., Joseph, M., & Diaz, J. (2019). Application of UNet Fully Convolutional Neural Network to Impervious Surface Segmentation in Urban Environment from High Resolution Satellite Imagery. *IGARSS 2019 - 2019 IEEE International Geoscience and Remote Sensing Symposium*, 3915–3918. https://doi.org/10.1109/IGARSS.2019.8900453

Miceli, G., & Braaten, J. (2021). *Sentinel-2 Cloud Masking with s2cloudless* [Jupyter Notebook]. Google. https://github.com/google/earthengine-community/blob/74cf65b61ccfc574d1ed33b9a8210e32eda14af3/tutorials/sentinel-2-s2cloudless/index.ipynb (Original work published 2019)

Misra, M., Kumar, D., & Shekhar, S. (2020). Assessing Machine Learning Based Supervised Classifiers For Built-Up Impervious Surface Area Extraction From Sentinel-2 Images. *Urban Forestry & Urban Greening*, *53*, 126714. https://doi.org/10.1016/j.ufug.2020.126714

MoDOR. (2013). *Nepal Road Standard 2070*. Government of Nepal Ministry of Physical Infrastructure & Transport. https://dor.gov.np/home/publication/general-documents/force/nepal-road-standard-2-7

MoUD. (2017). *National Urban Development Strategy 2017*. https://www.moud.gov.np/storage/listies/July2019/NUDS_PART_A.pdf

Nair, V., & Hinton, G. E. (2010, January 1). *Rectified Linear Units Improve Restricted Boltzmann Machines*. ICML. https://openreview.net/forum?id=rkb15iZdZB

Neale, M. C., & Maes, H. H. M. (2004). *Methodology for Genetic Studies of Twins and Families*. 308.

Novotny, V., & Chesters, G. (1981). *Handbook of nonpoint pollution*. Van Nostrand Reinhold Company. https://tamug-ir.tdl.org/handle/1969.3/24546

Nwankpa, C., Ijomah, W., Gachagan, A., & Marshall, S. (2020). *Activation Functions: Comparison of trends in Practice and Research for Deep Learning*.

Ongsulee, P. (2017). Artificial intelligence, machine learning and deep learning. *2017 15th International Conference on ICT and Knowledge Engineering (ICT KE)*, 1–6. https://doi.org/10.1109/ICTKE.2017.8259629

Parker, J. A., Kenyon, R. V., & Troxel, D. E. (1983). Comparison of Interpolating Methods for Image Resampling. *IEEE Transactions on Medical Imaging*, *2*(1), 31–39. https://doi.org/10.1109/TMI.1983.4307610

Parris, K. M. (2006). Urban amphibian assemblages as metacommunities. *Journal of Animal Ecology*, *75*(3), 757–764. https://doi.org/10.1111/j.1365-2656.2006.01096.x

Pauchard, A., Aguayo, M., Peña, E., & Urrutia, R. (2006). Multiple effects of urbanization on the biodiversity of developing countries: The case of a fast-growing metropolitan area (Concepción, Chile). *Biological Conservation*, *127*(3), 272–281. https://doi.org/10.1016/j.biocon.2005.05.015

Perez, F., & Granger, B. E. (2007). IPython: A System for Interactive Scientific Computing. *Computing in Science Engineering*, *9*(3), 21–29. https://doi.org/10.1109/MCSE.2007.53

Perry, T., & Nawaz, R. (2008). An investigation into the extent and impacts of hard surfacing of domestic gardens in an area of Leeds, United Kingdom. *Landscape and Urban Planning*, *86*(1), 1–13. https://doi.org/10.1016/j.landurbplan.2007.12.004

Pratiwi, H., Windarto, A. P., Susliansyah, S., Aria, R. R., Susilowati, S., Rahayu, L. K., Fitriani, Y., Merdekawati, A., & Rahadjeng, I. R. (2020). Sigmoid Activation Function in Selecting the Best Model of Artificial Neural Networks. *Journal of Physics: Conference Series*, *1471*, 012010. https://doi.org/10.1088/1742-6596/1471/1/012010

Rana, S., & Marwasta, D. (2015). Urbanisation trends in developing countries: Comparative study of Yogyakarta City and Kathmandu Valley. *Journal of Natural Resources and Development*, *5*. https://doi.org/10.5027/jnrd.v5i0.04

Reed, R., & MarksII, R. J. (1999). *Neural Smithing: Supervised Learning in Feedforward Artificial Neural Networks*. MIT Press.

Ronneberger, O., Fischer, P., & Brox, T. (2015). U-Net: Convolutional Networks for Biomedical Image Segmentation. *ArXiv:1505.04597 [Cs]*. http://arxiv.org/abs/1505.04597

Rose, A., Wilson, J. E., & Lavkulich, L. M. (2017). Analysis of Impervious Surface Area, and the Impacts on Soil-Based Agriculture and the Hydrologic Cycle: A Case Study in the Agricultural Land Reserve in Metro Vancouver, British Columbia, Canada. *Agricultural Sciences*, *08*(08), 837. https://doi.org/10.4236/as.2017.88062

Rousselet, G. A., & Wilcox, R. R. (2020). Reaction Times and other Skewed Distributions: Problems with the Mean and the Median. *Meta-Psychology*, *4*. https://doi.org/10.15626/MP.2019.1630

Rusk, N. (2016). Deep learning. *Nature Methods*, *13*(1), 35–35. https://doi.org/10.1038/nmeth.3707

Sakaguchi, I., Momose, T., & Kasubuchi, T. (2007). Decrease in thermal conductivity with increasing temperature in nearly dry sandy soil. *European Journal of Soil Science*, *58*(1), 92–97. https://doi.org/10.1111/j.1365-2389.2006.00803.x

Scalenghe, R., & Marsan, F. A. (2009). The anthropogenic sealing of soils in urban areas. *Landscape and Urban Planning*, *90*(1), 1–10. https://doi.org/10.1016/j.landurbplan.2008.10.011

Schowengerdt, R. A. (2006). *Remote Sensing: Models and Methods for Image Processing*. Elsevier.

Scott, A. J. (2008). Inside the City: On Urbanisation, Public Policy and Planning. *Urban Studies*, *45*(4), 755–772. https://doi.org/10.1177/0042098007088466

Serrano, W. (2017). Smart Internet Search with Random Neural Networks. *European Review*, *25*, 1–13. https://doi.org/10.1017/S1062798716000594

Shandilya, K., Shukla, S., & Pathak, V. (2013). *Applications of Remote Sensing*.

SHARMA, S. (2021, July 4). *Activation Functions in Neural Networks*. Medium. https://towardsdatascience.com/activation-functions-neural-networks-1cbd9f8d91d6

Slonecker, E. T., Jennings, D. B., & Garofalo, D. (2001). Remote sensing of impervious surfaces: A review. *Remote Sensing Reviews*, *20*(3), 227–255. https://doi.org/10.1080/02757250109532436

Sollins, P., Homann, P., & Caldwell, B. A. (1996). Stabilization and destabilization of soil organic matter: Mechanisms and controls. *Geoderma*, *74*(1), 65–105. https://doi.org/10.1016/S0016-7061(96)00036-5

Sonka, M., Hlavac, V., & Boyle, R. (2015). *Image Processing, Analysis, and Machine Vision* (4th ed.). Cengage Learning.

Soulé, M. E. (1991). Land Use Planning and Wildlife Maintenance: Guidelines for Conserving Wildlife in an Urban Landscape. *Journal of the American Planning Association*, *57*(3), 313–323. https://doi.org/10.1080/01944369108975502

Strohbach, M. W., Döring, A. O., Möck, M., Sedrez, M., Mumm, O., Schneider, A.-K., Weber, S., & Schröder, B. (2019). The “Hidden Urbanization”: Trends of Impervious Surface in Low-Density Housing Developments and Resulting Impacts on the Water Balance. *Frontiers in Environmental Science*, *7*. https://doi.org/10.3389/fenvs.2019.00029

Suardiwerianto, Yogi. (2017). *Flash flood modelling using data-driven models: Case studies of Kathmandu Valley (Nepal) and Yuna Catchment (Dominican Republic)*. Delft : UNESCO-IHE Institute for Water Education; https://doi.org/10.25831/gmss-t167

Tacoli, C. (2018). *Sustainable Cities, Human Mobility and International Migration: A Concise Report*. UN. https://doi.org/10.18356/a11581d8-en

Takebayashi, H., & Moriyama, M. (2007). Surface heat budget on green roof and high reflection roof for mitigation of urban heat island. *Building and Environment*, *42*(8), 2971–2979. https://doi.org/10.1016/j.buildenv.2006.06.017

Thapa, R. B., & Murayama, Y. (2009). Examining Spatiotemporal Urbanization Patterns in Kathmandu Valley, Nepal: Remote Sensing and Spatial Metrics Approaches. *Remote Sensing*, *1*(3), 534–556. https://doi.org/10.3390/rs1030534

Thapa, R. B., & Murayama, Y. (2012). Scenario based urban growth allocation in Kathmandu Valley, Nepal. *Landscape and Urban Planning*, *105*(1), 140–148. https://doi.org/10.1016/j.landurbplan.2011.12.007

VanderPlas, J. (2016). *Python Data Science Handbook: Essential Tools for Working with Data*. O'Reilly Media, Inc.

Weng, Q., Liu, H., & Lu, D. (2007). Assessing the effects of land use and land cover patterns on thermal conditions using landscape metrics in city of Indianapolis, United States. *Urban Ecosystems*, *10*(2), 203–219. https://doi.org/10.1007/s11252-007-0020-0

Wieland, M., & Pittore, M. (2014). Performance Evaluation of Machine Learning Algorithms for Urban Pattern Recognition from Multi-spectral Satellite Images. *Remote Sensing*, *6*(4), 2912–2939. https://doi.org/10.3390/rs6042912

Xian, G., Crane, M., & Su, J. (2007). An analysis of urban development and its environmental impact on the Tampa Bay watershed. *Journal of Environmental Management*, *85*(4), 965–976. https://doi.org/10.1016/j.jenvman.2006.11.012

Xu, H. (2006). Modification of normalised difference water index (NDWI) to enhance open water features in remotely sensed imagery. *International Journal of Remote Sensing*, *27*(14), 3025–3033. https://doi.org/10.1080/01431160600589179

Xu, H. (2008). A new index for delineating built-up land features in satellite imagery. *International Journal of Remote Sensing*, *29*(14), 4269–4276. https://doi.org/10.1080/01431160802039957

Xu, R., Liu, J., & Xu, J. (2018). Extraction of High-Precision Urban Impervious Surfaces from Sentinel-2 Multispectral Imagery via Modified Linear Spectral Mixture Analysis. *Sensors*, *18*(9), 2873. https://doi.org/10.3390/s18092873

Yeom, S., Giacomelli, I., Fredrikson, M., & Jha, S. (2018). Privacy Risk in Machine Learning: Analyzing the Connection to Overfitting. *2018 IEEE 31st Computer Security Foundations Symposium (CSF)*, 268–282. https://doi.org/10.1109/CSF.2018.00027

Yu, H., Zhao, Y., Fu, Y., & Li, L. (2018). Spatiotemporal Variance Assessment of Urban Rainstorm Waterlogging Affected by Impervious Surface Expansion: A Case Study of Guangzhou, China. *Sustainability*, *10*(10), 3761. https://doi.org/10.3390/su10103761